Salmonella enterica Typhimurium as a tumor-targeting immunotherapy vector

A Thesis
SUBMITTED TO THE FACULTY OF
UNIVERSITY OF MINNESOTA
BY

Jeremy Drees

IN PARTIAL FULFILLMENT OF THE REQUIREMENTS
FOR THE DEGREE OF
DOCTOR OF PHILOSOPHY

Janet L. Schottel

August 2015

ACKNOWLEDGEMENTS

There are many people without whom this work would have been difficult or even impossible. This list is by no means exhaustive and fails to acknowledge everybody who has supported me in my graduate education, to whom I am extremely grateful.

I would like to thank my advisor Dr. Janet Schottel, who has has taught me much about how to design experiments and present my ideas clearly. Her attention to detail is admirable and something that I know has helped me in my development as a scientist. One of the clear lessons that I learned from Janet when designing and interpreting experiments is "the devil's in the detail." Janet is full of integrity and was never afraid to speak her thoughts clearly and honestly, something that I admire a lot. I have never had to worry about whether Janet was "on my side" and always knew that she had my best interests in mind.

I would like to thank the remaining members of my thesis committee, including Dr. Christian Mohr, Dr. Christopher Pennell, and Dr. Matthew Mescher for their scientific expertise and input into my project. Each of my committee members has been very helpful and easy to work with.

I would like to thank Dr. Dan Saltzman, who has been a co-advisor in my research. The research presented in this thesis is a continuation of ideas initially pioneered by Dr. Saltzman in his PhD work, and the work performed was done so in Dr. Saltzman's laboratory and would have been impossible without him. Dan's positive outlook and his unique perspective and advice were always a refreshing start to the week.

I would like to thank Dr. Lance Augustin, who has been somewhat of a scientific mentor throughout my graduate career. Lance is a quick thinker and has a gift for problem solving, which was greatly appreciated when experimental results were difficult to interpret and saved me from going home frustrated on multiple occasions. Lance also had his nose in the scientific literature more than anybody else in the lab and was an "idea factory" for providing research direction and solutions to problems and hurdles that were encountered.

I would like to thank Mike Mertensotto for his indispensable work in the laboratory. Throughout my graduate studies, Mike has been a great help and has contributed significantly to a lot of the research presented in this thesis (specifically indicated in authorship notes and figure legends). Mike has particularly good molecular biology technical skills and helped me considerably in the cloning performed throughout my projects.

I would like to thank all of the funding sources that have made this research possible. This work has been funded in part by the Department of Surgery at the University of Minnesota, by a Department of Surgery Research Scholar of the Year Award, and by the Lung Cancer Research Foundation. Substantial funding was also provided by philanthropic organizations such as the ProjectStealth.org, Arnold S. Leonard Cancer Research Fund, StoneArch, and the Randy Shaver Cancer Research and Community Fund.

DEDICATION

This thesis is dedicated to my wife Jen, who is the most patient, loving, and supportive person I know.

And to my parents, who have loved and supported me from my youth and have always emphasized the importance of my education.

And to my friends, whose support and prayers have helped carry me through the finish line.

ABSTRACT

Interest in cancer immunotherapy has grown in recent years due to its potential for significant and durable therapeutic responses. Immune checkpoint blockade has emerged as an immunotherapy as a single agent but has even greater appeal when it is used in combination with other immunostimulatory approaches. However, the dosing of checkpoint blockade and its combinatorial use with other immunotherapies has been limited by systemic immune-related adverse side effects. One way to overcome these adverse effects is to deliver the therapeutic agents specifically to the tumor microenvironment. *Salmonella enterica* Typhimurium (*S.* Typhimurium) has been studied for cancer therapy due to its genetic manipulability and tumor-targeting propensity, and in this thesis, the potential of *S.* Typhimurium as a tumor-targeting immunotherapy vector was investigated. Functional antagonistic single chain antibodies (scFvs) against the immune checkpoints CTLA-4 and PD-L1 were isolated from an immunized chicken library and engineered for secretion from *S.* Typhimurium. The inherent anti-tumor properties and tumor-targeting capability of *S.* Typhimurium were then tested in transplanted primary and metastatic tumor models as well as a genetically engineered autochthonous BALB-neuT breast cancer model. In each of these models, *S.* Typhimurium demonstrated native anti-tumor efficacy; however the bacteria did not adequately colonize the autochthonous tumors of the BALB-neuT model. Disruption of tumor vasculature by treating BALB-neuT mice with a vasculature disrupting agent (VDA) improved the colonization of autochthonous tumors over 1000-fold to levels similar to those observed for transplanted tumors. Subsequent comparison of the tumor targeting capability and efficacy of *S.* Typhimurium engineered to secrete the antagonistic αPD-L1 (scFv) versus a control strain showed that secretion of the scFv

may further improve the colonization of autochthonous tumors, leading to a greater reduction in tumor burden of treated mice. These findings provide a proof of principle for the expression and delivery of functional immunotherapeutic single chain antibodies using *S.* Typhimurium, demonstrate *S.* Typhimurium's native tumoricidal activity independent of tumor-targeting, illustrate the importance of clinically representative tumor models when studying bacterial cancer therapy, and demonstrate the potential of VDA treatment to improve bacterial tumor-targeting. Collectively, this work illustrates *S.* Typhimurium's promise as a tumor-targeting immunotherapy vector.

TABLE OF CONTENTS

LIST OF TABLES

LIST OF FIGURES

CHAPTER 1

GENERAL INTRODUCTION

The National Cancer Institute Surveillance, Epidemiology, and End Results Program estimates that one in two men and one in three women will develop cancer in their lifetime. In the United States alone nearly every minute of every day a person dies due to cancer, resulting in approximately 500,000 cancer deaths each year. This is in spite of over 40 years of fighting a declared “war on cancer” (1). While exciting progress has been made in the treatment of some forms of cancer, it is often incremental, and fatalities due to the more deadly forms of cancer have remained largely unchanged in recent history. Victory in the war on cancer will depend on substantial advances in the diagnosis and treatment of the disease. One area that has demonstrated exciting potential in cancer treatment is immunotherapy, which is the utilization of the immune system to treat cancer.

TUMOR IMMUNOLOGY

Immunosurveillance

The theory of immunosurveillance claims that nascent tumors emerge sporadically throughout life, but are recognized and destroyed by the immune system before becoming clinically apparent (2), much like the immune system responding to and destroying a pathogen before the symptoms of infection appear. Historically, the theory of immunosurveillance of tumors was not widely accepted. After the notion was first proposed in 1909 by Paul Ehrlich (3), it was formally introduced by Marcfarlane Burnet and Lewis Thomas 50 years later (4, 5). However when tested experimentally, studies at the time demonstrated no difference in methylcholanthrene (MCA) carcinogen-induced

or spontaneous tumor incidence in athymic nude CBA/H mice when compared to wild type controls. In response to these experiments, the idea of immunosurveillance was widely unaccepted into the 1970's (2). The caveats of these studies, unknown at the time, included 1) the use of nude mice as a model of immunodeficiency, which are now understood to harbor both a fully-functional innate immune system, including functional natural killer (NK) cells, and even some degree of an adaptive immune system containing detectable numbers of αβ T-cells and 2) CBA/H mice that were used in the studies are particularly sensitive to the transforming effects of MCA due to their expression of a highly active enzyme isoform required to metabolize MCA into its carcinogenic form. Therefore, it may be that MCA-induced carcinogenesis in these mice was so effective that any protective immunity to tumor formation was insufficient to show a significant effect (2). Resurgence in the theory of immunosurveillance began in the 1990's, in light of a more detailed understanding of the components of the immunosurveillance network. Several reports in the subsequent decades demonstrated a greater tumor incidence and/or aggression in mice that are deficient in certain components of the immune system such as T, B and NKT cells; interferon gamma (IFNγ) production or sensitivity; monocytes; macrophages; perforin; TNF-related apoptosis inducing ligand (TRAIL); interleukin 12 (IL-12); and more (reviewed in (2)). In light of these studies and additional clinical observations, such as an increased incidence of several tumor types in patients with acquired immune deficiencies (6), immunosurveillance theory holds widespread acceptance in the scientific community today.

Immunoediting of tumors

Clinically apparent tumors by definition have avoided the surveillance of the immune system through a process termed “immunoediting.” This is thought to occur in three stages or “E’s” of immunoediting: *elimination*, *equilibrium* and *escape* (2).

Elimination phase: Immunosurveillance is represented during the *elimination* phase of immunoediting, in which nascent tumors are recognized by the immune system and effectively eradicated before they cause disease. Elucidating the components of an effective anti-tumor immune response is an ongoing area of investigation, and current understanding involves both the innate and adaptive arms of the immune system. Initially, the innate immune system may be alerted to a developing tumor by the damage it causes to local tissues (7, 8). This recruits cells of the innate immune system such as NK cells, NKT cells, γδ T-cells, and macrophages (2). Tumor cells may be recognized at this point by NKG2D receptors on NK cells and/or NKT cells recognizing NKG2D ligands expressed on the transforming cells. NKT cells have also been shown to respond to glycolipid complexes expressed on tumor cells during transformation (9). Ultimately, an important outcome of this initial recognition is the production of IFNγ. IFNγ signaling has several effects that drive the anti-tumor immune response at this stage, such as inducing the production of chemokines that in turn recruit additional immune cells to the tumor environment (2), inducing tumor-infiltrating macrophages to secrete low levels of IL-12, and stimulating NK cells to secrete additional IFNγ. IL-12 induces NK cell production of IFNγ, which in turn induces macrophage secretion of IL-12 in a positive feedback loop (10). This additional boost in IFNγ not only increases the cytotoxicity of NK cells but also results in anti-proliferative (11), pro-apoptotic (12), and anti-angiogenic (13, 14) effects in the tumor that cause tumor cell death. Additionally, IFNγ-activated macrophages can kill cells indirectly via the production of reactive oxygen species (ROS) or TNF-related apoptosis-inducing ligand (TRAIL) (15, 16). Ultimately, these activities result in the

availability of tumor antigens (TA) from dead tumor cells that allow the enlistment of the adaptive immune system to target tumor cells. Immature dendritic cells (DCs) recruited to the tumor environment in response to chemokine signals become activated in the presence of the NK cells and the cytokine milieu generated from the innate immune system (17). Activated DCs then pick up TA directly by phagocytizing tumor cell debris or indirectly by the transfer of heat shock protein/TA complexes to the DCs (18, 19). Activated, TA-loaded DCs then migrate to the tumor-draining lymph node (20, 21), where they present antigen to naïve CD4 T-cells in the presence of IL-12, inducing CD4 T-cell differentiation into activated T-helper 1 (Th1) cells, which in turn help the activation and proliferation of tumor-specific CD8 cytotoxic T-lymphocytes (CTL) by assisting DC-mediated cross presentation of TA (22, 23). The T-cell-mediated adaptive immune response then allows for the complete elimination of the developing tumor. Tumor-specific CD4 and CD8 T-cells accumulate in the tumor microenvironment, and CD4 T-cells produce interleukins 2 and 15 (IL2, IL15), which sustain the function and viability of tumor-specific CTL. CD8 T-cells kill tumor cells both directly, via the recognition of TA peptide on the surface of tumor cells in the context of major histocompatibility complex class 1 (MHC I), and indirectly via the production of high amounts of IFNγ, which (as described above) may cause pleotropic tumoricidal effects on cell cycle, apoptosis, angiogenesis, and macrophage activation. As this Th1-driven, CTL-mediated tumor elimination phase is TA-specific, it must be repeated for each new antigenically variant population of tumor cells that may appear.

Equilibrium phase: If a particularly prolific, genetically unstable tumor cell population is generated, it may avoid elimination and enter an *equilibrium* phase with the host immune system, wherein an IFNγ-driven cellular immune response kills tumor cells

at a rate that is enough to contain, but not fully abolish a tumor bed harboring genetically unstable cancer cells. This phase will often last several years in humans and is a crucial stage in cancer development. During this time, the host immune system exerts a relentless selection pressure on the developing tumor, which through a micro Darwinian-like selection will become edited for immunosuppressive characteristics that allow it to ultimately escape equilibrium and grow in the final *escape* phase as clinically apparent cancer (2).

Escape phase: Through the process of immunoediting, tumors develop immune hallmarks that are required for growth and progression in an immunocompetent host, such as the ability to evade immune recognition and the ability to suppress immune reactivity (24). Tumors are marked by an increasing genetic instability during development (25), and mutations in tumor antigens themselves or antigen presentation machinery that reduce the recognizability of the tumor cells by the adaptive system (termed “immunogenicity”) are selected for during immunoediting, resulting in less immunogenic tumor cells. Additionally, tumor cells have been reported to alter or lose MHC I surface expression, hampering antigenic peptide presentation to tumor specific T-cells and allowing them to evade recognition by the adaptive immune response (26, 27).

Immunosuppressive mechanisms of tumor cells

While immunoevasive strategies are problematic, they are not enough alone to prevent the generation an anti-tumor immune response. This is evidenced by most, if not all, tumors also acquiring additional mechanisms to suppress the host immune system to avoid destruction. Tumor cells will often directly release immunoinhibitory agents, such as cytokines including transforming growth factor beta (TGFβ) or interleukin 10 (IL-10), or factors such as the tryptophan catabolizing enzyme indolamine 2,3-dioxygenase

(IDO), which depletes available tryptophan that is essential for T-cell effector function (24). Additionally tumors recruit or induce the differentiation of immunosuppressive cell populations causing their accumulation in the tumor microenvironment (TME) and attenuating the effects of the immune system.

Regulatory T-cells

Regulatory T-cells (T-regs) are an immunosuppressive subset of CD4 T-cells that are often found in high concentrations in tumor tissues (28). The mechanisms of T-reg-mediated T-cell inhibition continues to be an area of active investigation, though evidence has been proposed for multiple mechanisms that may vary depending on tumor type or stage of development (reviewed in (29)) including the secretion of soluble or membrane-bound immunosuppressive molecules such as IL-10, TGFβ, and IL-35; the direct cytolysis of T-cells and possibly antigen-presenting DCs; disruption of T-cell metabolism by "starving" T cells of cytokine signals such as IL-2 or catalyzing the conversion of ATP to adenosine, which suppresses T-cell effector function; and by suppressing DC function by preventing maturation and expression of co-stimulatory molecules and inducing DC expression of IDO.

T-regs are important cell populations in peripheral tolerance that prevent the activation of high affinity self-reactive T-cells that have escaped negative selection in the thymus. As tumor-associated antigens are often not foreign in the way pathogenic antigens are, the enrichment of T-regs in the tumor microenvironment might be expected as the immune system attempts to prevent a cytotoxic response against what may largely be recognized as "self." In addition to the presence of these "natural" T-regs in the TME, tumors may also cause the accumulation of "induced" T-regs. In this case, tumor cells themselves or tumor associated cells will express factors such as TGFβ that

that can induce naïve CD4 cells to act like or differentiate into T-regs; these induced T-regs express the canonical FoxP3 transcription factor that characterizes natural T-regs and will suppress T-cell mediated immunity similarly to natural T-regs (29).

Tumor-associated macrophages

In addition to regulatory T-cells, tumors will often harbor large populations of immunosuppressive myeloid cells such as tumor-associated macrophages (TAMs). Typically, macrophages are described phenotypically as either classically activated (M1) or alternatively activated (M2). M1 macrophages are required for tumor immunosurveillance and protection against pathogens, while M2 macrophages are important in inflammation, angiogenesis, and wound healing. Current understanding suggests that M1 and M2 polarization is too simplistic to adequately characterize the diverse spectrum of phenotypes that are actually encountered *in vivo* (30); however for simplicity, this nomenclature will be used here while acknowledging its potential to over-simplify macrophage characterization. Instead of the M1-like macrophages desired for tumor elimination, tumors that have escaped immunosurveillance will be enriched with M2-like TAMs. Rather than expressing IL-12, activating NK and Th1 CD4 cells, and stimulating anti-tumor immunity, TAMs will actually be commandeered by the tumor to support tumor growth and inhibit anti-tumor immune responses. TAMs will display several M2-like characteristics that drive tumor progression including the promotion of angiogenesis (31) and the assistance in tumor cell intravasation and epithelial to mesenchymal transition, which drives tumor metastasis (32, 33). Additionally, TAMs have been implicated for many M2-like mechanisms of immunosuppression including but not limited to: the expression of surface-bound and secreted inhibitory factors such as HLA-G, an MHC molecule that may inhibit IFNγ-mediated CD4 T-cell activation (30), IL-

10, and TGFβ (34); the constitutive expression of the immunoinhibitory checkpoint ligands such as PD-L1 and B7-H4 and their up-regulation in hypoxic areas (35); the recruitment of T-regs via the expression of the CCL22 (36) and the induction of T-regs and direct suppression of T-cells via IL-10 and TGFβ (37-40); and by the expression and secretion of Arginase I (ArgI), which metabolizes L-arginine, an essential amino acid for maintaining the ζ-chain expression important for T-cell receptor (TCR) signaling (41).

Myeloid-derived suppressor cells

In addition to TAMs, populations of less mature myeloid cells are emerging as important immunomodulators in tumor immune escape. In a tumor-bearing host, a large collection of immature myeloid cells will accumulate in the tumor and spleen and suppress host anti-tumor immunity. These cells, termed myeloid-derived suppressor cells (MDCSs), are normally generated as myeloid cell precursors in the bone marrow of a healthy host and when transferred into a non-tumor bearing host will develop into mature macrophages and DCs; however if adoptively transferred into a tumor bearing host or cultured in the presence of tumor-derived soluble factors, these cells will remain MDSCs or differentiate into immunosuppressive TAMs (42). MDSCs, initially identified as Gr-1$^+$ and CD11b$^+$, have since been subdivided into Ly6G$^+$ granulocytic (G-MDSC) and Ly6C$^+$ monocytic (M-MDSC) subsets (the “Gr-1” antibody recognizes an epitope expressed on both Ly6C and Ly6G). G-MDSCs are usually the more numerous of the two populations in cancer and suppress CD8 T-cells primarily through the production of reactive oxygen species (ROS) (42). M-MDSCs, although less prevalent, are more immunosuppressive on a per-cell basis (43-45). M-MDSCs suppress T-cells primarily through ArgI expression and may subsequently develop into TAMs (42). While a relatively new area of ongoing study, MDCSs are thought to suppress the immune

system through multiple mechanisms, including: the depletion of L-arginine and L-cysteine by expression of metabolizing enzymes such as ArgI (46, 47); the generation of oxidative stress via the production of ROS and reactive nitrogen species (42), which effects T-cell ζ-chain expression (48), IL-2 receptor signaling (49), and TCR sensitivity (50); the inhibition of effector T-cell trafficking to the tumor by decreasing T-cell L-selectin expression (51); and the activation and expansion of T-regs possibly through cell-to-cell contact (52) or by the production of IL10, TGFβ, and/or retinoic acid (53-55).

Immunoinhibitory checkpoints

In addition to secretion of immunoinhibitory molecules and the recruitment of immunosuppressive cells, tumors will avoid elimination by taking advantage of immunoinhibitory checkpoints such as CTLA-4 and PD-1. These receptors are naturally important in peripheral tolerance and are up-regulated on T-cells shortly after activation. Their expression primes the T-cells for subsequent self-regulation by rendering the cells susceptible to homeostatic signals later in an immune response. As important molecules in the prevention of autoimmunity, mice deficient in either of these receptors develop severe autoimmune disorders shortly after birth (56). CTLA-4 is thought to antagonize T-cell activation by multiple mechanisms including competition with CD28 for costimulatory B7.1/B7.2 interaction, evidenced by CTLA-4's higher binding affinity for B7.1/B7.2, as well as intrinsic immunoreceptor tyrosine-based inhibitory motif-mediated signaling mechanisms that interfere with TCR signaling upon CTLA-4 binding to its ligands (56). Additionally, CTLA-4 is constitutively expressed on T-regs and is essential for their inhibitory activity (57, 58). PD-1, through engagement with its ligands PD-L1 and PD-L2 sends inhibitory signals through an immunoreceptor tyrosine-based switch motif to inhibit T-cell activation at the immunological synapse (59). PD-L1 is constitutively expressed on

T-regs and suppressive myeloid cells such as MDSCs and TAMs. Expression may also be increased in response to hypoxia (35). In addition to immune cells, PD-L1 is also directly expressed by tumor cells in several cancers as part of their immune-inhibitory repertoire and is correlated with a negative prognosis (60).

IMMUNOTHERAPY, CYTOKINES AND CHECKPOINT INHIBITION

Cytokine therapy

Cytokines are the primary messengers of the immune system, and the cytokine milieu present in the TME largely controls the activation or inhibition of an anti-tumor immune response. One strategy used to reverse tumor-mediated immune suppression is to manipulate the cytokine environment. To this end, systemic administration of immunostimulatory cytokines has been examined for efficacy in several cancer models, and cytokines such as IL-2 and IFNα have been used clinically for several years to treat malignancies such as metastatic melanoma and renal cell carcinoma (61). As immunological knowledge increases, more recently characterized cytokines are being tested for potential anti-tumor efficacy. IL-15, for example, elicits many of the beneficial effects of IL-2, but also promotes the formation of immunological memory and, unlike IL-2, does not preferentially induce the proliferation of T-regs (62).

While cytokine treatments have demonstrated modest clinical benefits, their successful usage has been largely limited by extreme toxicities including capillary leakage syndrome, fever, malaise, hypotension, renal dysfunction, hepatic dysfunction, and death (61, 63). For example, high dose IL-2 infusion is limited to a two-week regimen, and lower doses, while less toxic are less efficacious (61). Additionally, IL-12 has demonstrated dramatic anti-tumor effects in mouse models, but when tested clinically, systemic administration of this cytokine was stopped abruptly due to severe

toxicities (64). In addition to their toxic effects, direct T-cell-stimulatory methods such as cytokine treatment may be naturally limited by inducing the surface expression of immunoinhibitory checkpoints such as CTLA-4 and PD-1, which serve as the “brakes” of the immune system by priming the TIL for inactivation and limiting the effectiveness of immunostimulatory therapy.

Immunoinhibitory checkpoint blockade

Further insights into the primary regulatory role of inhibitory checkpoints led to their suggestion as a target for therapy. This alternative approach would “remove the brakes” of the immune system to activate T-cells rather than directly stimulating them with cytokines. In the late 1990s and early 2000s, a fully humanized anti-CTLA-4 antibody (Ipilimumab) entered clinical trials, and for the next decade, anti-CTLA-4 demonstrated efficacy in several cancer types, including melanoma (65-67), renal cell carcinoma (68), prostate cancer (69), urothelial carcinoma (70) and ovarian cancer (71). The efficacy observed with anti-CTLA-4 therapy lead to its eventual approval by the food and drug administration (FDA) for clinical use in 2011. Similarly and not far behind, PD-1/PD-L1 antagonism was tested in several clinical trials for the treatment of melanoma, renal cell carcinoma, non-small cell lung cancer (72), and bladder cancer (73), which lead to FDA approval of two humanized anti-PD-1 antibodies, pembroluzimab and nivolumab, at the end of 2014. While immune checkpoint blockade has significantly improved the treatment of cancers such as advanced metastatic melanoma, only a minority of treated patients actually responds to anti-PDL1 or anti-CTLA-4 antibodies alone; however, the durability of the response is often impressive with patients surviving years or even decades after treatment (74).

Toxicity of checkpoint blockade

In spite of these successes, inhibitory checkpoint blockade treatments have been associated with systemic autoimmune side effects that result from blocking important peripheral tolerance mechanisms. These side effects, termed autoimmune related adverse events (irAEs), are common and are caused most often by the infiltration of highly activated CD4 and CD8-T cells and the production of inflammatory cytokines in normal tissues. The side effects are not surprising given preclinical studies demonstrating that CTLA-4-deficient mice die early after birth due to lympho-proliferative disease and autoimmunity (75, 76), and blockade studies using antibodies have demonstrated the development of diabetes, demyelinating lesions, encephalomyelitis and colitis (77-79). In humans, the most common irAEs in response to ant-CTLA-4 therapy affect the GI tract, liver, skin and endocrine system (80) and affect ~60% of patients. Severe Grade 3 (requiring hospitalization) to Grade 5 (mortality) toxicities appear in 15-20% of patients (81, 82), which makes the likelihood of a patient developing a severe irAE in response to the drug at least as common as the patient responding favorably to the therapy (83). Blockade of PD-1/PD-L1 seems to result in a somewhat more favorable toxicity profile than CTLA-4 blockade. This may be explained by PD-1/PD-L1 acting more peripherally at the tumor site, while CTLA-4 acts more centrally in lymphoid organs (84). Adverse events in response to anti-PD-1/PD-L1, like anti-CTLA-4, are immune related, and include fatigue, decreased appetite, diarrhea, nausea, dyspnea, vomiting, rash, pyrexia, and headache (85), and severe adverse events occur in about 14% of patients receiving the anti-PD-1 antibody nivolumab (81). Unfortunately, the severity of the adverse events associated with checkpoint blockade seems to correlate with efficacy, as patients who experience higher-grade irAEs are more likely to show a therapeutic response, and higher doses of checkpoint inhibitors

have been demonstrated to increase both therapeutic response rates and severe irAE incidence (81, 86). This correlation makes intuitive sense, as the same immunostimulatory mechanisms of action responsible for the therapeutic benefit are also the cause of the adverse events. While irAEs are often successfully managed by administration of systemic corticosteroids (81), they have indeed restricted checkpoint blockade administration to doses that are therapeutically suboptimal: in a phase II dose-escalation study including 217 patients (86), ipilimumab was administered at 0.3, 3, or 10mg/kg doses, and while a significantly greater response rate was observed for the 10mg/kg dose, the percentage of patients with serious adverse events at this level was more than triple the 3mg/kg dose. The current FDA-approved dose of ipilimumab (and nivolumab) is 3mg/kg, reflecting the decision to avoid adverse events at the cost of potentially greater therapeutic benefit.

Combinatorial immunotherapy

Recently researchers have begun the clinical investigation of concomitantly blocking both CTLA-4 and PD1/PD-L1. This combinatorial approach is attractive because these receptors signal through non-redundant pathways, and often the activation resulting from CTLA-4 blockade can induce the expression of both PD-1 and PD-L1 in the tumor (74). In a recent phase II trial with 142 patients with metastatic melanoma (82), the efficacy of ipilimumab alone was compared to the combination of ipilimumab and nivolumab. The researchers reported an objective response rate of 61% in patients given the combination, which included a 22% complete response rate. These results were significantly greater than the objective response rate of 11% in patients given ipilimumab plus placebo (and no complete responses). While certainly an exciting improvement in efficacy, the combination also more than doubled the occurrence of

severe adverse events (grade 3 or higher), including 54% for the combination and 24% for ipilimumab plus placebo, illustrating again the correlation between efficacy and toxicity.

Intuitively, the optimal immune-stimulatory approach would include both blocking immunoinhibitory mechanisms while simultaneously stimulating directly with stimulatory molecules. This could be likened to both stepping on the gas and releasing the brakes at the same time. This combinatorial approach of administering a “positive” direct stimulatory signal such as IL-15 with a “negative” blocking signal to abrogate the resultant immune inhibitory signals has been illustrated preclinically. In metastatic colon cancer (87) and prostate (88) tumor models, Yu and colleagues treated mice with either IL-15 or antibody blockade of CTLA-4 and PD-L1 versus combinatorial treatment with both IL-15 and antibody blockade. IL-15 treatment alone, while slightly reducing tumor burden, led to upregulation of PD-1 on $CD8^+$ T-cells and increased secretion of IL-10, limiting efficacy; however when administered in combination with the antibodies, IL-10 secretion was reduced, and CTL-mediated killing and IFNγ secretion were increased leading to a greater anti-tumor response and rate of survival. While proof of principle has been established, this combinatorial method has received surprisingly little clinical investigation. As observed when anti-CTLA-4 was combined with anti-PD-1 (82), the synergistic efficacy of cytokine and checkpoint blockade combination therapy may likely be accompanied with synergistic immune-related toxic effects, as both are the result of an accelerated immune system. Therefore, successful clinical application of this combinatorial approach may not be realized until the potential toxicities are addressed. One approach that would limit the potential systemic toxicity would be the delivery of stimulatory molecules specifically to the diseased tumor microenvironment. This would avoid the inflammatory off-target effects that are responsible for the majority of irAEs.

This approach would require a suitable vector that is able to target the tumor tissue and deliver the therapeutic molecules. In this dissertation the case will be made that bacteria, specifically attenuated Gram-negative, facultative anaerobic strains such as *Salmonella* are promising candidates for this task.

BACTERIA AS A CANCER THERAPY

History

Long before the advent of modern immunotherapy, bacteria have been used to stimulate an anti-tumor response. The potential of bacteria for cancer therapy may have been partly realized as early as 1813, when it was reported that cancer patients who developed gangrenous *Clostridium* infections seemed to have tumor regression (89). Subsequently, the German physician W. Busch performed the first intentional bacterial cancer treatment in 1868, before bacteria were even known to cause disease. Busch cauterized a female patient's neck tumor and placed the woman in a bed previously occupied by a patient suffering from "erysipelas," a *Streptococcus pyogenes* infection. The patient became infected, and rapid tumor clearance occurred. Unfortunately the patient died 9 days later due to the infection (90). In the subsequent decades, many physicians tried to improve this therapy using different bacteria or bacterial components. The most notable was William Coley, who injected cancer patients with a combination of heat-killed *Streptococcus pyogenes* and *Serratia marcescens*, termed "Coley's Toxins." (91). Despite successes, the strong inflammatory side effects of the treatment caused by the immune system reacting to the toxins were difficult to control at the time. Additionally, the growing popularity of surgery, radiation and chemotherapy in the 20th century challenged the continued use of Coley's Toxins. The proponents of these newer therapies refused the use of Coley's Toxins, and the FDA eventually retracted the use of

the toxins in 1962 (92). Interestingly, a study in 2003 performed by Hoption Cann *et al* using data from the Surveillance Epidemiology End Result Cancer Registry examined the 10-year survival rates of patients treated with modern conventional external cancer therapies and those introduced by Coley (93). The study reported that despite the billions of dollars spent developing modern conventional therapies, patients treated with these therapies have not fared better than those treated with the therapy started by Coley over 100 years ago, which prompted the authors to ask, “Where would cancer treatment be today if equivalent effort and funds has been used to develop a better understanding of the treatment pioneered by Coley?”

Tumor-targeting propensity of Salmonella

Interest in bacterial cancer therapy has recently resurged due to a better understanding of both bacteria and the mammalian immune system. Preclinical reports describing bacterial anticancer therapies have increased exponentially in the last decade (94), particularly those reporting the use of Gram-negative facultative anaerobic strains such as *Salmonella enterica* and *Escherichia coli* (*E. coli*). Attenuated *Salmonella enterica* Subs. *enterica* serovar: Typhimurium (*S.* Typhimurium) has several characteristics that make it suitable for cancer therapy. Perhaps the most appealing is the propensity of the bacterium to preferentially accumulate in tumor tissue with ratios of over 1000/1 compared to tissues high in reticuloendothelial cells such as the liver and spleen. This ratio is even higher when compared to other organs (94). This phenomenon is likely due to a number of causes including: entrapment of *S.* Typhimurium in the chaotic vasculature of tumors; flooding into tumors following inflammation (95); chemotaxis toward compounds produced by tumors (96, 97); preferential growth in the hypoxic nutrient rich tumor-microenvironment (96, 98); and protection from surveillance

of the immune system (99). It is generally considered that the tumor-targeting is more of a passive selection rather than an active trafficking in which the attenuation inhibits the bacteria's ability to avoid immune-mediated clearance unless they are in the immune privileged site of the tumor, wherein they thrive in the hypoxic environment with little competition for nutrients as they feed on sloughed dead cells and necrotic tissue (90).

Natural cytotoxicity of Salmonella

Another beneficial characteristic of bacteria such as *S.* Typhimurium for cancer therapy is the natural cytotoxicity caused by the organisms. This toxicity by itself has been sufficient to cause tumor regression in many cancer models, and is described to be the result of immune stimulation, competition for nutrients and/or the direct induction of apoptosis of tumor cells by bacterial toxins (90, 99). Since many bacterial strains will accumulate in tumor tissue, these effects are largely contained within the local tumor microenvironment. Therapeutic success due to the natural immune stimulatory effect of bacteria has been demonstrated historically with Coley's Toxins and more recently with live, attenuated strains of *Clostridium* and *Salmonella* (94). Additionally, the use of an attenuated strain of *Mycobacterium bovis* called Bacille Calmette-Guérin, originally developed as a vaccine strain against tuberculosis, is routinely used in clinics to successfully treat bladder cancer, although its mechanism of action is unclear (90).

Genetic manipulability of Salmonella, delivery of therapeutic agents

Finally, increased microbiological understanding and advances in molecular biology and recombinant technology have allowed researchers to genetically manipulate bacteria to improve its usefulness as a cancer therapy. Researchers have engineered several attenuated strains of *S.* Typhimurium to remove its virulence while maintaining

its tumor-targeting propensity. Additionally, *S.* Typhimurium can be engineered as a delivery system to actively express and secrete therapeutic proteins within the TME. Tumor vasculature, compared with normal tissue, is chaotic with large intercapillary distances; this impedes the delivery of conventional therapeutic molecules deep into tumor tissue (100). *S.* Typhimurium as a delivery vehicle enables intratumoral targeting of therapeutic agents. Through flagellar motility, *S.* Typhimurium can actively swim away from tumor vasculature and penetrate more deeply into tumor tissue than passive therapeutic molecules (94, 101), and preferential accumulation of the bacteria in tumor tissue allows for tumor-targeted delivery and prevention of systemic side effects associated with many therapeutic molecules. Using this approach, bacteria have been utilized pre-clinically for the tumor-specific delivery of cytotoxic agents such as: cytolysin A, Fas ligand, tumor necrosis factor alpha (TNFα) and TRAIL and immunostimulatory cytokines and chemokines such as: interleukin 2 (IL-2), interleukin-18 (IL-18), LIGHT, and CCL21 (94). Additionally, *S.* Typhimurium has been engineered to express prodrug-converting enzymes in tumor tissue and to transfer genetic material for expression in mammalian cells such as plasmids containing genes for cytotoxic and anti-angiogenic agents, cytokines and growth factors, tumor antigens, and gene-silencing shRNA (94).

Preclinical successes of* Salmonella-*based cancer therapy

The antitumor efficacy and tumor-targeting propensity of *S.* Typhimurium has been demonstrated in several transplantation mouse models of subcutaneous, orthotopic and metastatic tumors. These include, but are not limited to: breast cancer, colon cancer, hepatocellular carcinoma, melanoma, neuroblastoma, pancreatic cancer, prostate cancer, osteosarcoma and spinal cord glioma (for review see (94)). Researchers have reported reproducibly high tumor colonization numbers of 1×10^7 to

1×10^9 colony-forming units (cfu) per gram (g) of tumor tissue when bacteria are injected intravenously (IV) and have demonstrated partial or complete regression of transplanted tumors along with increases in survival time of treated tumor-bearing mice. In these preclinical studies, several different attenuated strains of *S.* Typhimurium were used including: A1-R, auxotrophic for leucine and arginine (102); SL7207 and related strains, auxotrophic for aromatic amino acids (95, 103, 104); χ4550, attenuated by knockout of cyclic adenosine monophosphate signaling (105), and perhaps the most widely used strain VNP20009, which, among many other mutations, lacks lipopolysaccharide (LPS) and is auxotrophic for purines (106).

Failure of Salmonella *to consistently colonize human tumors*

The promising preclinical efficacy reported has led to three clinical trials in which *S.* Typhimurium was administered IV to cancer patients (107-109). In each trial, the attenuated vaccine strain VNP20009 (Δ*msb*, Δ*purI*) was used. The results of these trials were largely disappointing and have since been attributed to poor tumor colonization; of a combined 32 patients, only six were found to contain the bacterium in the tumors, indicating a problem with tumor-targeting in clinical disease. The failure to colonize has since been attributed by some to be the result of an over-attenuation of the strain due to its (LPS) deficiency (90). The *msb* knockout strain is unable to synthesize lipid A, the base structure of LPS. This attenuating mutation greatly diminishes the TNFα response to infection in humans, which reduces the virulence and toxicity of the strain. However, this TNFα response may be important for tumor colonization by increasing permeability of tumor vasculature, which leads to a Lipid A-dependent blood influx that carries the bacteria into the tumor. This hemorrhage then leads to the development of a large necrotic core where the bacteria localize and proliferate (95). In support of this

hypothesis, Yu and colleagues demonstrated that depleting TNFα caused a reduction in hemorrhage and a delay in tumor colonization in mice (95). Therefore, using attenuated *Salmonella* strains that are Lipid A^+ may rescue tumor colonization in humans. Alternatively, it was recently demonstrated that co-administration of purified Lipid A with VNP20009 reduced the variability of colonization and led to more thorough penetration throughout the tumor tissue (110).

TRANSPLANT VERSUS AUTOCHTHONOUS TUMOR MODELS

Clinical relevance of transplant versus autochthonous tumor models

The failure to consistently target human tumors in the VNP20009 trials was somewhat surprising, particularly in light of the extensive preclinical demonstrations of successful tumor-targeting by this strain in several mouse models. This discrepancy may be due to the artificiality of the tumor models that have been used to demonstrate the tumor-targeting propensity of *S.* Typhimurium strains. Virtually all preclinical reports of tumor-targeting *Salmonella* strains have based conclusions on experiments performed in "transplant" cancer models. In these models, a suspension of cells from cancer cell lines or actual pieces of human or mouse tumors are transplanted into a particular organ in the mouse, or more commonly, into the subcutaneous compartment. These experiments are most often performed in immunocompetent mice that develop subcutaneous tumors after injection of a syngeneic mouse tumor cell line. While these models offer more experimental control and may reduce variability, they do not accurately mimic the complexities of the natural tumor development that is encountered in human disease. In contrast to transplant tumors, "autochthonous" tumors that have developed from a single cell are a more accurate representation of human cancer. In autochthonous models, tumor development is typically driven by transgenic oncogene expression in certain

organs or by a topical application of a mutagen such as 3-methylcholanthrene, which causes mutations that drive tumorigenesis.

Important differences between transplant and autochthonous tumor models

The differences between transplant and autochthonous tumor models are extensive and may help explain the discrepancy between successful targeting of tumors in transplant mouse models and unsuccessful targeting of human tumors. First, vasculature development and maturity in autochthonous tumors differs significantly from that observed in transplanted tumors (111). In autochthonous tumor development, tumor angiogenesis occurs in organs over a long period of time while tumor cells are transforming and cell populations are evolving (111). During this time tumor cells may also be coopting normal vessels for their blood supply (112). In contrast, transplanted tumor vasculature develops rapidly and is induced throughout its development by fully transformed tumor cells. Tumor vasculature that results from these differences differs significantly in morphology and maturity. Autochthonous tumors will often contain more mature vasculature that is characterized by a high degree of pericyte coverage, a sign of vessel maturity. In contrast, the vasculature of transplant tumors contains less pericyte coverage and is primarily neovasculature (111). The differences in vasculature maturity between autochthonous and transplanted tumors has led to differences in responses to therapeutic agents such as IL-12 (111), anti-angiogenic agents (113, 114) and vasculature disrupting agents (115). Similarly, differences in tumor vasculature maturity may vitally affect hemorrhage-dependent bacterial tumor colonization described by Leschner and colleagues (95), as less mature vasculature of transplant tumors may more readily permeabilize and hemorrhage in response to bacterial treatment than the more mature vasculature of autochthonous tumors.

Second, transplant tumors will often differ from autochthonous tumors in the extent of necrosis they contain. When cancer cell lines are inoculated into the subcutaneous environment, the majority of the transplanted cells die, leading to an early artificial necrosis and an acute inflammatory response surrounded by a thin rim of viable tumor cells. This necrotic artifact often remains for about 2 weeks, at which point most transplanted tumors are about 1 cm in diameter (116). Autochthonous tumors, having developed from a single cell over a longer period of time, do not contain this necrotic artifact. Additionally, necrosis in transplanted tumors can be caused by the less mature, more chaotic vasculature preventing adequate oxygen diffusion throughout the rapidly growing inoculated tumor (117). Human tumors and autochthonous tumor models, having developed over longer periods of time with coincident development of vasculature may be less consistently necrotic. The presence of necrosis is likely important for effective and lasting colonization of tumors, as the majority of colonizing bacteria in mouse models are found in necrotic tumor regions (118). However, the degree of colonization in tumor tissue may not be determined by pre-existence of necrosis alone, as colonization has been observed in less necrotic tumors (118). Additionally, the hemorrhage of immature blood vessels in transplant tumors initially caused in response to *S.* Typhimurium may induce the formation of habitable necrotic areas, in which case necrosis would be the result of tumor colonization rather than the cause; this hemorrhagic necrosis might be prevented in the more mature, less hemorrhage-prone vasculature of autochthonous tumors.

Third, immunological differences may affect bacterial tumor-targeting. Immune-mediated clearance of bacteria from tumors may be a limiting factor in colonization (118). Unlike in autochthonous tumors, the process of immunoediting (discussed in the “Tumor Immunology” section) that shapes the immune microenvironment of human

tumors is largely absent in transplant tumor models. Rather, the immune response against tumors in transplant models is largely shaped by the transplant itself, including the initial inflammatory response against the inoculation wound and the death of the majority of the transplanted cells. Since transplant recipient mice will typically only live for a few weeks post tumor inoculation, it is difficult to separate this acute inflammatory response from an anti-tumor immune response that would appear in an established tumor microenvironment (119). These differences in tumor immunology have led to experimental differences in immunosurveillance and therapeutic immune responses between autochthonous and transplanted tumors of identical origin (120), and may indeed lead to differences in functional draining lymphatics and populations of phagocytic cells that would play a role in the clearance of bacteria from tumor tissue.

CONCLUSION AND HYPOTHESIS

Immunotherapies have demonstrated exciting potential in the treatment of cancer. Theoretically, the immune memory generated during a proper anti-tumor immune response would not only remove systemic metastases but would also prevent relapse of disease. This is illustrated by the relatively longer disease-free survival of many responders to successful immunotherapy compared to conventional therapies, particularly when more than one immunotherapeutic agent is used in combination. However, immunotherapies such as cytokine administration and/or immune checkpoint blockade strategies are limited in their administration by systemic immune-related adverse side effects, and these irAEs are compounded when multiple agents are used simultaneously. One approach to avoid these toxicities is to deliver the therapeutic molecules specifically to the TME in order to avoid their systemic inflammatory effects. In this thesis, the applicability of *S.* Typhimurium for such a role is investigated. Attenuated

S. Typhimurium will be assessed initially for its ability to express and secrete functional cytokines and antagonistic single chain antibodies against CTLA-4 and PD-L1. Secondly the native anti-tumor efficacy and tumor-targeting propensity of *S.* Typhimurium will be investigated in multiple models including both transplanted and autochthonous tumors. The overall hypothesis for this thesis is stated as: Recombinant attenuated *Salmonella enterica* Typhimurium is a promising tumor-targeting immunotherapy vector.

CHAPTER 2

EXPRESSION AND SECRETION OF FUNCTIONAL IMMUNOMODULATORY PROTEINS IN ATTENUATED *SALMONELLA ENTERICA* TYPHIMURIUM

Authorship Note: Jeremy Drees performed all experimental work in this chapter alone or with assistance from colleagues with the following exceptions: the surface plasmon resonance measurements to measure affinity (Table 2-1) were performed by LakePharma (Belmont, CA); the colonization and growth curve experiments (Figure 2-10A and B) and protein preparation and western blots (Figure 2-11B) were performed by Michael Mertensotto (Research Scientist U of MN Dept. Surgery).

INTRODUCTION

The ability to genetically engineer *Salmonella* to express recombinant proteins of interest make it appealing as a deliver system for therapeutic proteins. Our lab has experience using the attenuated *S.* Typhimurium strain χ4550 (*Δcya, Δcrp, Δasd)* to deliver a truncated human IL-2 protein to stimulate T-cells and mediate tumor regression in murine models of neuroblastoma (121), metastatic osteosarcoma (122), and

metastatic colon cancer (123-125). This bacterium, named SalpIL-2, was given orally to mice, and while efficacious, may have been limited by a truncation in the recombinant human IL-2 sequence that may have affected its bioactivity. Additionally, SalpIL-2 was not engineered to actively secrete the IL-2 molecule, making its dissemination dependent on the lysis of the bacterial cells. Improved efficacy of bacterially delivered agents may be realized if they are actively secreted into the extracellular space, where they are required for the signaling through receptors on the surface of effector cells.

As discussed, the immunoinhibitory checkpoints CTLA-4 and PD-1 are expressed on activated T-cells and are constitutively expressed by T-regulatory cells. Inhibiting the binding of these receptors to their ligands, B7.1/2 and PD-L1 respectively, would remove this auto-inhibitory mechanism making simultaneous cytokine stimulation presumably much more effective. Conventionally, these signals are blocked using antagonistic antibodies, but because antibodies are too complex for efficient expression in *Salmonella,* we propose to express the binding portion of the antibody, including the variable light (V_L) and heavy (V_H) portions of one arm of an antibody combined via a flexible peptide linker. This type of construct is termed a single chain variable fragment (scFv). scFvs can retain specificity and affinity for their antigens with the reduced complexity of a single polypeptide chain without the Fc or other constant region making them suitable for bacterial expression (126). There are a few reports that describe antagonistic anti-mouse CTLA-4 scFvs (127, 128); however, data about their biological activity or binding characteristics is lacking, and since they were cloned from monoclonal antibody (mAb) hybridomas, there is no surety of their expression in a bacterial host. Additionally, there are no antagonistic anti-mouse PD-L1 scFv sequences to our knowledge.

Typically, scFvs are cloned from the variable regions of existing high-affinity B-cell hybridomas, which often results in scFvs that are unstable, of low affinity, or fold incorrectly due to the absence of stabilizing constant regions. These limitations have restricted their use as blocking agents (129). Selection for scFvs by phage display can overcome some of these limitations but is most often performed on suboptimal variable region libraries from naïve mammalian hosts, preventing the isolation of high-affinity scFvs (130). Alternative hosts, such as chickens, have been shown recently to be more effective for scFv development (130). The avian germline sequences encoding Ig variable regions are well suited for scFv library development. Consisting of a single set of V_H and V_L regions, the entire Ig repertoire can be easily captured via PCR (131). Additionally, scFvs generated from chicken variable-region libraries typically have higher affinities due to the greater immune response to mammalian proteins generated in a non-mammalian host. Other advantages include greater inherent stability of polypeptides generated from chicken variable regions (130) and the reported successes of multi-antigen immunizations (132-134). For these reasons, we constructed an immunized chicken scFv library and used phage display to successfully isolate biologically active antagonistic scFvs against mouse PD-L1 and CTLA-4 that are readily expressed and secreted as soluble protein from *Salmonella*.

In this chapter, the hypothesis that *Salmonella* can be engineered to successfully express and secrete immunotherapeutic proteins is explored by describing the development of recombinant *Salmonella* strains that secrete biologically active antagonistic scFvs against CTLA-4 and PD-L1. The aim is to ultimately use these strains in combination with strains that secrete immunostimulatory cytokines such as IL-2 and IL15 for the delivery of combinatorial immunotherapy to the tumor microenvironment.

METHODS

Development and characterization of scFvs

Chicken immunizations and IgY purification

Immunizations were based on a protocol developed by Finlay et al (135), and were performed at Aves Labs (Oregon). Three female chickens of egg-laying age were immunized intramuscularly with purified recombinant mouse CTLA-4 and PD-L1 (Sino Biological). The immunization regime included four intramuscular injections three weeks apart: 1) 50 µg of each protein emulsified in complete Freund's adjuvant; 2) 50 µg of each protein in incomplete Freund's adjuvant; 3 and 4) 25 µg of each protein in incomplete Freund's adjuvant. Eggs were collected for 10 days before immunization and after final the immunization. IgY from egg yolk was purified at Aves Labs (Oregon).

IgY ELISA

High protein-binding 96-well plates (Costar: 3590) were coated with 1.25 µg/ml recombinant PD-L1 (Sino biological: 50010-M08H) in 0.1 M sodium carbonate pH 9.5 overnight at 4ºC. Plates were washed three times in PBS + 0.1% Tween-20. Plates were blocked using 5% milk for two hours at room temperature and washed as before. Varying dilutions of IgY from each chicken were added to plates and incubated for 90 minutes at room temperature. Plates were washed, and bound IgY was detected using an anti-IgY-HRP conjugate (Aves Labs: H-1004) diluted 1:5000 in 5% milk for 90 minutes at room temperature followed by washing and detection with OptEIA substrate (BD: 555214) for 30 minutes according to manufacturers' protocol. Absorbance at 450 nm was corrected for background by subtracting absorbance at 570 nm.

RNA isolation and cDNA generation

Chickens were sacrificed and their spleens were frozen in RNAlater (Qiagen). Total RNA was isolated from 200 mg of each spleen using an RNeasy Midi Kit (Qiagen) according to manufacturers' instructions. cDNA was generated from total RNA using SuperScript^{TM} 1st Strand Synthesis System for RT-PCR (Life Technologies) with random hexamers according to manufacturers' instructions.

PCR synthesis of scFv library

Library synthesis was performed according to methods published by Finlay *et al* (135), including PCR primers and temperature parameters. Briefly, V_L and V_H libraries were amplified from cDNA from each chicken using PCR primers flanking the variable regions. PCR reactions were repeated 10 times with new cDNA to in order to retain as much library diversity as possible. Resulting DNA fragments were purified from an agarose gel using a Qiaquick Gel Extraction Kit (Qiagen) and pooled for each chicken. Individual V_L and V_H region libraries were randomly combined with the addition of a flexible peptide linker using splice overlap extension PCR with defined primers (135), and 4 µg of gel-purified scFv DNA from each chicken was combined to generate the final scFv library.

Ligation and transformation of TG1 cells for phage display

The scFv library was ligated into pComb3x phagemid vector (from Dr. Barbas, Scripps Research Inst.). Before ligation, 40 µg of pComb3x vector and 10 µg of the combined scFv library were digested with Sfi1 in a 200 µl final reaction volume (New England Biolabs) according to manufacturers' instructions for 8 hours at 50ºC. Digested fragments were separated by gel electrophoresis and extracted from agarose using a Gel Extraction Kit (Qiagen). The pComb3x vector was treated with Antarctic

phosphatase (New England Biolabs: M0289S) to prevent self-ligation according to manufacturers' instructions. Phosphatase was removed before ligation using a PCR cleanup Kit (Qiagen). The pComb3x vector and scFv library were ligated with T4 DNA ligase (New England Biolabs) using 1.5 µg of vector and 1 µg scFv library for a 1:3 vector to insert molar ratio in 200 µl total reaction volume for 16 hours at 16ºC. Following ligation, the DNA library was freed of enzyme and ligation buffer using a PCR Cleanup Kit and eluted in 40 µl sterile deionized water. The entire ligation was added to 300 µl of electrocompetent *E. coli* TG1 cells (Agilent Technologies), and cells were electroporated according to manufacturers' instructions, rescued in 5 ml of pre-warmed S.O.C. medium, and the entire transformation plated on 2x yeast-tryptone agar containing 100 µg/ml carbenicillin in a 22x22 cm Qtray (Genetix) and incubated overnight at 37ºC. A 100 µl aliquot of the transformation was serially diluted and plated for counting to determine the theoretical library diversity. After incubation, colonies were scraped from Qtrays in 20 ml 2x yeast-tryptone broth + 15% glycerol and stored in aliquots at -80^{o}C for phage display and panning.

Phage display and panning for binding sequences

Phage display and binding screens were performed according to methods published by Finlay et al (135). Briefly, the *E. coli* TG1 cells containing the scFv library were infected with M13K07 helper phage (New England Biolabs). Infected cultures were grown overnight and phage displaying the scFvs were precipitated and allowed to bind immobilized PD-L1 (Sino Biological: 50010-M08H). Unbound phage were removed by washing 10 times with PBS-0.1% Tween-20 and 10 times with PBS. Antigen-bound phage were eluted with 0.1 M glycine pH 2.2 and used to infect *E. coli* strain ER2738 (Agilent Technologies), which were spread onto QTrays containing 50 µg/ml

carbenicillin. The selection and re-infection procedure was repeated for four total rounds. An aliquot of input and output phage was titered for each panning round to monitor enrichment of binding sequences.

ELISA screen for binding sequences

Several colonies from the output of round 4 of panning were tested for antigen binding. Colonies were inoculated into individual wells of a 96-deepwell plate (Eppendorf: 951033502) containing 1ml of 2x YT medium containing 100 µg/ml carbenicillin and induced with 0.02 mM IPTG at log phase. Induced cultures were grown overnight, and the periplasmic protein was extracted via osmotic shock in 100 µl of sterile, ice-cold H_2O. High protein-binding 96-well plates (Costar: 3590) were coated with 1.25 µg/ml recombinant PD-L1 or CTLA-4 (Sino Biological) in 0.1 M sodium carbonate pH 9.5 overnight at 4ºC. Plates were washed four times in PBS + 0.1% Tween-20 and blocked using 200 µl 5% milk for two hours at room temperature. Periplasmic protein containing scFvs (50 µl) was mixed with 50 µl of 10% skim milk, added to plate-bound antigen, and incubated for two hours at room temperature. Plates were washed and bound scFv was detected using 0.5 µg/ml anti-*hemagglutinin* tag/HRP conjugate (GenScript: A00169) in 5% milk, followed by incubation with OptEIA substrate (BD: 555214) for 30 min according to manufacturers' protocol. The top five binding scFvs were sequenced and Top 10F' *E. coli* cells (Life Technologies: C3030-03) were transformed for subsequent protein expression and characterization.

Expression, purification and detection of scFv

E. coli Top10F' cells harboring phagemid with the selected scFv sequences (αPD-L1 scFv) were grown in 250 ml 2x YT medium, induced at log phase with IPTG at

a final concentration of 1 mM and incubated at 37° C overnight at 250 RPM. Cultures were pelleted at 4000×g for 15 minutes and resuspended in 30 ml of 20% sucrose, 50 mM Tris-HCl, 1 mM EDTA and incubated with mild shaking for 15 minutes at room temperature. Bacteria were at pelleted at 4°C and resuspended in 6 ml ice-cold sterile H_2O to release the periplasmic fraction via osmotic shock. scFvs were purified from total periplasmic protein using 100 µl of His-Tag Isolation & Pulldown beads per 1 ml of periplasmic protein (Life Technologies: 10103D) according to manufacturers' instructions. Purified protein was then desalted twice in PBS using Amicon® Ultra 0.5 ml 10K centrifugal filters (Millipore: UFC501008) and quantified using a BCA protein assay (Pierce®) for subsequent experiments.

Protein was isolated from culture media after 0.22 µm filtration to remove all cells and TCA precipitation (10% TCA in acetone) on ice for 2 hours. Precipitated protein was pelleted at 10,000 RCF for 30 minutes and dissolved in SDS sample buffer (Boston Bioproducts) for gel analysis.

For detection of scFvs, protein was denatured in SDS sample buffer and separated on 10-20% gradient polyacrylamide gels. Proteins were detected using either Coomassie stain (GelCode Blue, Thermo Scientific) or transferred to a PVDF membrane and detected with anti-hemagglutinin-HRP conjugate (GenScript: A00169).

Affinity mearsurements by surface plasmon resonance (SPR)

To measure binding kinetics, SPR was performed at LakePharma using an Octet QKe system (ForteBio). Anti-hFc kinetic grade biosensors (ForteBio: 18-5060) were hydrated in sample diluent (0.1% BSA in PBS and 0.02% Tween 20) and preconditioned in 10mM glycine pH 1.7. Mouse PD-L1 human Fc fusion protein (R&D systems: 1019-B7) was reconstituted at 100 µg/mL in PBS and was further diluted to 10 µg/mL with

sample diluent for loading. The PD-L1-Fc solution was immobilized onto anti-hFc biosensors for 120 seconds. After the baseline was established for 120 seconds in sample diluent, the biosensors were moved to wells containing either αPD-L1 scFv or one of three monoclonal anti-mouse PD-L1 antibodies: 10F9G2 (Biolegend: 12403), 1-111a (eBioscience: 14-9971) or MIH5 (eBioscience: 14-5982) at a series of concentrations to measure the association. Association was observed for 120 seconds and dissociation was observed for 300 seconds for each protein of interest in the sample diluent. The K_{on} and K_{off} rates were measured by fitting of kinetics sensorgrams to a monovalent binding model using Octet software on global fitting (1:1 binding). K_D was calculated for each protein of interest by the K_{off}/K_{on} ratio.

αPD-L1 scFv T-cell stimulation assay

M450 tosylactivated beads (Life Technologies: 140.13) were coated with 3 µg anti-CD3 antibody (BioLegend: clone 17A2) and 2 µg mouse PD-L1-Fc chimera (R&D Systems: 1019-B7) according to manufacturers instructions. Control beads were coated with 3 µg of anti-CD3 and 2 µg human Fc control protein (Abcam: 90285). Anti-CD3/PD-L1-coated beads were then blocked with varying concentrations of either αPD-L1 scFv, an antagonistic anti-PD-L1 positive control mAb (clone 10F.9G2), or Fc protein as a negative control, for 2 hours at 37^{o} C. Primary T-cells were purified from murine splenocytes using T-cell purification columns (R&D Systems: MTCC-10) and incubated at a 1:1 bead:cell ratio with coated/blocked beads for 4 days in RPMI medium (Gibco) containing 10% fetal bovine serum, 2mM l-glutamine and 2µg/mL B7.1-Fc protein (R&D Systems: 740-B1) at 37^{o}C in 5% CO_2. Following incubation, culture supernatant was tested for IL-2 secretion using an ELISA (BD OptEIA^{TM} Mouse IL-2 ELISA Set) according to manufacturers' instructions.

Anti-CTLA-4 scFv antagonistic binding assay

96-well plates (Costar® 3590) were coated with recombinant mouse CTLA-4 (Sino Biological) at 1.25 µg/mL and incubated overnight. Plates were washed 3x in PBS+0.1%Tween-20 and blocked for 90 minutes at room temperature with 5% milk. Recombinant hB7.1-Fc fusion protein (Sino Biological) was added to plates at a concentration of 1.25 µg/mL along with varying concentrations of either anti-CTLA-4 mAb (clone: 63828, R&D Systems), anti-CTLA-4 scFv or a negative control (anti-PD-L1) scFv and incubated at room temperature for 120 minutes. After washing, bound hB7.1-Fc fusion protein was detected with anti-human Fc-HRP antibody (Millipore) diluted 1:50,000 in 5% milk followed by incubation with BD OptEIA™ TMB substrate according to manufacturer's instructions.

In vivo survivability experiments

Female BALB/c mice of 10-12 weeks of age were injected IV with the indicated *S.* Typhimurium strain. Mice were euthanized 21 days post-*S.* Typhimurium administration. Indicated tissues were harvested and minced with sterile razor blades to about 1 mm diameter pieces. Minced tissues were then homogenized in 3 ml of sterile PBS using gentleMACS M Tubes (Miltenyi Biotec) with a gentleMACS Tissue Dissociator (program RNA_01). The homogenates were serially diluted in sterile PBS, plated on LB agar, and incubated for 16-18 hours at 37°C for CFU enumeration.

For tumor survivability studies, 4T1 breast cancer cells (ATCC #CRL-2539) were grown in RPMI-1640 medium containing 10% fetal bovine serum. Cells were detached from flasks using 0.05% trypsin-EDTA, counted with a hemocytometer, washed with sterile PBS, and diluted to the appropriate concentration prior to injection. Mice were

given a subcutaneous injection of 1×10^5 4T1 cells in 50 µL of sterile PBS superficial to the right inguinal mammary fat pad. 11 days post-tumor inoculation, mice were similarly injected with the indicated strain, and tumor tissue was harvested, homogenized, and plated as were other tissue samples.

Salmonella *strains and expression systems*

Attenuated Salmonella *strains*

Attenuated *S.* Typhimurium strain χ4550 (*Δcya, Δcrp, Δasd)* was a gift from Roy Curtiss III (Arizona State University). χ4550 is deficient in aspartate semialdehyde dehydrogenase (*asd*), which allows for plasmid maintenance by encoding *asd* on its expression plasmid. Attenuated *S.* Typhimurium strain SL3261 (Δ*aroA*, Δ*hisG*) was obtained from the *Salmonella* Genetic Stock Centre (SGSC #439). The strain "SalpNG" was constructed by transforming χ4550 with pNG, a plasmid containing cDNA coding for the *asd* gene to complement the χ4550 requirement for diaminopimelic acid. To construct plasmid pNG, plasmid pYA292 (136) was cut with EcoRI and HindIII, the ends filled in, and the plasmid recircularized to eliminate the LacZ(alpha) coding sequence. SL3262 (Δ*aroA*, Δ*hisG, Δasd*) was generated by knocking out the *asd* gene from SL3261 using the phage λ Red recombinase method (137) and two PCR primers: FWD: CGGCCTACAGAACCACACGCAGGCCCGATAAGCGCTGCAAATTGTGTAGGCTGGAGCTG and REV: CACAGGATACTGGCGCGCATACACAGCACATCTCTTTGCAGTCCATATGAATATCCTCCTTAGTTC. Transforming SL3262 with the pNG plasmid generated the strain DSpNG.

Plasmid construction, recombinant gene cloning

All bacterial plasmid construction and recombinant cDNA cloning (including scFv and cytokine cDNA sequences, secretion accessory proteins, and periplasmic chaperone proteins) were accomplished by PCR amplification of the desired sequences, insertion into the vector via blunt-end ligations, and electroporation into electrocompetent cells using standard techniques. To increase electroporation efficiency, ligations were cleaned before electroporation using a Qiagen PCR Cleanup Kit. Correct orientation of gene inserts was validated by restriction digests and agarose gel separations of DNA fragments.

RESULTS

Isolation and characterization of single chain antibodies against murine CTLA-4 and PD-L1

Immunoglobulin library development

To develop the immune library, three female chickens of laying age were immunized simultaneously with purified PD-L1 and CTLA-4 protein intramuscularly four times over a period of nine weeks. Eggs from each chicken were collected before and after the immunization, and egg yolk immunoglobulin (IgY) was purified in order to verify successful sensitization to PD-L1 and CTLA-4. Pre- and post-immune IgY were qualitatively compared for antigen specificity using an ELISA with plate-bound PD-L1 and CTLA-4. Each chicken demonstrated a robust increase in antigen specificity in response to the immunization (Figure 2-1).

Total RNA was isolated from the spleens of immunized chickens. cDNA was generated from RNA using reverse transcriptase and random hexamers. The V_H and V_L sequences were amplified from cDNA using PCR primers flanking the variable regions (Figure 2-2A). The resulting variable domain fragments were randomly combined with

the addition of a linker sequence (Figure 2-2B) generating the full-length scFvs. The resulting individual scFv libraries were combined with equal representation from each chicken and ligated into the pComb3x phagemid vector (138). Electroporation into *E. coli* TG1 cells resulted in $2.5x10^8$ colonies, which represents the theoretical library diversity of unselected scFvs. While the size of the library allows for $2.5x10^8$ different scFv sequences, the library likely consisted of replicates of high affinity scFv sequences that would have been enriched *in vivo* during clonal expansion and affinity maturation of B-cells recognizing immunogenic epitopes on PD-L1 and CTLA-4. Next, phage display was used to enrich for antigen-specific scFvs from the immunized sequence pool and to select the highest binding scFvs for further characterization.

Phage display and panning

The scFv library is contained within the pComb3x vector (Figure 2-3), which expresses scFvs as fusion proteins attached to the p3 coat protein of M13 filamentous phage. The library was rescued via infection with helper phage, which provided the accessory proteins necessary for replication in and release from infected *E. coli*. Phage precipitated from infected cultures displayed the encoded scFvs on their surface and were incubated with immobilized recombinant PD-L1 or CTLA-4 to allow binding. Rigorous washing removed unbound phage, and the bound phage were eluted, titered, amplified and used to re-infect *E. coli*. This panning procedure was repeated for a total of four rounds for each antigen. The output phage titer after the first round of selection was ~$1x10^4$ for each antigen, implying that only one in ~25,000 clones of the original immune library bound antigen strongly enough to be selected by phage display. These binding sequences were enriched in subsequent rounds of panning as output titers increased. There was not an increase in output titer from round 3 to 4, which may be

explained by reaching a maximum occupancy of available antigen in these rounds (Figure 2-4A). However, there may have been further enrichment of strongly binding scFvs during round four as they competed for antigenic “space.” The binding capabilities of several scFvs from the output of the final round of panning was tested with an ELISA against PD-L1 or CTLA-4; the majority of the selected scFvs bound their antigen in varying degrees when compared to negative controls (Figure 2-4B). The DNA sequences of the top five binding scFvs for both antigens were determined. All five PD-L1-binding scFvs shared the same sequence, which was labeled “αPD-L1 scFv.” Three of the top five CTLA-4 binding scFvs shared the same sequence, which was labeled “αCTLA-4 scFv.” These sequences have been submitted to the GenBank database under accession numbers KF041825 and KF041824, respectively.

Expression, purification and binding capability of soluble scFvs

In order to express the scFvs as mature proteins without the fused P3 peptide for further characterization, the non-suppressor *E. coli* strain Top10F’ was transformed with phagemid harboring the αPD-L1 scFv or αCTLA-4 sequence and induced for protein production. The mature scFv contains the C-terminal hemagglutinin (HA) and polyhistidine tags for detection and purification (Figure 2-3). Soluble scFv was detected in *both the periplasm and culture supernatant of transformed cells using an anti-HA-tag/HRP conjugate (Figure 2-5A).* The OmpA signal peptide directs type II sec-dependent secretion into the periplasmic space; therefore we suspect the scFv detected in the culture supernatant is due to passive leakage of the scFv across the outer membrane or cell lysis resulting in the accumulation of periplasmic proteins in the supernatant.

Soluble scFvs were purified from the periplasmic protein of recombinant Top10F' cells using cobalt-based immobilized metal affinity chromatography. ScFvs were eluted in imidazole solution and desalted using 10kD molecular weight cutoff filters. Approximately 1 mg of purified *αPD-L1 scFv was* obtained from the periplasmic protein extraction of 250 ml of culture. A high degree of purity was achieved as indicated by separation on SDS-PAGE and Coomassie blue staining (Figure 2-5B). By evaluating band intensity of protein gels, we estimated that over half of the protein was found in the periplasm and culture supernatant of recombinant bacteria (not shown). In addition to the supernatant and periplasm, each scFv was found in the cytoplasm and insoluble fraction of cell lysates. There was some difficulty in the production and purification of αCTLA-4 scFv, which hindered the subsequent purification and binding affinity characterization of the protein when produced from E. coli.

Binding affinity of αPD-L1 scFv

To address the potential of bacterially delivered αPD-L1 scFv for PD-L1 blockade, we examined the affinity of αPD-L1 scFv to its antigen using surface plasmon resonance (SPR), which can directly measure the rate of binding of antibodies to their antigens (K_{on}) and the rate at which the antibody/antigen complex dissociates (K_{off}). Affinity to antigen is often expressed as a dissociation constant (K_d), which is the molar concentration of an antibody at which half of the total available antigen is bound by the antibody, calculated as the ratio of K_{off}/K_{on}. The higher an antibody's affinity, the lower its K_d. We utilized a PD-L1-Fc chimera as the target antigen, which allowed capturing the PD-L1 antigen onto a biosensor in the correct orientation. The PD-L1-coated biosensor was immersed in an scFv-containing solution, the αPD-L1 scFv was allowed to bind the captured antigen, and the bound scFv was measured over time to give a K_{on} value.

Moving the biosensor into a buffer solution containing no scFv allowed the measurement of K_{off}. In addition to αPD-L1 scFv, three commercially available antagonistic blocking mAbs against murine PD-L1 were tested for comparison (clones 10F.9G2, MIH5 and 1-111a). The, K_{off}, K_{on} and K_d values of αPD-L1 and the mAbs are shown in Table 2-1. Due to difficulties in the expression and purification of αCTLA-4 scFv (see chapter 2 discussion), the binding affinity of this molecule was not tested.

Biological activity of αCTLA-4 and αPD-L1 scFvs

CTLA-4 when binding to its ligand B7.1 inhibits T-cell activation. Therefore a functional antagonistic scFv must inhibit CTLA-4/B7.1 binding. In order to assay for αCTLA-4 scFv blocking activity an *in vitro* competitive binding assay was used. Plates coated with purified CTLA-4 protein bound B7.1 (Figure 2-6A). However when αCTLA-4 scFv was added, CTLA-4/B7.1 binding was inhibited in a dose-dependent manner. Blocking activity was compared to the conventional αCTLA-4 mAb clone 63828 and to a αPD-L1 scFv as a negative control (Figure 2-6A).

In order to assay for blocking activity of αPD-L1 scFv, we utilized a T-cell activation assay. Activated T-cells will begin to proliferate and secrete effector molecules such as interleukin 2 (IL-2). PD-L1 attenuates T-cell activation in response to antigen by binding its receptor PD-1, expressed on T-cells during activation. This interaction inactivates T-cells, reducing effector function and IL-2 secretion. Therefore, blocking PD-1/L1 activity increases T-cell activation, indirectly stimulating proliferation and IL-2 secretion. To determine if αPD-L1 scFv has PD-1/L1 antagonistic activity, T-cells were activated in the context of PD-L1 and observed for a rescue of IL-2 secretion by the addition of αPD-L1 scFv. In order to mimic an antigen presenting or target cell, tosylactivated beads were coated with an anti-CD3 mAb. The anti-CD3 antibody binds to

the CD3 subunit of the TCR and acts as a non-specific primary signal for T-cell activation. In addition to anti-CD3, tosylactivated beads were coated with either PD-L1-Fc fusion protein, “PD-L1(+) beads,” or Fc control protein, “PD-L1(-) beads.” Primary T-cells were purified from the spleens of Balb/C mice and cultured in the presence of either PD-L1(-) beads or PD-L1(+) beads. In addition, the culture medium was supplemented with B7.1-Fc protein to facilitate co-stimulation of T-cells. In the presence of PD-L1(-) beads, T-cells expanded and produced IL-2, measured by an ELISA of the culture supernatant on day 4 of incubation (Figure 2-6B). Conversely, when cultured in the presence of PD-L1(+) beads, T-cell activation was prevented, as indicated by a reduction in IL-2 secretion. However, when PD-L1(+) beads were blocked with αPD-L1 scFv, T-cell activation was rescued, as indicated by a dose-dependent increase in IL-2 production. The T-cell stimulatory activity of αPD-L1 scFv was compared to the mAb 10F.9G2, which had shown the highest affinity to PD-L1-Fc of the antibodies tested (Table 2-1). The αPD-L1 scFv was found to be as effective as 10F.9G2 at stimulating T-cells in the context of PD-L1 (Figure 2-6B). Therefore both scFvs demonstrated antagonistic biological function against immune checkpoint receptor-ligand binding and were ready for recombinant expression in *S.* Typhimurium.

Recombinant scFv expression in* S. *Typhimurium

Attenuated Salmonella *strains and plasmid*

The attenuated strains of *S.* Typhimurium focused on in this study are χ4550 and SL3261. These strains were chosen based on previous experience with χ4550 and several reports demonstrating successful tumor colonization with SL3261 (90). χ4550 is an *asd*$^{-}$ strain that lacks aspartate semialdehyde dehydrogenase and therefore cannot synthesize diaminopimelic acid (DAP), an essential component of the bacterial cell wall.

Bacterial plasmid maintenance is therefore maintained by complementing *asd* on our basic expression plasmid, pNG (Figure 2-7A). χ4550 cells that do not contain a plasmid must be grown in medium supplemented with DAP and will not survive *in vivo*. The *asd* complement system removes the need for antibiotic selection of transformants and allows for continual recombinant plasmid maintenance in an animal host. In addition to *asd,* the basic pNG plasmid contains a p15 origin of replication, leading to 15-20 plasmid copies per cell, and the *trc* promoter (139) upstream from the cloning site (Figure 2-7A). The *trc* promoter (139) is a Lac-based promoter modified from the *lac* operon found in *E. coli* that is constitutively active in *Salmonella* due the absence of a functional *lac* operon and LacI repressor protein.

Periplasmic scFv expression in attenuated Salmonella

When expressed in bacteria, scFvs are typically fused to an N-terminal type II secretion tag. This facilitates secretion into the more oxidative environment of the periplasm, where stabilizing disulfide bond formation occurs more readily (140). Since the scFvs had been selected by phage display using an OmpA secretion tag, we chose this tag for type II secretion in χ4550. Sequences for αCTLA-4 scFv and αPDL1 scFv were inserted into the pNG expression vector under the constitutively active *trc* promoter to generate pTrc-OmpA-αCTLA-4 and pTrc-OmpA-αPD-L1, respectively (Figure 2-7B). Recombinant plasmids were then used separately to transform electrocompentent χ4550 to generate SalpαCTLA-4 and SalpαPD-L1. These strains were grown in culture overnight and prepped for recombinant scFv expression. Coomassie-stained protein gels revealed high quantities of αPDL1 scFv in both the periplasm and culture supernatant of SalpαPD-L1 (Figure 2-8A) however, the growth rate of SalpαPD-L1 was slower than χ4550 containing a control pNG plasmid (SalpNG), and the culture

contained a white precipitate thought to be caused by bacterial cell lysis (not shown). SalpαPD-L1 cell lysis during culturing may explain the slower growth rate, the presence of the precipitate, and the accumulation of the scFv in the culture supernatant in the absence of an extracellular secretion mechanism. In contrast to SalpαPD-L1, very little to no αCTLA-4 scFv was observed in the SalpαCTLA-4 culture (Figure 2-8A). Subsequent analysis revealed a mutation that occurred during the culturing of SalpαCTLA-4 that inserted a premature stop codon. These observations indicated that forced periplasmic expression of the scFvs is deleterious to the fitness of χ4550, particularly expression of the αCTLA-4 scFv. This was verified by subsequent SalpαCTLA-4 cloning attempts resulting in strains with unique mutations to the cDNA or promoter sequence that prevented αCTLA-4 scFv expression. Therefore, generation of SalpαCTLA-4 was unsuccessful at this point.

To determine whether the altered growth kinetics of SalpαPD-L1 affected its *in vivo* survivability, 4T1 tumor-bearing mice were orally gavaged with SalpNG or SalpαPD-L1 and examined for tumor colonization. Each tumor from mice treated with SalpNG contained viable bacteria; however tumors from mice treated with SalpαPD-L1 did not contain bacteria (Figure 2-9A). This suggests that constitutive expression of periplasmic αPDL1 scFv reduces the fitness of SalpαPD-L1 and its survivability *in vivo.* The attenuating effects of periplasmic protein expression may be caused by the aggregation of mis-folded recombinant scFvs affecting the fitness of the bacteria. This issue has been partially addressed by Schaefer and Pluckthun (141), who observed greater success in recombinant periplasmic scFv expression in *E. coli* by co-expressing multiple periplasmic chaperones (FkpA, SurA, Skp, DsbA, and DsbC) on a separate plasmid. We investigated if this approach would lessen the deleterious effects of periplasmic αPDL1 scFv expression in SalpαPD-L1. The chaperone proteins were cloned into the pTrc-

OmpA-αPD-L1 plasmid forming pCH-OmpA-αPD-L1 (Figure 2-7C) and the resulting construct was used to transform χ4550 to generate "SalpCH-αPD-L1." The co-expression of periplasmic chaperone proteins seemed to improve the health of the cells in culture, indicated by a lack of precipitate and an improved growth rate (not shown). In addition, αPDL1 scFv was no longer found in the culture supernatant, indicating that bacterial cells were no longer lysing due to scFv expression (Figure 2-8B). However, periplasmic chaperone co-expression did not improve the *in vivo* survivability defects of periplasmic αPD-L1 scFv expression (Figure 2-10A). To determine if chaperone expression itself affected *in vivo* survivability, we tested *S.* Typhimurium expressing periplasmic chaperones alone (SalpCHAP) and found that periplasmic chaperone expression actually reduced the *in vivo* survivability of the bacteria (Figure 2-10A), despite having no apparent effect on *in vitro* growth (Figure 2-10B). Therefore, it was apparent that periplasmic secretion was impractical for *in vivo* bacterial delivery of scFvs.

Extracellular secretion of scFvs in attenuated Salmonella

We next sought to investigate whether *Salmonella* could be engineered to actively secrete the recombinant scFvs out of the bacterial cell and into the extracellular space. Extracellular secretion was desirable for two reasons: it would not require lysis of the bacterial cell in order to deliver the anti-tumor agents, leading to a more consistent delivery of therapeutic proteins during bacterial tumor colonization, and secreting the proteins through the inner and outer membrane to the extracellular space could circumvent the attenuating effects we observed with periplasmic secretion.

Successful secretion of recombinant proteins from *Salmonella* has been reported using Type I, Type III, and flagellin secretion systems. These mechanisms involve fusing

an N or C-terminal tag to the protein of interest, which is recognized by periplasmic proteins that mediate the secretion of the tagged protein out of the cell. Several secretion tags were fused to the αPDL1 scFv sequence and assayed for secretion; the descriptions of these systems and the results obtained are summarized in Table 2-2. Ultimately, successful secretion of both scFvs was achieved using the hemolysin (Hly) secretion system, based on the type I secretion of the hemolysin protein in Gram-negative bacteria such as *E. coli.* In this system, hemolysin (Hly A) is recognized by the inner membrane protein HlyB via a 60 amino acid C-terminal signal sequence (HlyA-ss). HlyB, in concert with the inner membrane protein HlyD and the outer membrane protein TolC, forms a channel through which the target protein unfolds as it is secreted out of the cell where it then refolds (142). Secretion using the Hly system was accomplished in *Salmonella* by encoding the HlyB and HlyD accessory proteins on our expression vector (TolC is constitutively expressed in *Salmonella*) and fusing the αPDL1 scFv sequence with the C-terminal HlyA-ss sequence to generate pTrc-αPDL1-Hly and pTrc-αCTLA4-Hly (Figure 2-7D), which when electroporated into χ4550 generated SalpαPDL1-Hly and SalpαCTLA4-Hly, respectively. αPDL1 scFv and αCTLA4 scFv were found exclusively in the culture medium of SalpαPDL1-Hly and SalpαCTLA4-Hly (Figure 2-11A). To verify that this was due to secretion of the molecules and not cell lysis, the expression of DnaK was also examined as a cytoplasmic control protein (Figure 2-11A). The Hly system not only allowed for secretion of the αPDL1 scFv, but also removed the *in vivo* survivability defects that were observed with periplasmic secretion (Figure 2-9B). Additionally, the Hly secretion system improved the cloning and expression issues with the αCTLA-4 scFv sequence that were encountered when attempting to initially clone this sequence in *Salmonella*.

The Hly secretion system was also utilized to generate scFv-secreting strains based on the SL3261 attenuated *Salmonella* strain (Δ*aroA*, Δ*hisG*). These strains, named DSpαPDL1-Hly and DSpαCTLA4-Hly, secreted their recombinant scFvs at levels similar to SalpαPDL1-Hly and SalpαCTLA4-Hly (Figure 2-11B). Although unlikely, the presence of the Hly-ss on the mature scFvs may prevent them from binding their ligands. To test this possibility, an ELISA was performed to determine the binding capability αPDL1 scFv against PD-L1-Fc-coated plates. In this assay, the scFv bound its ligand in a dose-dependent manner, which indicated that the Hly-ss sequence does not interfere with the ligand-binding region of the protein (Figure 2-11C).

DISCUSSION

Generation of functional immune checkpoint-blocking scFvs

Immunized avian libraries have been used before to generate high affinity scFvs (130). In addition to the benefits described in the introduction of this chapter (page 27), selection of functional scFvs using phage display was advantageous by selecting only functional scFvs that can be expressed in Gram-negative bacteria, which increased the likelihood of successful downstream expression in *Salmonella*. The scFvs and the molecules they block are roughly the same size, and theoretically many ligand-binding scFvs selected during panning would bind their antigen in areas that would not block signaling. We were fortunate to find that both of the scFvs selected from our phage display pool actually blocked the receptor/ligand binding of their target proteins. Indeed, when the library was subsequently revisited (for experiments irrelevant to this thesis), scFv sequences were characterized that bound their antigen but did not interrupt receptor/ligand binding.

Typically, antibody affinities in response to immunization will be in the 10^{-7}-10^{-10} M range (143). We observed a notably high affinity with a K_d value of $7.11x10^{-10}$ M for αPD-L1 scFv binding to PD-L1-Fc, especially when compared to the reported K_d of the cellular PD-1/PD-L1 interaction of $4.17x10^{-6}$ (144). This could be attributed to the higher affinity that is typical of chicken derived anti-mammalian variable regions after immunization (130) and the use of phage display to select the highest affinity scFv from the immunized library. However, when compared to the antagonistic mAbs tested, the scFv had a slightly lower affinity than MIH5 and was more than an order of magnitude lower than 10F.9G2 and 1-111a. In many cases, scFvs will bind antigen more weakly than full-length antibodies, as an scFv has only one antigen-binding Fv region, and a full-length mAb has two Fv regions. When the antigen is carrying more than one available antigenic determinant, such as in the case of PD-L1-Fc (the Fc portion of this protein causes dimerization), the bivalent avidity of two binding sites adds a considerable advantage by decreasing the K_{off} of the mAb, as both antigen-antibody bonds must be broken simultaneously before dissociation can occur (145). We suspect this difference accounts for the lower affinity of αPD-L1 scFv when compared to the mAbs, as the calculated differences in K_D are largely reflective of K_{off} rather than K_{on} (Table 1).

While αPD-L1 scFv binds PD-L1 more weakly than 10F.9G2, it demonstrated comparable blocking activity to the full-length mAb. This may be because the affinity of both αPD-L1 scFv and 10F.9G2 are several orders of magnitude above the affinity of PD-L1 to its receptor PD-1, and are both in the upper theoretical limit of antibody affinity (145). Their blocking ability may therefore be limited more so by diffusion rates and the proximity and availability of antigen rather than by their rate of dissociation. Additionally, while more PD-L1 molecules may remain unbound in the case of αPD-L1 scFv when

compared to 10F.9G2, these antibodies are comparable in their ability to block PD-L1/PD-1 inhibitory signals in a cellular context.

Expression and secretion of recombinant proteins in Salmonella

When producing scFvs, it is not unusual to encounter problems with solubility and proper folding (146), and in most cases, scFvs generated in bacteria will accumulate as insoluble protein in inclusion bodies and require extra steps to refold before functional use (147-151). We did not encounter these issues with the αPD-L1 scFv when expressed in *E. coli*, which eased the production and purification of the protein. However there was some difficulty in the production of soluble αCTLA-4 scFv, which hindered the subsequent characterization and binding affinity of the protein, but sufficient amounts of soluble protein were generated to determine its antagonistic bioactivity.

Even though both αPD-L1 scFv and αCTLA-4 scFv were expressed and secreted to the periplasm in *E. coli* for selection by phage display, their constitutive expression and periplasmic expression in *Salmonella* proved deleterious for the bacteria as evidenced by the slowed growth in culture and lack of *in vivo* survivability in the case of SalpαPDL1. These negative effects were seemingly more pronounced in the initial attempts to clone the αCTLA-4 scFv in *Salmonella* (echoing the expression issues of this scFv encountered in *E. coli*); in this case, the only recoverable transformants had recombinant pTrc-OmpA-αCTLA-4 plasmids with altered sequences that prevented expression of the scFv. These deleterious effects may have been due to an accumulation of potentially poorly folded and/or aggregated scFvs in the periplasmic space, which can sometimes accompany recombinant scFv expression in bacteria. While the co-expression of recombinant periplasmic chaperone proteins may have prevented lysis of scFv-secreting bacterial strains *in vitro*, the expression of these

chaperone proteins *in vivo* lessened the survivability of the bacteria. Therefore, we hypothesized that extracellular secretion would not only allow the accumulation of scFvs in the extracellular space without bacterial cell lysis, but also would increase the fitness of the bacteria by circumventing the periplasmic accumulation of the scFvs that may have been the cause of these attenuating effects. In support of this, we found that type I extracellular secretion of αPD-L1 scFv via the Hly system eliminated the burdening effects of this expression and increased the *in vivo* survivability of the recombinant bacteria. Therefore utilizing the Hly secretion system allowed for the generation of attenuated strains of *S.* Typhimurium that successfully secreted scFvs that block PD-L1 or CTLA-4. Additionally, the same expression and secretion system has been applied in our lab to generate strains that secrete the biologically active stimulatory cytokines IL-2 and an IL-15/IL-15 receptor alpha fusion protein. Ultimately, SalpαPD-L1-Hly and SalpαCTLA-4-Hly would be used in combination with these cytokine-secreting strains to deliver a combinatorial immunostimulatory therapy to the tumor microenvironment.

The goal of this study was to investigate the ability of *S.* Typhimurium to express and secrete immunostimulatory proteins, with a specific focus on PD-L1 and CTLA-4 immune checkpoint-blocking scFvs. At a minimum, this work serves as a proof of principle demonstrating the expression capabilities of attenuated *S.* Typhimurium. Ultimately, the strains generated would be assayed alone and in combination for their ability to deliver therapeutic concentrations of their recombinant proteins to the tumor microenvironment. The remaining chapters of this thesis will investigate the tumor-targeting potential of the more well-characterized αPD-L1 scFv, with the assumption that reasonably similar results could be expected for the delivery of other scFvs in parallel or future studies.

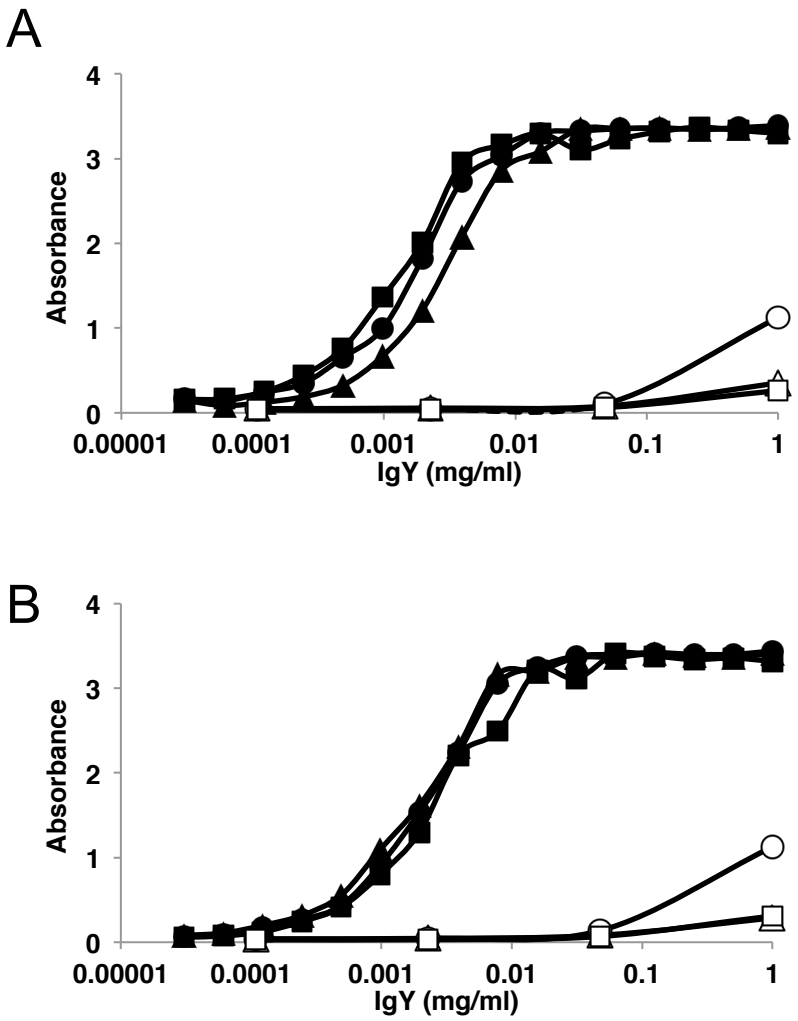

Figure 2-1. Immunized chickens develop strong Ig responses against CTLA-4 and PD-L1 antigens.

Figure 2-1. Immunized chickens develop strong Ig responses against CTLA-4 and PD-L1 antigens. IgY purified from host chickens before (open symbols) and after immunizations (filled symbols) was tested for antigen specificity. Antibody concentration was normalized and compared in triplicate by ELISA against plate-bound mouse CTLA-4 **(A)** or PD-L1 **(B)** as the target antigen. Bound IgY was detected using anti-chicken IgY-HRP conjugate (Aves Labs) and BD OptEIA^{TM} TMB substrate. Absorbance was measured at 450nm and corrected for 570nm background absorbance. Chickens 1, 2 and 3 are represented by ▲, ● and ■ symbols, respectively.

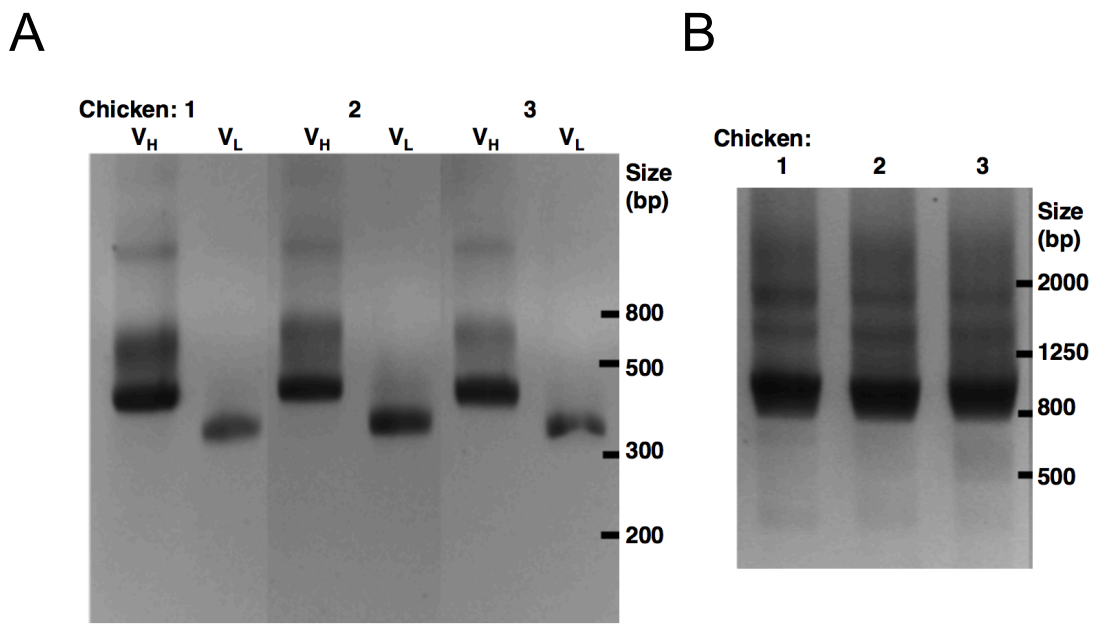

Figure 2-2. Chicken variable regions were amplified and combined to generate the scFv library.

Figure 2-2. **Chicken variable regions were amplified and combined to generate the scFv library. (A):** V_H and V_L sequences (~450 and 350 bp, respectively) were amplified from chicken cDNA using PCR with primers flanking the variable regions. **(B):** After gel purification, V_H and V_L sequences were combined with splice-overlap extension PCR to generate full length scFvs of about 800-900 bp. Multiple PCR reactions were combined to generate >1 µg of purified DNA after gel extraction.

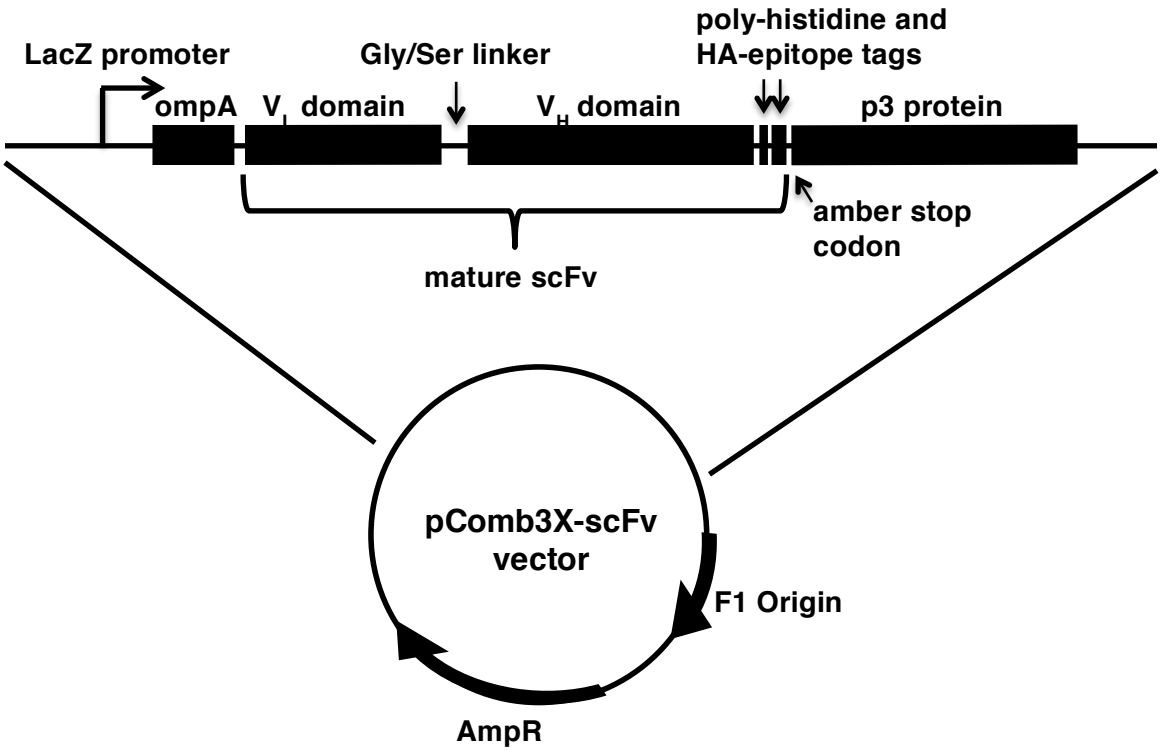

Figure 2-3. Schematic representation of the pComb3x phagemid vector including the scFv library.

Figure 2-3. Schematic representation of the pComb3x phagemid vector including the scFv library. The scFv library is expressed as a P3 fusion protein in amber suppressor strains of *E.coli* for phage display and panning. In non-suppressor strains of *E. coli*, the amber stop codon is recognized and soluble scFv protein is expressed without the p3 protein. The ompA signal sequence is cleaved in the periplasm, leaving mature scFv that consists of the variable regions and the C-terminal HA and His tags.

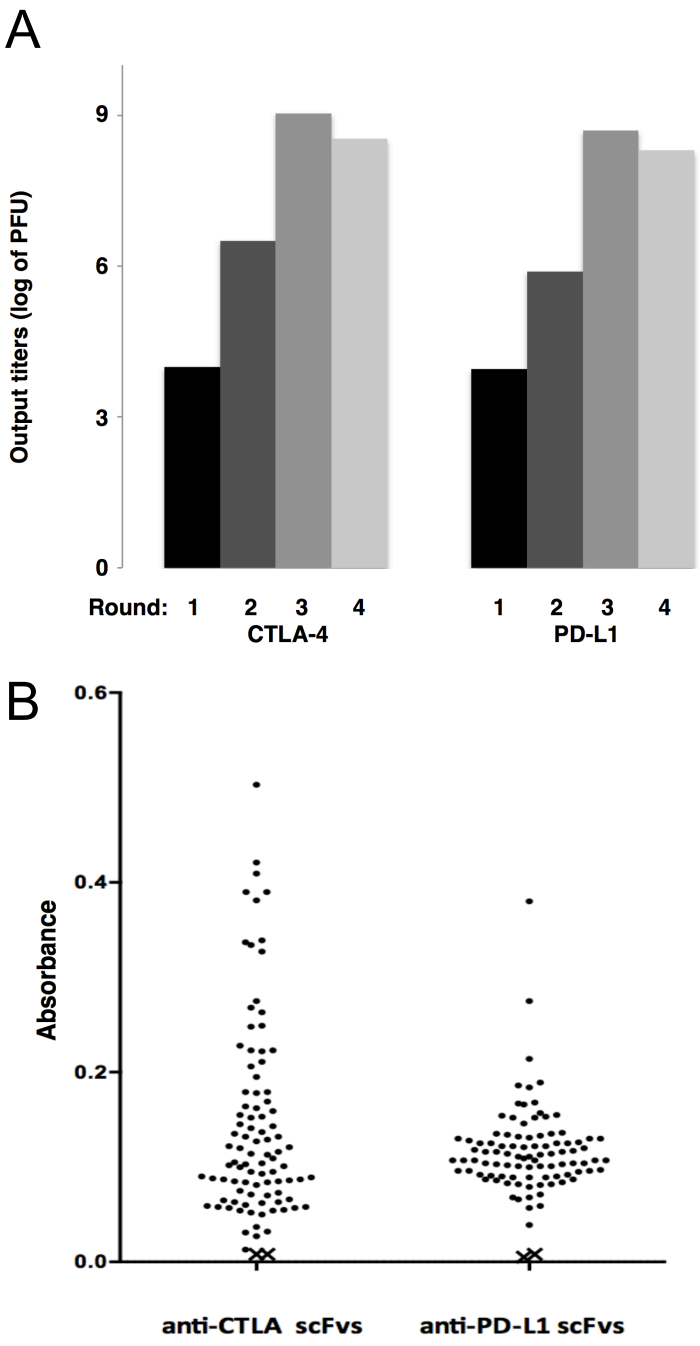

Figure 2-4. Antigen-specific scFvs were enriched from the immunized library and demonstrated antigen-binding capability.

Figure 2-4. Antigen-specific scFvs were enriched from the immunized library and demonstrated antigen-binding capability. **(A):** Output phage titers were measured with each round of panning. Output phage were enumerated by infecting excess ER2738 *E. coli* cells with an aliquot of phage eluted after selection and plating for colony formation on 2xYT agar containing carbenicillin. Each colony formed corresponded to a single plaque-forming unit (PFU) of phage. **(B):** ELISA of selected scFvs from panning output round 4. Soluble protein was prepared from the periplasm of *E. coli* TG1 cells containing scFv sequences from round 4 of panning. Protein was tested for binding to recombinant plate-bound PD-L1 or CTLA-4. Absorbance was measured at 450nm and corrected for absorbance at 570nm. Each dot represents an individual scFv from the enriched library. The five top binding scFvs were selected for sequencing and further characterization. Negative controls containing no periplasmic protein are indicated by the X symbols.

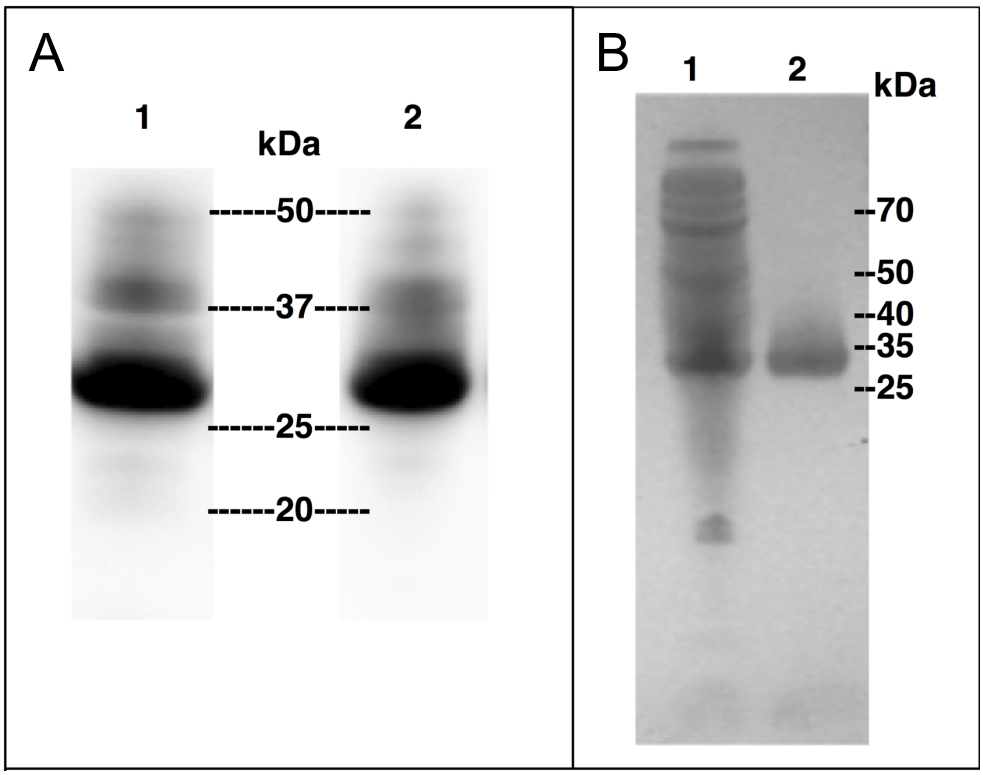

Figure 2-5. Soluble αPD-L1 scFv is detected in the periplasm and culture supernatant of *E. coli* and is readily purified.

Figure 2-5. Soluble αPD-L1 scFv is detected in the periplasm and culture supernatant of *E. coli* and is readily purified. *E. coli* T10F' cells were transformed with phagemid harboring the αPD-L1 scFv sequence (for schematic, see Figure 2-3). **(A):** Western blot of soluble αPD-L1 scFv in culture supernatant (lane 1) and periplasm (lane 2) of bacterial cultures using an anti-HA tag-HRP conjugate. **(B):** Total periplasmic protein was isolated (lane 1), and αPD-L1 scFv was purified using IMAC beads (lane 2). Proteins were visualized using Coomassie Brilliant Blue dye.

Table 2-1: Antibody affinity measurements. *SPR measurements were performed at LakePharma (Belmont, CA).*

Antibody[a]	$\mathbf{K_d}$ (M)	$\mathbf{K_{on}}$ (1/Ms)	$\mathbf{K_{off}}$ (1/s)
10F.9G2 (Biolegend)	1.67×10^{-11}	7.22×10^{5}	1.21×10^{-5}
1-111a (eBioscience)	5.66×10^{-11}	1.31×10^{6}	7.43×10^{-5}
MIH5 (eBioscience)	2.05×10^{-10}	1.04×10^{6}	2.13×10^{-4}
αPD-L1 scFv	7.11×10^{-10}	4.91×10^{5}	3.94×10^{-4}

[a] Vendor sources for monoclonal antibodies are shown in parentheses.

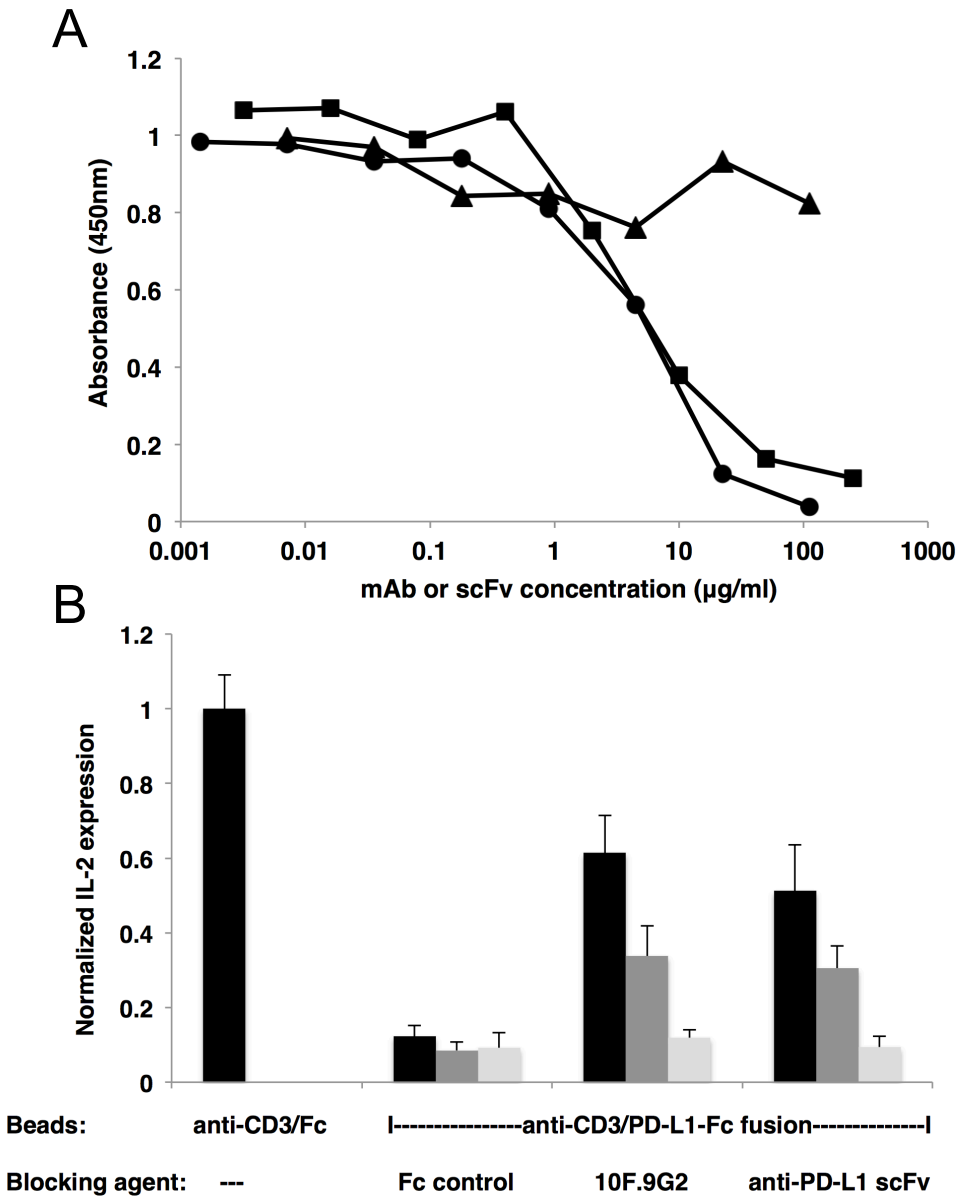

Figure 2-6. ScFvs demonstrate antagonistic biological activity.

Figure 2-6. ScFvs demonstrate antagonistic biological activity. (A) Anti-CTLA-4 scFv blocks CTLA-4 binding to B7.1. B7.1-Fc fusion protein was incubated with plate-bound CTLA-4 in the presence of anti-CTLA-4 scFv (●), a positive control anti-CTLA-4 blocking mAb (■) or a non-specific anti-PD-L1 scFv (▲). B7.1-Fc fusion protein binding was detected using anti-Fc HRP antibody. Absorbance was measured at 450nm and corrected for absorbance at 570nm. **(B)** Tosylactivated beads were coated with a stimulatory anti-CD3 mAb and either PD-L1-Fc fusion protein (anti-CD3/PD-L1-Fc fusion; PD-L1^{+}), or Fc control (anti-CD3/Fc; PD-L1^{-}). To test the blocking activity of the scFv, PD-L1^{+} beads were blocked with 10μg (■), 1μg (■) or 0.1μg (■) of purified αPD-L1 scFv and incubated with T-cells from Balb/c mice for 4 days. To measure T-cell activation, IL-2 secretion after incubation was quantified using ELISA. Beads were blocked with human Fc protein or 10F.9G2 mAb as negative and positive controls, respectively. Experiments were performed in triplicate; results were normalized to the IL-2 secretion with the PD-L1^{-} beads in each experiment and combined for the data shown. Error bars indicate +/- standard deviation.

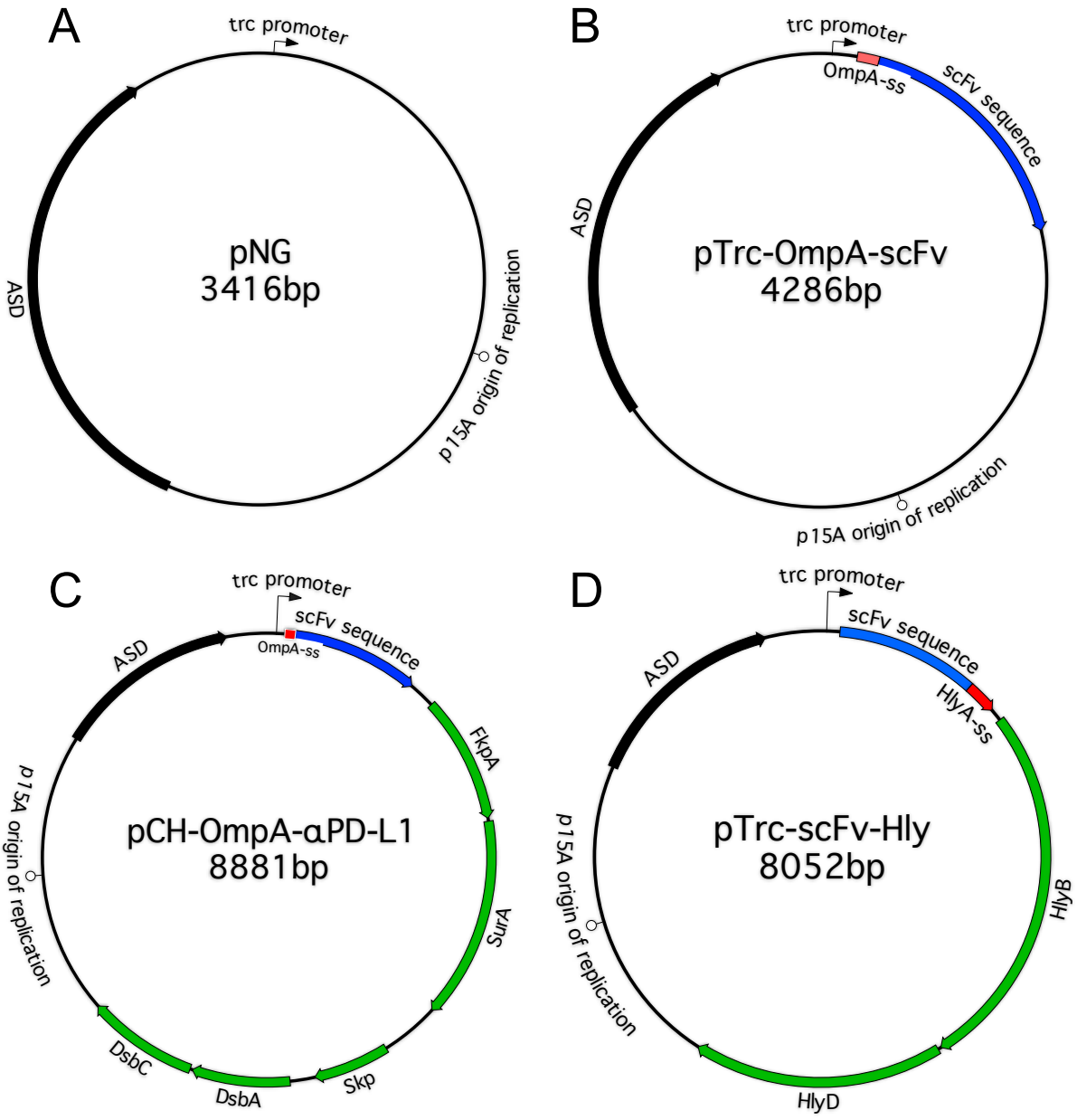

Figure 2-7. Plasmid vector maps along with their size and recombinant protein sequences.

Figure 2-7. Plasmid vector maps along with their size and recombinant protein sequences. Sizes of each vector are shown below the vector name in nucleotide base pairs (bp). The *asd* gene, *Trc* promoter, and *p15A* origin of replication are found in each plasmid. Blue “scFv sequence” gene denotes the sequence for either αCLTA-4 or αPD-L1 scFv, depending on the plasmid. Accessory chaperone or secretion protein genetic sequences are indicated in green.

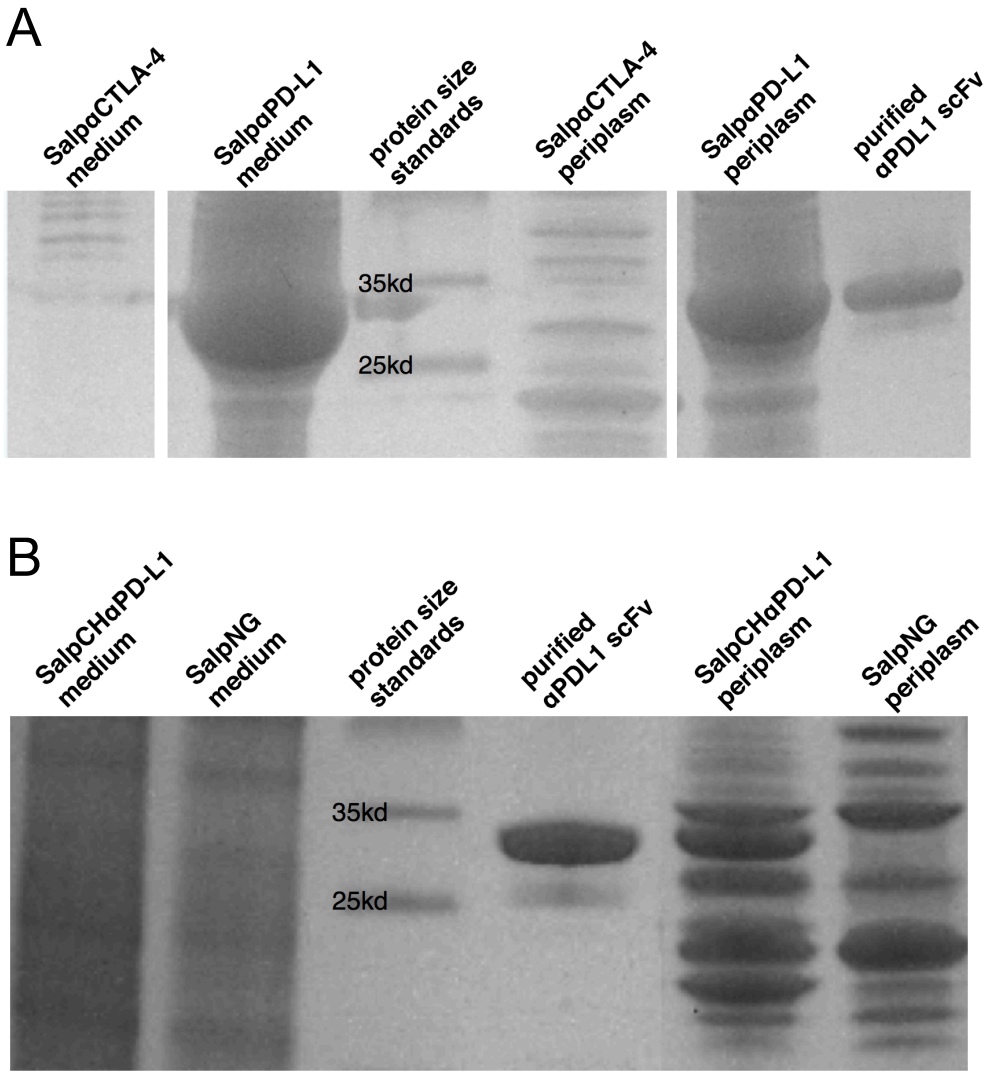

Figure 2-8. Secretion of scFvs into the periplasm.

Figure 2-8. Secretion of scFvs into the periplasm. (A) αPD-L1 scFv but not αCTLA-4 scFv is found at high quantities in the periplasmic space and culture supernatant of overnight bacterial cultures. Purified αPDL1 scFv was used for size comparison. **(B)** Coexpression of periplasmic chaperone proteins (CH) maintains periplasmic expression but prevents the accumulation of αPDL1 scFv in the culture supernatant. A SalpNG culture was used as a negative control for expression, and purified αPDL1 scFv was used for size comparison. In both (A) and (B), polyacrylamide gels were stained with Coomassie for protein visualization. Lighter exposure of panel B shows a clearer picture for lanes one and two, with no notable scFv bands. Additionally, western blots against polyhistadine tags verify no scFv in the medium in these lanes (not shown).

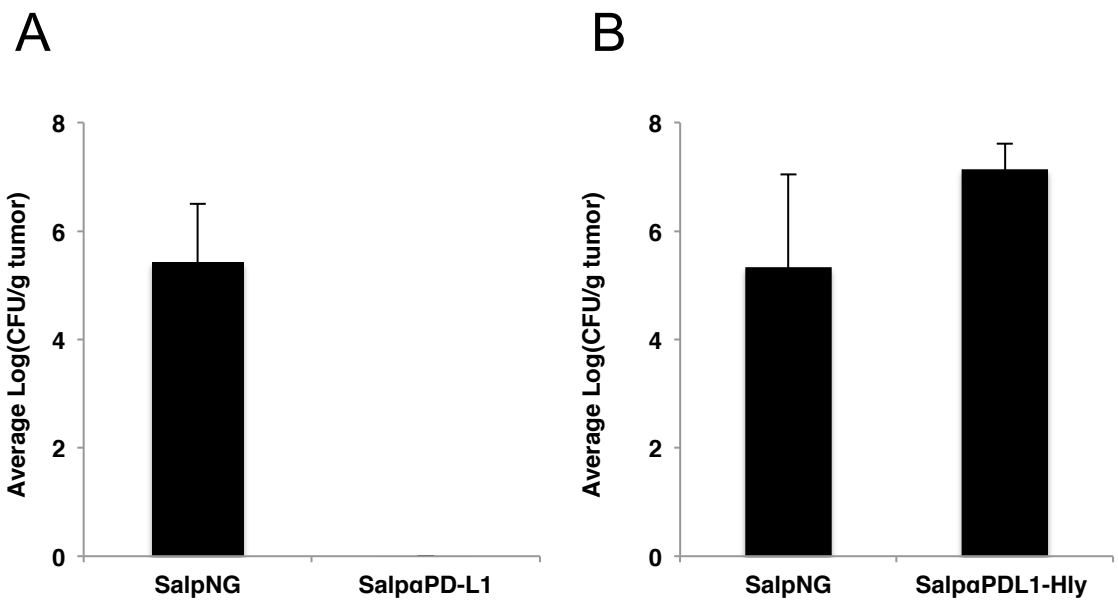

Figure 2-9. The location of αPD-L1 scFv affects the *in vivo* survivability of attenuated *Salmonella*.

Figure 2-9. The location of αPD-L1 scFv affects the *in vivo* survivability of attenuated *Salmonella*. Mice bearing subcutaneous 4T1 tumors were injected intravenously with 5×10^4 CFU of either SalpNG or SalpαPD-L1 in **(A)** or SalpNG and SalpαPDL1-Hly in **(B)**. Tumors were harvested after 3-4 weeks, homogenized, plated and incubated overnight for colony formation and enumeration. Periplasmic scFv expression of SalpαPD-L1 reduced intratumoral colonization of the bacterium compared to the SalpNG control (A). Extracellular scFv-secreting SalpαPDL1-Hly colonized tumors at least as well as the SalpNG control (B). Bars indicate the average of 4 mice, and error bars = 1 standard deviation.

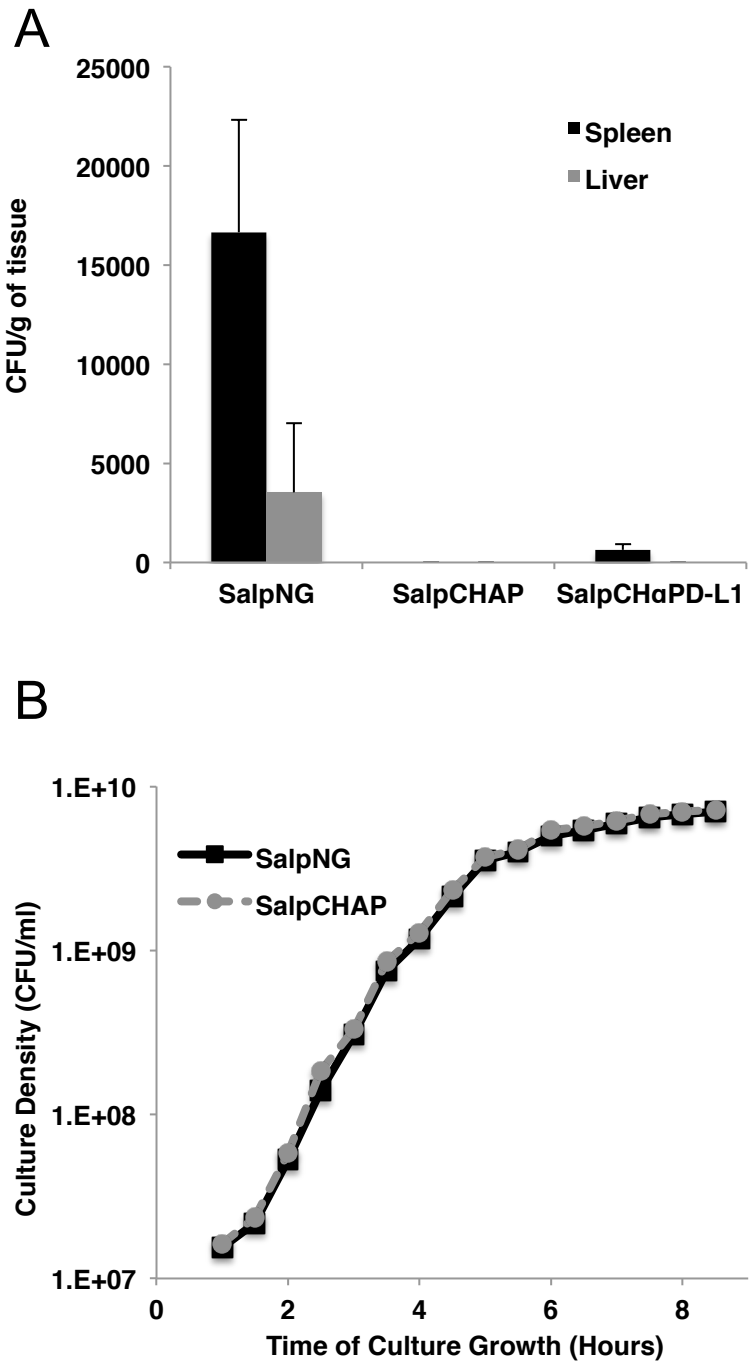

Figure 2-10. Recombinant periplasmic chaperone expression reduces *Salmonella* strain survival *in vivo* while not affecting *in vitro* growth rate.

Figure 2-10. Recombinant periplasmic chaperone expression reduces *Salmonella* strain survival *in vivo* while not affecting *in vitro* growth rate. (A) Mice were injected with 5×10^4 CFU of either SalpNG, SalpCHαPD-L1, or SalpCHAP. Animals were sacrificed 3 weeks later and their tissues were homogenized, plated, and incubated overnight for CFU enumeration. Experiments were performed twice on 3 mice each (6 mice total). Bars show the average result of all mice. Error bars indicate 1 standard deviation. **(B)** SalpNG and SalpCHAP were grown at 37°C in LB and plated every 30 minutes to enumerate CFU/ml over time.
Experiments in this figure were performed by Michael Mertensotto.

Table 2-2: Extracellular secretion systems tested. Multiple systems reported to successfully secrete proteins from *Salmonella* were tested for scFv secretion. Their descriptions, references, and findings are summarized.

Tag ID	Secretion system	Reference	Tag description	Accessory proteins required?	Successful secretion of scFvs from *Salmonella*?
Yops	*Yersinia* outer proteins (Yops) type III secretion signal.	(152, 153)	8 amino acid N-terminal secretion signal: MISSSSIS	no	may improve intracellular expression, but no secretion detected.
Flag	Segment of the flagellin protein sequence (amino acids 26-47) directs secretion of protein through bacterial flagella.	(154)	22 amino acid N-terminal secretion signal.	no, bacterium needs active flagella	no protein secretion detected.
YebF	*sec*-dependent extracellular secretion used to produce proteins toxic to host bacteria	(155)	21 amino acid N-terminal tag. Cleaved in the periplasm before extracellular secretion	no	no protein secretion detected.
Hly	Type I secretion signal used for native hemolysin secretion.	(156, 157)	60 amino acid C-terminal HlyA-ss tag.	HlyB and HlyD	yes (see figure 2-11)

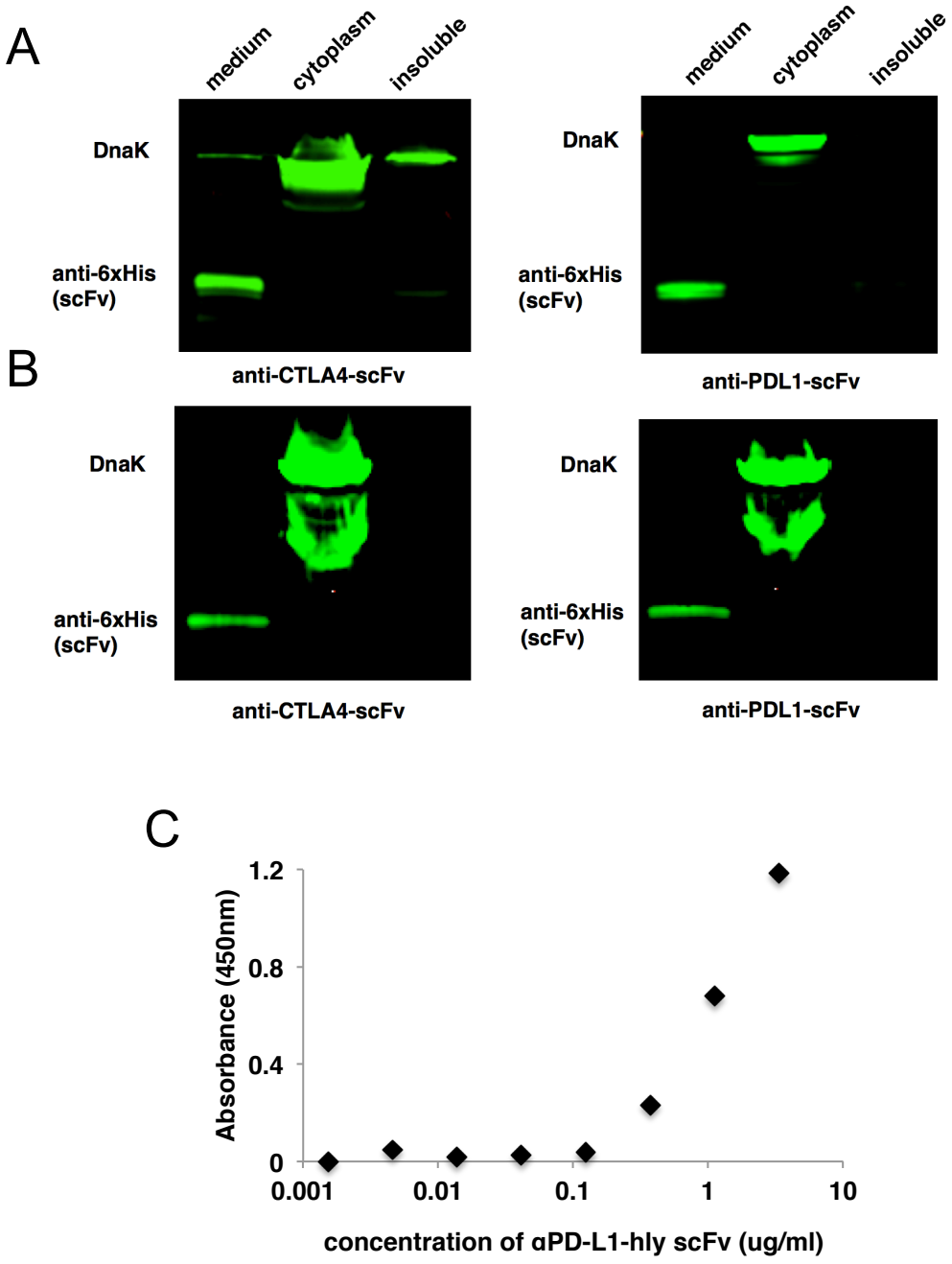

Figure 2-11. The Hly secretion system mediates successful extracellular secretion of both αPD-L1 and αCTLA-4 scFvs.

Figure 2-11. The Hly secretion system mediates successful extracellular secretion of both αPD-L1 and αCTLA-4 scFvs. (A) SalpαCTLA-4-Hly and SalpαPD-L1-Hly were grown in culture overnight. The supernatant (medium), cytoplasm and insoluble fraction of cell cultures were isolated and examined by Western blot for the presence of scFv using anti-His-tag and and IR800 secondary antibodies. Both scFvs were found exclusively in the culture supernatant. DnaK was detected by antibody binding as a cytoplasmic control to verify secretion rather than cytoplasmic leakage or cell death. **(B)** The SL3261-based attenuated strains DSpαCTLA-4-Hly and DSpαPD-L1-Hly were tested for extracellular secretion as in (A). DnaK is sometimes detected as a doublet protein band and did so in these blots, which does not affect the interpretation of results. **(C)** The αPD-L1-scFv tagged with the HlyA-ss was tested in an ELISA to determine whether the HlyA-ss prevented antigen-binding. Plates were coated with PD-L1-Fc protein, and varying concentrations of purified αPD-L1-Hly scFv were tested for binding. Bound scFv was detected using an anti-HisTag-HRP conjugate.
Protein preparation and Western blotting for the gels in panel (B) were performed by Michael Mertensotto.

CHAPTER 3

ATTENUATED *S.* TYPHIMURIUM DEMONSTRATES ANTI-TUMOR EFFICACY INDEPENDENT OF TUMOR COLONIZATION

Authorship Note: Jeremy Drees performed all experimental work in this chapter alone or with assistance from colleagues including Michael Mertensotto (Research Scientist U of MN Dept. Surgery) and Lance Augustin (Assistant Prof. U of MN Dept. Surgery).

Reprint Disclaimers:
Sections of this chapter have been adapted with permission from *Anticancer Research,* International Institute of Anticancer Research
Citation: *Drees J, Mertensotto M, Liu G, Panyam J, Leonard A, Augustin L, Schottel J, Saltzman D. Attenuated* Salmonella enterica *Typhimurium reduces tumor burden in an autochthonous breast cancer model. Anticancer Res. 2015; 35: 843-9.*

INTRODUCTION

The characteristics of tumors that affect their susceptibility to *S. enterica* Typhimurium (*S.* Typhimurium) colonization (outlined in Chapter 1, page 16) are general features that would theoretically be relevant to many types of cancer and are not dependent on tissue locations or the expression of specific tumor antigens. Therefore, successful development of salmonellae-based cancer therapy would likely have widespread application in several types of solid cancers. We investigated this potential by assessing the anti-tumor efficacy and tumor-targeting propensity of attenuated *S.* Typhimurium in a variety of murine tumor models including osteosarcoma pulmonary metastases, subcutaneous and metastatic breast cancer, and transgenic autochthonous breast cancer.

Osteosarcoma is a disease with a peak incidence in early adolescence. Current therapies have increased the 3-year survival of patients with local disease to greater than 70%. However, in patients with metastatic disease, often presenting as pulmonary metastases, disease-free survival is limited to less than 30% (158). In mice, metastatic

osteosarcoma can be modeled using K7M2 cells. The K7M2 cell line was derived from a metastasis on the lung of a mouse with metastatic osteosarcoma, and when injected into the bone of BALB/c mice, this cell line will give rise to tumors that will metastasize to the lungs. Alternatively, the cell line can be injected directly into the bloodstream of mice, wherein it travels to the lungs and forms tumors that model pulmonary metastases (159).

Breast cancer is the most common cancer among women, including over 200,000 new diagnoses every year (U.S. Cancer Statistics Working Group, 2011). The most common diagnosis is ductal carcinoma, a cancer of the ductal cells of the mammary glands. Invasive ductal carcinoma can spread to other parts of the breast and into other parts of the body. There are several mouse models of invasive breast cancer; however, the focus of this thesis will be on the metastatic 4T1 tumor model and the transgenic BALB-neuT model. The 4T1 cell line is a highly metastatic cell line derived from a mouse mammary tumor (160) and is is often used to study breast cancer metastases due to its highly metastatic potential. A subcutaneous inoculation of 4T1 cells into BALB/c mice will develop a primary tumor that metastasizes into the lungs in >95% mice (160). The BALB-neuT model is a genetically engineered mouse (GEM) model of invasive breast cancer on the BALB/c background that expresses a constitutively active rat Her2 receptor (*neu*) driven by the mouse mammary tumor virus promoter. As opposed to transplant models such as such the 4T1 model, BALB-neuT mice positive for the transgene develop cancer over several months, which appears on the mammary pads of female mice as palpable tumors around 16 weeks of age. The tumors closely resemble the aggressive Her2-driven cancer found in human patients (161).

In this chapter, the tumor-targeting propensity, immune effects, and anti-tumor efficacy of attenuated *S.* Typhimurium were investigated in multiple models including

subcutaneous and metastatic transplanted tumors as well as transgenic autochthonous tumors.

METHODS

S*. Typhimurium strains and preparation for injection*

S. Typhimurium strain χ4550 (*Δcya, Δcrp, Δasd*) was used as the host strain for these experiments (105). Plasmid pNG was used as the cloning vehicle, and bacteria carrying pNG are referred to as SalpNG. SalpαPDL1-Hly are *S.* Typhimurium carrying the pNG plasmid with the αPDL1-Hly scFv gene. SalpαCTLA4-Hly are *S.* Typhimurium carrying the pNG plasmid with the αCTLA4-Hly scFv gene. See Figure 2-7 for the relevant plasmid maps.

Overnight cultures of SalpNG or indicated strain were grown in LB (10 g tryptone, 10 g NaCl, 5 g yeast extract per 1 L dH_2O). Cells were chilled in ice water, pelleted and resuspended in ice cold 15% glycerol in LB. Aliquots were then flash frozen in liquid nitrogen and stored -80°C. One vial from each batch was thawed and plated to determine live colony-forming units (CFU)/mL of bacterial stock after thawing. Before treatment, frozen bacteria were thawed at 37°C and diluted in phosphate-buffered saline (PBS) to the indicated concentrations and injected in a 100µl injection volume.

Animal care

BALB-neuT and BALB/c mice were maintained in specific pathogen free conditions and fed standard mouse chow (Harlan). Animals were cared for by the University of Minnesota's Research Animal Resources, and all animal use was approved by the University's Institutional Animal Care and Use Facility.

K7M2 tumor studies

For metastatic osteosarcoma experiments, K7M2 osteogenic carcoma cells (ATTC: CRL-2836) were grown in RPMI-1640 medium containing 10% fetal bovine serum. Cells were detached from flasks using 0.05% trypsin-EDTA, counted with a hemocytometer, washed with sterile PBS, and diluted to the appropriate concentration prior to injection. Female Balb/c mice were injected via the tail vein with $5x10^5$ K7M2 osteogenic sarcoma cells. SalpNG was administered intravenously 7 to 14 days post tumor inoculation as indicated. Mice were either sacrificed 14-21 days post treatment for tumor burden studies or when they were moribund for survival studies. To estimate tumor burden in the lungs of mice, lungs were excised, rinsed with PBS and dried with sterile guaze. The average lung weight of tumor-free (0.18 g, based on 10 mice) was subtracted from the lung weight of tumor-burdened mice (sex and age-matched) to calculate “net tumor burden.”

4T1 tumor studies

4T1 cells (ATCC #CRL-2539) were grown in RPMI-1640 medium containing 10% fetal bovine serum. Cells were detached from flasks using 0.05% trypsin-EDTA, counted with a hemocytometer, washed with sterile PBS, and diluted to the appropriate concentration prior to injection. Female BALB/c mice of approximately 12 weeks of age were given a subcutaneous injection of 1×10^5 4T1 cells in 50 µL of sterile PBS superficial to the right inguinal mammary fat pad. Tumor growth was measured over time by caliper. Mice were treated with SalpNG or SalpαPD-L1-Hly by IV injection 11 days post tumor inoculation. In the indicated experimental groups, mice were injected with 125µg of αPD-L1 mAb (10F.9G2, BioXCell) twice weekly for the duration of the experiment and/or 125µg of αCD137 (3H3, BioXCell) twice weekly for two weeks. At the

conclusion of the experiments, tumors were weighed, homogenized, diluted, and plated; plates were incubated overnight to determine CFU/gram of tissue. In some cases, lungs were removed and weighed to determine net pulmonary metastatic burden as in the K7M2-treated mice.

BALB-neuT tumor studies

Genotyping for the *neu* transgene was performed by Transnetyx on male and female pups in the BALB-neuT mouse colony. Breeding pairs consisted of heterozygous males and homozygous negative females. Female mice that were positive for the *neu* transgene were monitored for tumor development. Upon initial tumor palpation (~16 weeks), mice were injected IV with 6×10^4 CFU of the indicated *S*. Typhimurium strain. Tumors were measured weekly with a digital caliper, and individual tumor volumes were calculated as spheroid ($L \times W^2 \times 0.52$). Individual tumor volumes were added to give total tumor burden for each mouse. For survival studies, mice were monitored for survival and euthanized if they became moribund or if a single tumor reached 2 cm^3 in volume.

Bacterial tissue colonization experiments

For bacterial tissue colonization experiments, tumor-bearing mice were sacrificed 17-21 days post-treatment. Spleens and tumors were harvested from mice and minced to ~1 mm^3 pieces. Resulting samples were homogenized in 5 ml of sterile PBS in gentleMACS M Tubes with Strainers (Miltenyi Biotec) using a gentleMACS Tissue Dissociator and running program RNA_01. The homogenate was serially diluted in sterile PBS and plated on LB agar containing 100 µg/ml nalidixic acid for selection. Plates were incubated overnight at 37°C, and CFU were enumerated the next day.

Tissue preparation for flow cytometry

Tumors, spleens or tumor-bearing lungs were homogenized using a Mouse Tumor Dissociation Kit (Miltenyi Biotec) according to manufacturer's instructions. Cell suspensions were stained or cells were fixed and permeabilized for intracellular staining of Foxp3 and IFNγ after extracellular staining using the Foxp3 Transcription Factor Staining Buffer Set (eBioscience). Cells were gated and identified as follows: CD8 T-cells ($CD8^+$), CD4 T-cells ($CD4^+$), Th1 cells ($CD4^+$, $IFN\gamma^+$), T-regs ($CD4^+$, $CD25^+$, $Foxp3^+$) NK cells ($CD8^-$, $CD4^-$, $CD49b^+$), monocytic MDSCs ($CD45^+$, $CD11b^+$, $Ly6C^{Hi}$), granulocytic MDSCs ($CD45^+$, $CD11b^+$, $Ly6G^{Hi}$). Cells/sample were enumerated using CountBright absolute counting beads (Life Technologies). Cells/gram measurements were calculated based on the percent of sample analyzed, tumor weight, and homogenate volume. Antibody conjugates were purchased from BioLegend: αCD8/FITC (100705), αCD4/PerCP-Cy5.5 (100539), αCD49b/PE/Cy7 (108921), αCD45.2/BV510 (109837), αCD25/BV650 (102038), αCD11b/BV650 (101239), αPDL1/PE-Cy7 and isotype control (400617, 124313); BD Pharmingen: αLy6C/PerCP/Cy5.5 (560525) and αLy6G/AF700 (561236), and αFoxp3/AF700 (ebioscience: 56-5773-80).

In order to differentiate tumor leukocytes from blood leukocytes in K7M2 mice, we performed intravascular staining, adopted from Anderson *et al* (162), using an αCD45.2/PE antibody (Biolegend: 109808). Briefly, mice were injected IV with 4μg of CD45.2/PE antibody in 200μl of PBS and euthanized 4 minutes later using IV Beuthanasia D. The only cells that stained positively with PE were those in the blood stream; these cells were gated out from the analysis. Blood and inguinal lymph nodes were collected from mice for positive and negative *in vivo* staining controls, respectively.

All flow cytometry was performed on an LSR II flow cytometer (BD Biosciences) with FACS Diva acquisition software. Subsequent analysis was performed using FlowJo (version X).

RESULTS

S*. Typhimurium exhibits anti-tumor efficacy in transplanted metastatic and subcutaneous tumor models*

Before determining the therapeutic efficacy of the recombinant scFv-secreting strains (SalpαPDL1-Hly and SalpαCTLA4-Hly), we investigated the anti-tumor efficacy of SalpNG. As described in the introduction (page 17), *S.* Typhimurium has demonstrated native tumoricidal effects in multiple murine tumor models. However, these effects have not been characterized for the SalpNG bacterium. Additionally, the models that describe the anti-tumor effects of *S.* Typhimurium treatment used subcutaneous transplant models in which a tumor develops from a suspension of cells or a tumor piece that has been transplanted into the subcutaneous space. Therefore, we investigated the anti-tumor capabilities of *S.* Typhimurium treatment in a more diverse set of mouse models including both transplanted primary and metastatic tumors as well as autochthonous tumors.

SalpNG reduces tumor burden and increases survival in K7M2 osteogenic sarcoma.

To model osteosarcoma pulmonary metastases, BALB/c mice were injected IV with the metastatic osteogenic sarcoma cell line K7M2, which caused the development of numerous metastasis-like tumors in the lungs of inoculated mice. The total tumor weight in the lungs was determined by subtracting the average weight of tumor-free lungs from age and sex-matched mice from the weight of lungs from tumor-bearing

mice. When left untreated, by 28 days post-tumor cell inoculation, mice contained an average of 0.4 g of tumor in their lungs (Figure 3-1A). A single intravenous (IV) treatment of 5×10^4 CFU of SalpNG 7 days post-tumor cell inoculation reduced the tumor burden by approximately 80% (Figure 3-1A). Similar results were obtained when mice were treated 14 days post-tumor cell inoculation (Figure 3-1B). This reduction corresponded to an approximate 120% increase in average survival time from 29 days to 64 days post treatment (Figure 3-1C).

SalpNG reduces the percentage of infiltrating T-regs and increases CD4 T-cell IFNγ expression in K7M2 osteosarcoma.

To investigate the immune-modulating effects of SalpNG treatment on tumor-infiltrating lymphocytes, an intravascular staining method developed by Anderson and colleagues (162) was adapted for the K7M2 model. In order to differentiate between the blood lymphocytes in the lung vasculature and lung tissue/tumor-infiltrating lymphocytes, an αCD45.2/PE antibody was injected IV into tumor-bearing mice. The antibody specifically stained all leukocytes in the blood of the mice for four minutes before they were rapidly euthanized and their lungs homogenized and diluted to prevent antibody percolation into lung tissue. In subsequent flow cytometry analysis of infiltrating cells, those positive for PE staining were gated out of the analysis as blood cells (Figure 3-2A). Lymphocytes from blood and lymph nodes were harvested from each mouse and stained *ex vivo* with αCD45.2/BV650. These served as positive and negative technical controls for blood-specific PE staining (Figure 3-2B and C).

The $CD4^+$ T-cell compartment of untreated K7M2 tumor-infiltrating lymphocytes was highly enriched for $Foxp3^+$, $CD25^+$ T-regs, which comprised an average of approximately 60% of $CD4^+$ cells. However, treatment with SalpNG reduced this

percentage to about 25% (Figure 3-2D-F). Additionally, SalpNG treatment increased $CD4^+$ IFNγ expression, indicating an increase in Th1 cells in K7M2 tumors (Figure 3-2G-I). There was no significant change in $CD8^+$ T-cell IFNγ expression (not shown). These changes suggest an immunostimulatory effect of SalpNG treatment.

SalpNG reduces metastatic tumor burden in 4T1 breast cancer.

To determine if the antitumor effects of SalpNG observed in K7M2-treated mice would also affect tumors generated from the invasive metastatic 4T1 breast cancer cell line, mice bearing 4T1 tumors were treated IV with 5x10^4 CFU of SalpNG. The resulting primary tumors were reduced approximately 30% compared to saline-treated controls (Figure 3-3A). To determine an effect on metastases, lungs were also harvested and weighed as with K7M2 mice to estimate metastatic tumor burden in the lungs. The difference in lung metastases between SalpNG-treated and PBS-treated groups was more dramatic than what was observed for the primary tumor, with an approximate 88% reduction in response to SalpNG treatment (Figure 3-3B).

αPDL1 scFv secretion does not improve anti-tumor efficacy of S. Typhimurium in 4T1 tumors.

In order to investigate the functionality of bacterially delivered αPDL1 scFv, a model with adequate tumor colonization that would respond to PD-L1 blockade was required. Hirano and colleagues recently reported a complete clearance of 4T1 tumors in BALB/c mice given a combination of an immune-stimulating agonistic αCD137 mAb and an inhibitory αPD-L1 mAb (163). Given our experience with the 4T1 model and the tumor-colonization observed in 4T1 tumors (Figures 2-9B and 3-8B), we sought to replicate the efficacy observed by Hirano and colleagues and validate a bacterially

delivered checkpoint blockade by treating 4T1 tumor-bearing mice with a combination of αCD137 and SalpαPDL1-Hly. In this experiment, a combination of αCD137 mAb and αPD-L1 mAb was used as a positive control for efficacy as reported (7). Additionally, SalpNG was tested as a control for comparison to SalpαPD-L1-Hly alone. Mice were treated with the indicated strains when tumors reached approximately 100 mm^3 by caliper. Indicated mice were given intraperitoneal αCD137 mAb twice weekly for two weeks and/or αPD-L1 mAb twice weekly for the duration of the experiment. While a modest effect on the primary tumor was observed for both SalpNG and SalpαPDL1-Hly, there was no significant difference in efficacy between these strains (Figure 3-4A). Additionally no improvement over SalpNG was observed in mice given both SalpαPDL1-Hly + αCD137 mAb treatment or the combination of αCD137 and αPD-L1 mAbs (Figure 3-4A). Mice given a combination of SalpNG and αPD-L1 mAb were excluded from the analysis due to lethal toxicity that occurred when these treatments were combined. Additionally, a similar efficacious effect of SalpNG treatment was observed on lung metastases as seen in previous experiments; however, there was no difference between SalpNG and SalpαPDL1-Hly (Figure 3-4B). Tumors from mice treated with either SalpNG or SalpαPDL1-Hly were homogenized, diluted, and plated as before to verify 4T1 tumor colonization. SalpNG and SalpαPDL1-Hly colonized tumors with an average of approximately 4×10^7 and 6×10^7 CFU/g of tumor, respectively, at 22 days post bacterial treatment.

S*. Typhimurium exhibits anti-tumor efficacy in a transgenic, autochthonous breast cancer model*

SalpNG reduces tumor burden and increases survival of BALB-neuT mice.

There are many differences in tumors generated in transplant models and those that model autochthonous (i.e. developed from a single cell in its place of origin) tumor development (see introduction pages 21-23). Virtually all preclinical reports of *S.* Typhimurium-based cancer therapy in mice have been performed in transplanted tumor models. Therefore in order to investigate the anti-tumor properties of SalpNG in an autochthonous tumor model, a GEM model of mammary carcinoma was used. Mammary fat pad tumors in female BALB-neuT mice became palpable (~50-60 mm^3) around 16 weeks of age. At this time (day 0), the mice typically had 1-3 palpable tumors. These tumors enlarged over time, and new tumors appeared on the remaining fat pads, usually until each mammary pad developed a tumor. Individual tumors were measured weekly by caliper, and their volume was calculated and combined to give a total tumor burden measurement for each mouse. When left untreated, average total tumor burden per mouse reached 5.66 cm^3 by day 35 (Figure 3-5A). In contrast, if the mice were given a single IV injection of 6x10^4 CFU of SalpNG at day 0, tumor progression was significantly delayed, and average total tumor burden at day 35 was only 0.85 cm^3, corresponding to an 85% tumor reduction (Figure 3-5A). This correlated to a significant increase in survival time of SalpNG-treated mice (median = 66 days) when compared to untreated mice (median = 35 days) (Figure 3-5B). In order to test if multiple injections of SalpNG improved efficacy, the experiments were repeated with mice treated on day 0 and every 21 days following. No difference in tumor burden or survival was observed between single and multiple treatments (data not shown).

Efficacy of S*. Typhimurium is correlated with increased infiltration of cytotoxic lymphocytes.*

An important role of NK cells and CD8 T-cells in the anticancer efficacy of χ4550-based strains has been demonstrated using transplant models (123). In order to examine the role of these immune cells in BALB-neuT breast cancer, tumors from mice were homogenized 21 days post-treatment, and tumor-infiltrating lymphocytes were isolated and characterized using flow cytometry. Tumors from treated mice contained greater than 10-fold more infiltrating CD8 T-cells than tumors from untreated mice. Similarly, infiltrating NK cell numbers were approximately 6-fold greater in treated mice, indicating an immune response in reaction to SalpNG treatment (Figure 3-6A). CD4 T-cells were also examined, but the difference between the treated and untreated groups was insignificant (data not shown).

Treatment with S*. Typhimurium increases monocytic myeloid-derived suppressor cells both systemically and within tumors.*

In spite of a reduction in tumor burden and an increase in survival time of BALB-neuT mice, eventually all treated mice succumbed to disease. We examined changes in myeloid-derived suppressor cell (MDSC) numbers as a potential contributor to tumor progression. MDSCs are a suppressive subset of immature myeloid cells that express CD11b and the Gr-1 epitope and are present in several cancer models including BALB-neuT breast cancer (161). MDSCs are conventionally subdivided into monocytic ($Ly6C^{Hi}$) and granulocytic ($Ly6G^{Hi}$) subsets, and while both subsets have been implicated in tumor immunosuppression and cancer progression, monocytic MDSCs have been shown to be more consistently immunosuppressive on a per-cell basis than granulocytic MDSCs (for more detail on MDSCs, see introduction pages 8, 9). We investigated whether SalpNG treatment affected MDSC presence in tumor tissue. When examined 21 days post-treatment, tumors from treated mice displayed a greater than 10-fold increase

in monocytic MDSCs, while granulocytic MDSCs were not significantly affected (Figure 3-6B-C). In addition, the ratio of monocytic to granulocytic MDSCs in the spleen was increased in response to treatment, suggesting that the increase in tumor-infiltrating monocytic MDSCs was due to a systemic immunological effect of the bacteria rather than a tumor-specific effect (Figure 3-6D).

ScFv-secreting strains did not improve anti-tumor efficacy in BALB-neuT mice over SalpNG.

To determine if the recombinant strains that secrete immune checkpoint inhibiting scFvs characterized in Chapter 2 would demonstrate greater anti-tumor efficacy than SalpNG, tumor-bearing BALB-neuT mice were treated as before but instead with a combination of SalpαPDL1-Hly and SalpαCTLA-4-Hly. These strains were used in combination due to the reported advantages of combinatorial immune checkpoint blockade (see introduction page 86). No significant improvement in efficacy over SalpNG was observed with the recombinant scFv strains (Figure 3-7A). This was despite tumor specific expression of PD-1 on infiltrating CD8 T-cells and PD-L1 expression in the tumor (Figure 3-7B-C).

Tumor-targeting of attenuated* S*. Typhimurium is inconsistent between tumor models

The lack of an efficacious improvement against BALB-neuT tumors using the scFv-secreting strains may be due to a lack of sufficient tumor-targeting. The propensity of *S*. Typhimurium to preferentially accumulate in tumor tissue over healthy tissues has been reported extensively (94). However, these observations have been from experiments performed in subcutaneous and orthotopic transplant mouse models.

Therefore we investigated the tumor-targeting propensity of SalpNG in autochthonous tumors in the BALB-neuT model. Twenty-one days following treatment with SalpNG, tumors and spleens were removed, homogenized and plated onto selective nutrient agar for colony formation. No CFU were found in any of the tumors processed. In contrast, CFU were found in each spleen tested, with an average of 1.5×10^4 CFU/gram tissue (Figure 3-8A).

The lack of tumor-targeting in the BALB-neuT model may explain the insignificant difference in efficacy between SalpNG and the scFv-secreting strains. Tumors from the K7M2 and 4T1 models were similarly examined for bacterial tumor-targeting. Unlike BALB-neuT tumors, 4T1 tumors contained approximately 1×10^7 CFU/g of tumor tissue at 17 days post treatment, compared to approximately 1×10^5 CFU/g of spleen (Figure 3-8B). CFU numbers in K7M2 tumors were difficult to quantify due to treated mice having such small tumor masses in their lungs, but by homogenizing and plating whole lungs and estimating tumor mass from total lung mass, CFU/g of tumor values were approximated. While bacteria were usually present to some degree in K7M2 tumors, the numbers were highly variable and were several orders of magnitude less than values commonly reported for tumor colonization (Figure 3-8C). Therefore despite the efficacy observed in all of the models tested, only the subcutaneously inoculated 4T1 tumors contained substantial bacterial colonization.

DISCUSSION

S. Typhimurium exhibits anti-tumor efficacy and immune effects in transplanted and autochthonous tumor models.

The native cytotoxicity of Gram-negative bacteria has led to its application as a single agent for the preclinical treatment of many tumor types (reviewed in (94)). We

observed a reduction in tumor burden in response to IV treatment with an attenuated *S.* Typhimurium strain carrying an empty expression vector (SalpNG) in mouse models of K7M2 osteosarcoma, 4T1 primary and metastatic breast cancer, and BALB-neuT autochthonous breast cancer.

The efficacious effects of *S*. Typhimurium have been attributed to immune stimulation, competition for nutrients and/or the direct induction of apoptosis of tumor cells by bacterial toxins (90, 99). Where examined, the efficacy we observed was correlated with an increased tumor infiltration of immune cells and a reduction in suppressive populations such as T-regs. Therefore, we believe the anti-tumor efficacy was mainly the cause of a general immune-stimulation in response to the bacteria that in turn stimulated an anti-tumor immune response. Although it is not clear whether the changes in tumor-infiltrating lymphocytes observed in K7M2 and BALB-neuT tumors of treated mice were tumor-specific or *Salmonella* specific, we suspect they are tumor specific because these changes were observed in tumors that were not colonized by *S.* Typhimurium.

Along with cytotoxic lymphocytes, we observed an increased number of monocytic MDSCs in the tumor tissue of SalpNG-treated BALB-neuT mice. This change was likely due to systemic immune-modulatory effects of the bacteria rather than a tumor-specific response, as we also observed an enrichment of monocytic MDSCs in the spleen. The lipopolysaccharide surface molecules on *S.* Typhimurium have been shown to increase the presence and suppressive activity of MDSCs (164, 165), and a recent report demonstrated the recruitment of monocytic MDSCs from the bone marrow to tissues during *S.* Typhimurium infection (166). The potential efficacy of *S.* Typhimurim-based cancer immunotherapy may not be fully realized until MDSC recruitment and/or inhibitory activity is addressed.

S. *Typhimurium efficacy was not improved by recombinant αPDL1-scFv secretion.*

We observed greater than 1×10^7 CFU/g of 4T1 tumor tissue 22 days post-treatment. According to Hirano and colleagues (7), if *Salmonella*-delivered αPD-L1 scFvs were properly blocking PD-1/L1 signaling, the tumors in mice treated with SalpαPDL1-Hly + αCD137 mAb would have been cleared; yet we observed no difference in anti-tumor efficacy between SalpNG and SalpαPDL1-Hly + αCD137 mAb. It could be that SalpαPDL1-Hly did not colonize 4T1 tumors at levels high enough to deliver a therapeutic concentration of αPDL1-scFv. However, we were also unable to reproduce the tumor clearance that was reported by treating mice with αCD137 and αPD-L1 mAbs (163). Therefore, the 4T1 model may not be a suitable model to test for functional PD-L1 blockade.

Additionally, in K7M2 and BALB-neuT models we observed no difference in efficacy between SalpNG and either SalpαPDL1-Hly or the combination of SalpαPDL1-Hly and SalpαCTLA-4. However, since there was a lack of adequate tumor colonization in these models, and thus no delivery of the scFvs to tumor tissue, improved efficacy over SalpNG would not be expected.

S. *Typhimurium tumor-targeting is inconsistent between tumor models.*

Interestingly, there were little to no bacteria colonizing the tumor tissue of two of the three models tested. Therefore, we conclude that the observed efficacy and immune cell recruitment were due to a systemic immune stimulation rather than a tumor microenvironment-specific stimulation. This may have also been true of the efficacy observed in the 4T1 model, as there was a less dramatic anti-tumor effect on the

colonized primary tumor than there was on the systemic metastases measured in the lungs.

The lack of tumor colonization in the K7M2 model could be explained by technical limitations and/or the metastatic tumors being insufficiently developed in the lungs of inoculated mice by the time bacteria were administered. However, the lack of tumor colonization in the BALB-neuT model was unexpected given the empirical evidence of attenuated *S.* Typhimurium strains accumulating to high levels in tumors in subcutaneous or orthotopic models. This observation may be attributed to differences in tumor development and microenvironment physiology between autochthonous tumors and tumors developed in transplantation models (167).

It is becoming increasingly clear that necrosis in tumors is important for bacterial colonization (118). Early necrosis in transplanted tumor models is often caused by the death of a majority of the inoculated tumor cells leading to an early inflammatory response and a necrotic center (116, 169). Since this necrosis is absent in early stage autochthonous tumors, future studies might benefit from the inclusion of radiation therapy or other strategies such as the addition of a vascular-disrupting agent to cause necrosis of tumor tissue and allow colonization to the degree that is observed in transplant models. Also, differences in vasculature development between autochthonous and transplant tumor models have lead to varying responses to treatments such as interleukin-12 (111). These differences may have similar implications in bacterial tumor colonization. The more chaotic and less mature vasculature that characterizes transplantation tumors may more readily hemorrhage in response to *S.* Typhimurium than the more mature vasculature of autochthonous tumors. This may allow the bacteria to more easily colonize transplant tumors than autochthonous tumors, as hemorrhaging

of tumor blood vessels may be required for infiltration of the bacteria into the tumor tissue (95).

The differences in tumor-targeting between preclinical transplant and autochthonous models could potentially explain the lack of bacterial colonization in tumor biopsies of reported clinical trials (107-109) that used attenuated *S.* Typhimurium for cancer treatment and might illustrate a limitation of *S.* Typhimurium as a viable tumor-targeting cancer therapy. Therefore, it may be prudent to specifically address *S.* Typhimurium's tumor-targeting capability before further assessment of its potential for delivery of cytokines or immune checkpoint blockades. Achieving consistent tumor-targeting in an autochthonous tumor model will likely be more predictive of successful targeting of human tumors. Advances in bacterial tumor-targeting will be addressed in the next chapter of this thesis.

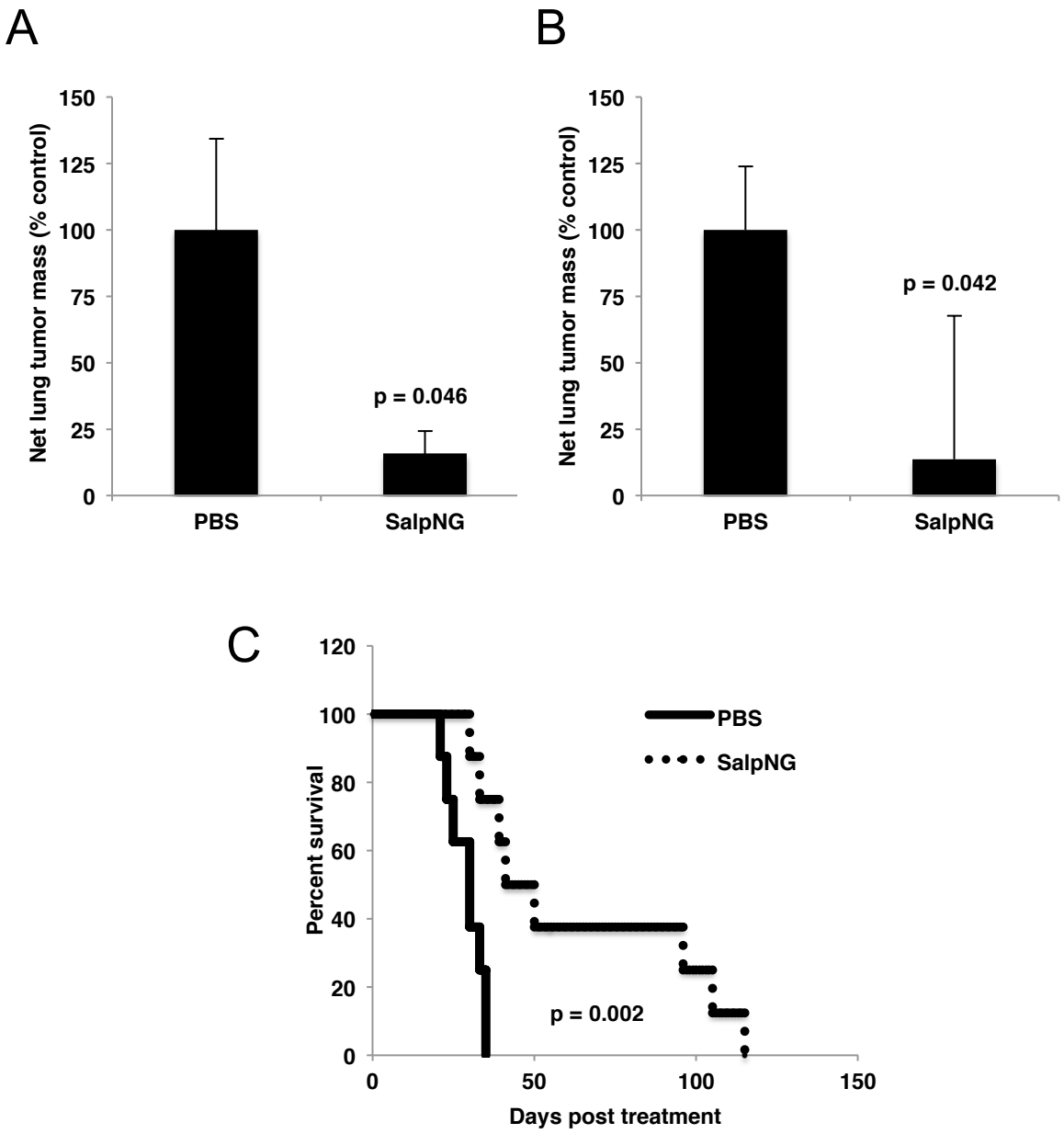

Figure 3-1: SalpNG demonstrates native anti-tumor efficacy in K7M2 pulmonary metastases.

Figure 3-1: SalpNG demonstrates native anti-tumor efficacy in K7M2 pulmonary metastases. (A) and **(B):** BALB/c mice were inoculated IV with 5×10^5 K7M2 osteosarcoma cells on day 0. Mice were treated with 5×10^4 CFU of SalpNG or saline control (PBS) on day 7 (A) or day 14 (B). On day 28, mice were harvested and "net tumor mass" was calculated for each mouse as lung weight – average lung weight of tumor free age/sex matched mice. Average values for treated mice are displayed as a percent of PBS-treated controls in each experiment. Bars indicate average of 4 (A) and 5 (B) mice per cohort. Error bars indicate 1 stdev. **(C)** Kaplan-meier curve comparing the survival of 8 mice per cohort inoculated and treated as in panel B. P-values were generated using a students unpaired T-test for (A) and (B) and a log-rank test for (C).

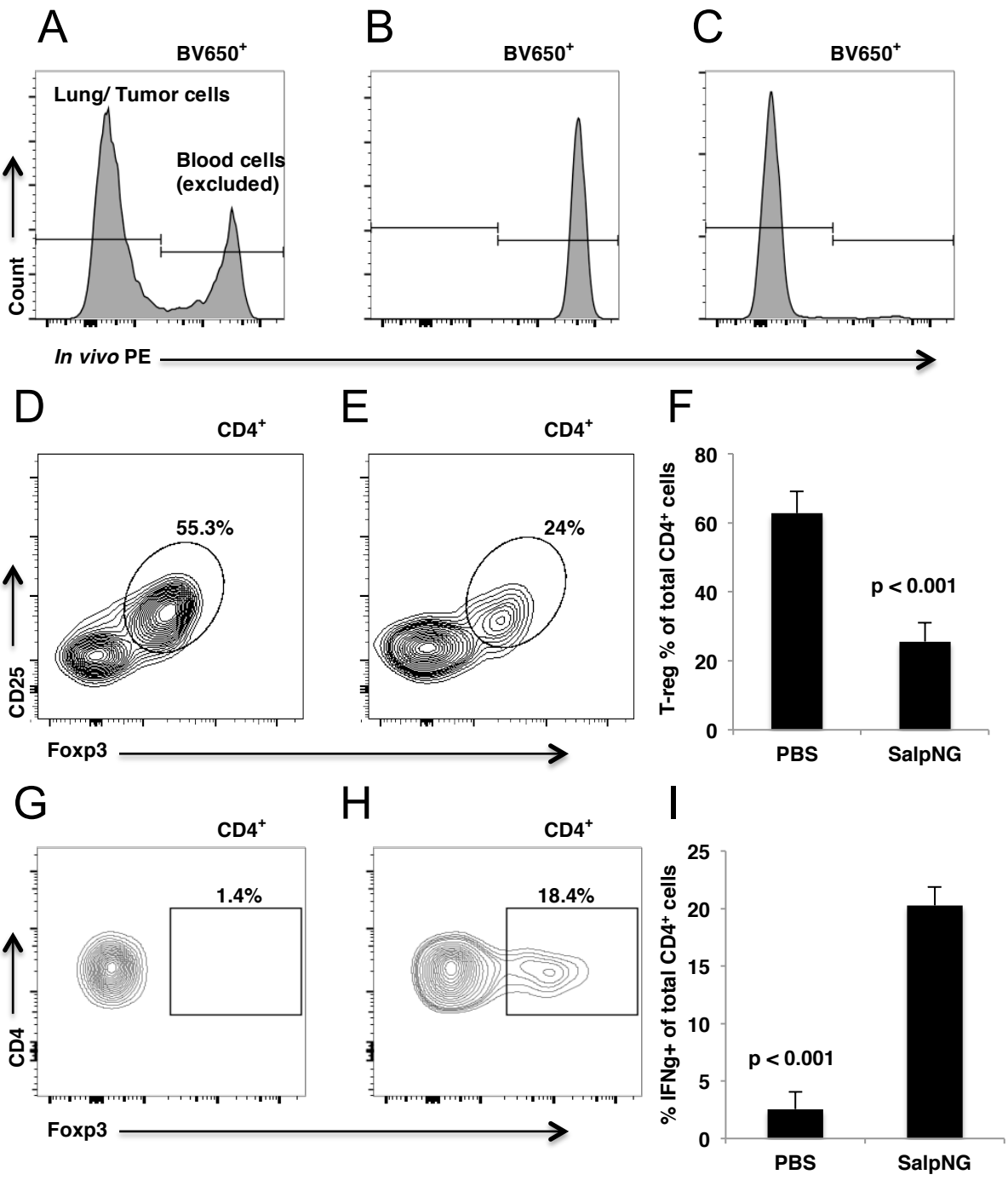

Figure 3-2: SalpNG treatment decreases the percentage of infiltrating T-regs and increases IFNγ expression of infiltrating CD4$^+$ T-cells.

Figure 3-2: SalpNG treatment decreases the percentage of infiltrating T-regs and increases IFNγ expression of infiltrating $CD4^+$ T-cells. (A-C) Intravascular staining allows the differentiation of leukocytes in lung/tumor tissue from blood leukocytes. An αCD45.2/PE antibody was injected into mice before harvesting and allowed to stain leukocytes in the blood. Cells isolated from homogenized lung tissues were then stained *ex vivo* with αCD45.2/BV650. $BV650^+/PE^+$ cells were excluded from analysis as blood cells and $BV650^+/PE^-$ cells were further analyzed in panels (D-I). A representative plot is shown in (A). Cells from blood (B) and lymph nodes (C) from each mouse were also stained as positive and negative controls, respectively, for CD45.2/PE staining. **(D-F)** Cells isolated from lungs of mice inoculated with K7M2 cells and treated two weeks later with PBS or SalpNG were fixed and stained for CD25 and Foxp3 expression. T-regs were defined as ($CD4^+$, $CD25^+$, $Foxp3^+$). Representative plots for PBS-treated and SalpNG-treated mice are shown in (D) and (E), respectively, and values for multiple mice are quantified in (F). **(G-I)** Cells prepped as in panels D-F were stained for intracellular IFNγ. Representative plots for PBS-treated and SalpNG-treated mice are shown in (G) and (H), respectively, and values for multiple mice are quantified in (I). N=4 mice/group. Bars indicated average + 1 standard deviation. P-values were generated using a student's unpaired T-test.

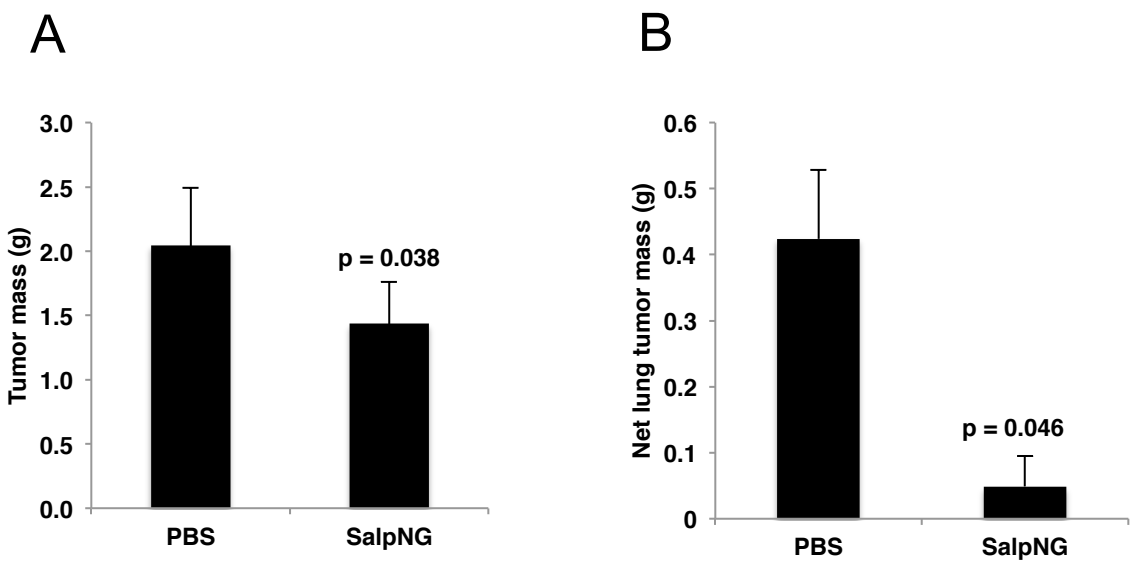

Figure 3-3: SalpNG treatment slightly reduces primary tumor burden and greatly reduces pulmonary metastases of 4T1 breast cancer.

Figure 3-3: SalpNG treatment slightly reduces primary tumor burden and greatly reduces pulmonary metastases of 4T1 breast cancer. (A) BALB/c mice were inoculated subcutaneously with 4T1 breast cancer cells on day 0 and treated IV with either PBS or 5×10^4 CFU SalpNG on day 11. Tumors were harvested on day 28 and weighed. **(B)** Mice inoculated and treated as in (A) were sacrificed 22 days post treatment, and their lungs were weighed to determine net tumor mass in lungs. N=6 mice/group in (A) and 3 mice/group in (B). Bars indicated average + 1 standard deviation. P-values were generated using a student's unpaired T-test.

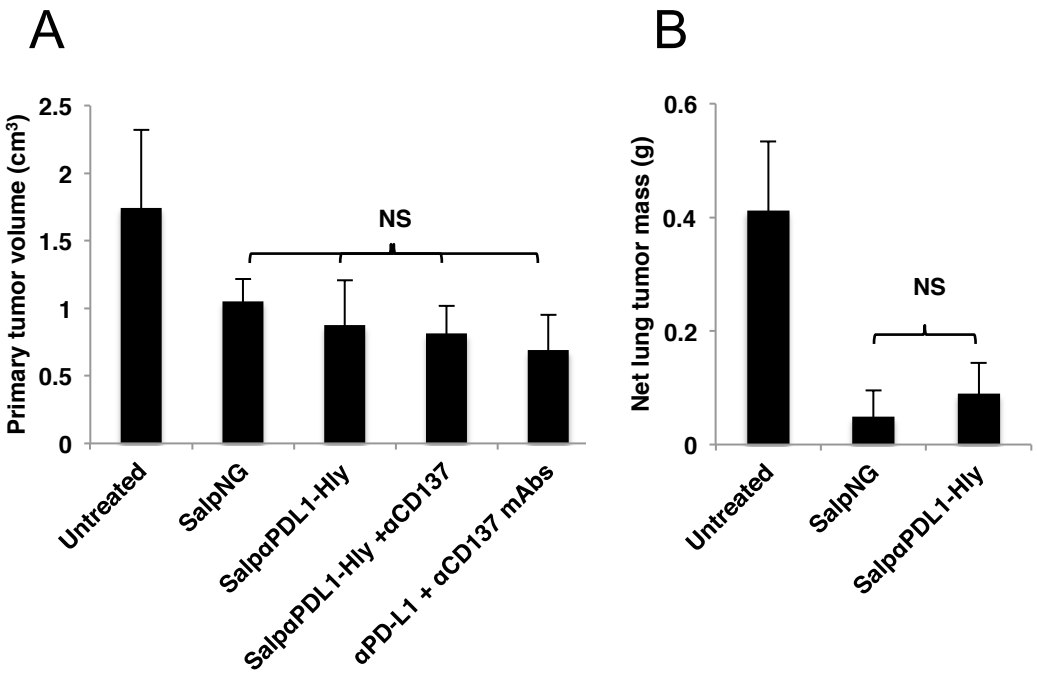

Figure 3-4: αPD-L1 scFv secretion does not improve anti-tumor efficacy of *Salmonella* in 4T1 tumors.

Figure 3-4: αPD-L1 scFv secretion does not improve anti-tumor efficacy of *Salmonella* in 4T1 tumors. BALB/c mice were inoculated subcutaneously with 4T1 (day 0) and treated with the indicated *S.* Typhimurium strains and/or antibodies. Bacteria were given as a single IV injection of 1×10^6 CFU on day 11, mAbs were injected IP at 125μg/injection twice weekly starting on day 11 and continuing two weeks for αCD137 and for the duration of the experiment for αPD-L1. Average tumor volume on day 28 (measured by caliper: $L\times W^2\times0.52$) is displayed for 4 mice per cohort in **(A)** and average net tumor mass of lung metastases on day 32 is displayed for 4 mice per cohort in **(B)**. Error bars indicate 1 standard deviation. NS= no significant difference based on ANOVA in A and a Student's unpaired T-test in B.

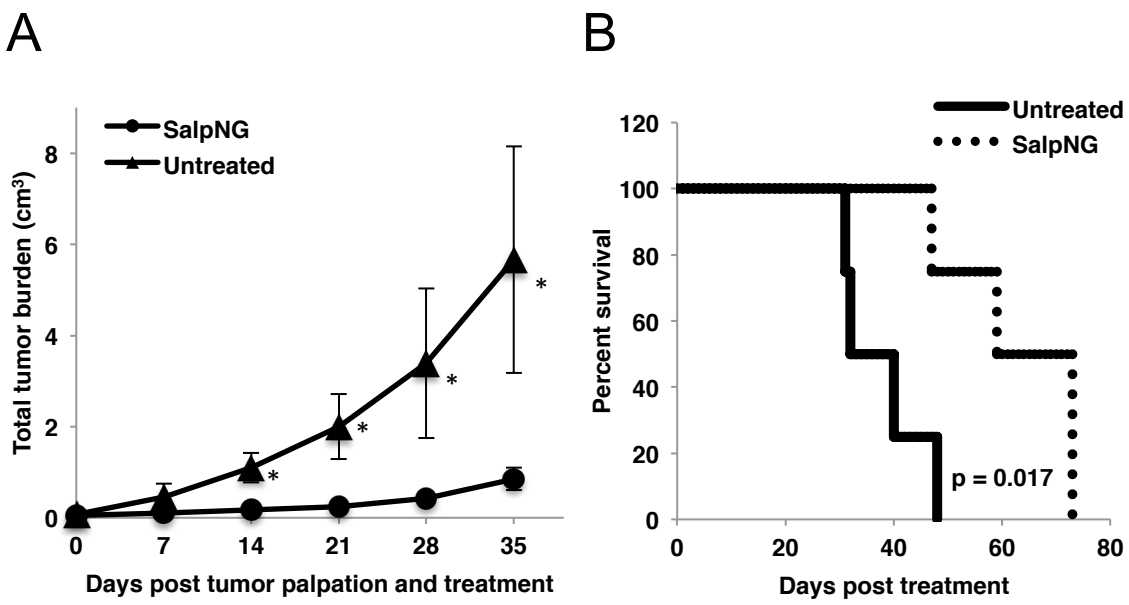

Figure 3-5: SalpNG reduces tumor burden and increases survival of BALB-neuT mice with autochthonous tumors.

Figure 3-5: SalpNG reduces tumor burden and increases survival of BALB-neuT mice with autochthonous tumors. (A) Mice were monitored for tumor development. Upon tumor palpation (day 0), mice were either treated with a single dose of 6×10^4 CFU of SalpNG or left untreated. Total tumor size was measured over time. Data displayed is an average + 1 standard deviation of 4 mice per group. * = p-value < 0.05 **(B)** Kaplan-Meier survival plot of treated and untreated mice shown in panel A. P-value was generated using the log-rank test.

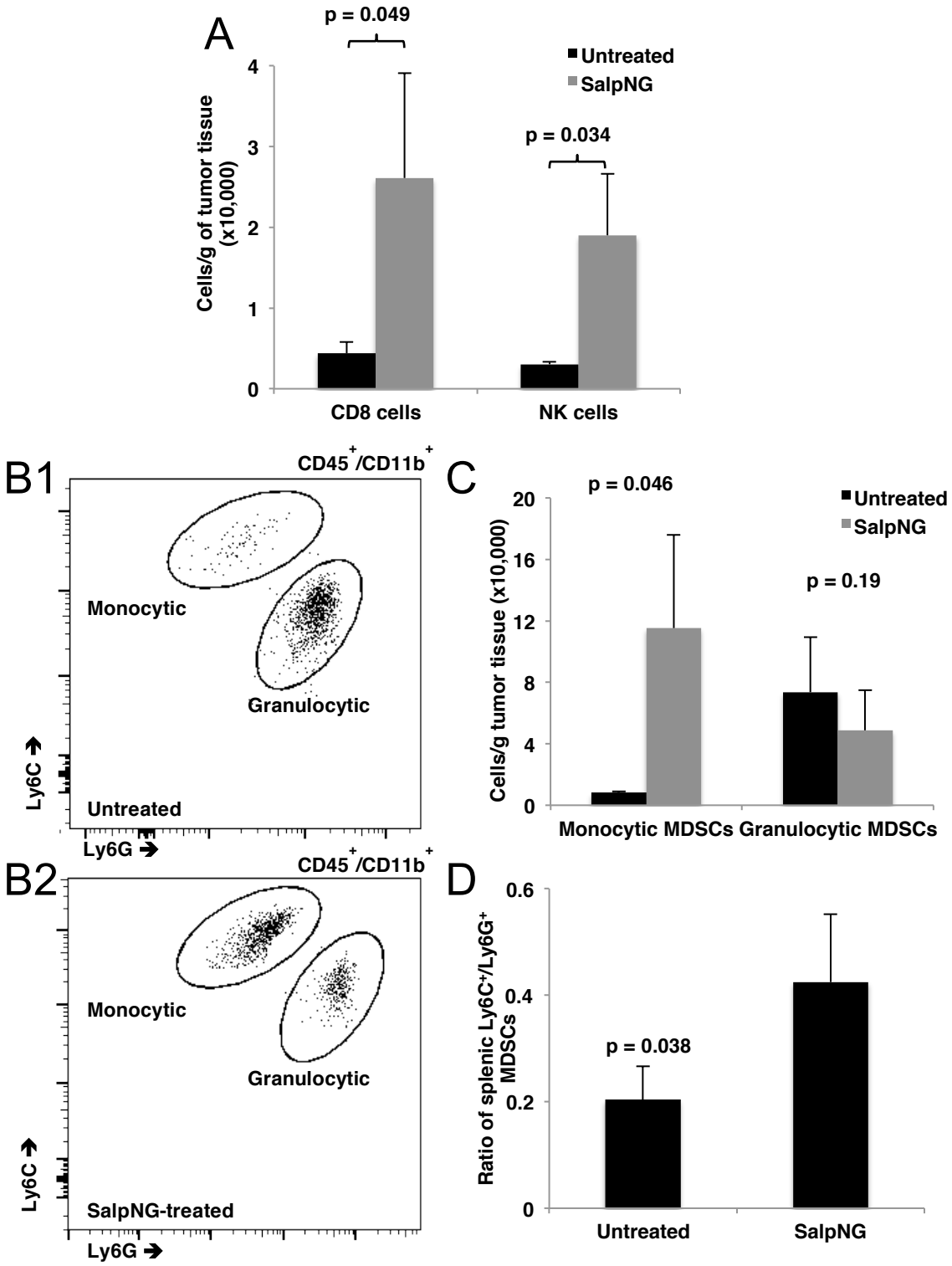

Figure 3-6: SalpNG treatment increases tumor infiltration of cytotoxic lymphocytes and causes enrichment of monocytic MDSCs.

Figure 3-6: SalpNG treatment increases tumor infiltration of cytotoxic lymphocytes and causes enrichment of monocytic MDSCs. (A) Infiltrating lymphocytes were isolated from the tumors of mice 21 days after SalpNG treatment. Cells were labeled with antibodies and analyzed using flow cytometry. CD8 and NK cells per gram were calculated based on tumor mass and cells counted. **(B-D)** MDSCs in tumor and spleen homogenates from treated or untreated mice were labeled with antibodies and identified using flow cytometry as monocytic ($Ly6C^{Hi}$) or granulocytic ($Ly6G^{Hi}$). Representative plots are shown in B1 (untreated) and B2 (treated), and resulting cells per gram of tumor tissue were quantified for multiple mice in (C). In (D) the average ratio of monocytic/granulocytic MDSCs in spleens from treated or untreated mice was calculated. Bars represent the average of 3 mice + 1 standard deviation. p-values were calculated using a Student's unpaired T-test.

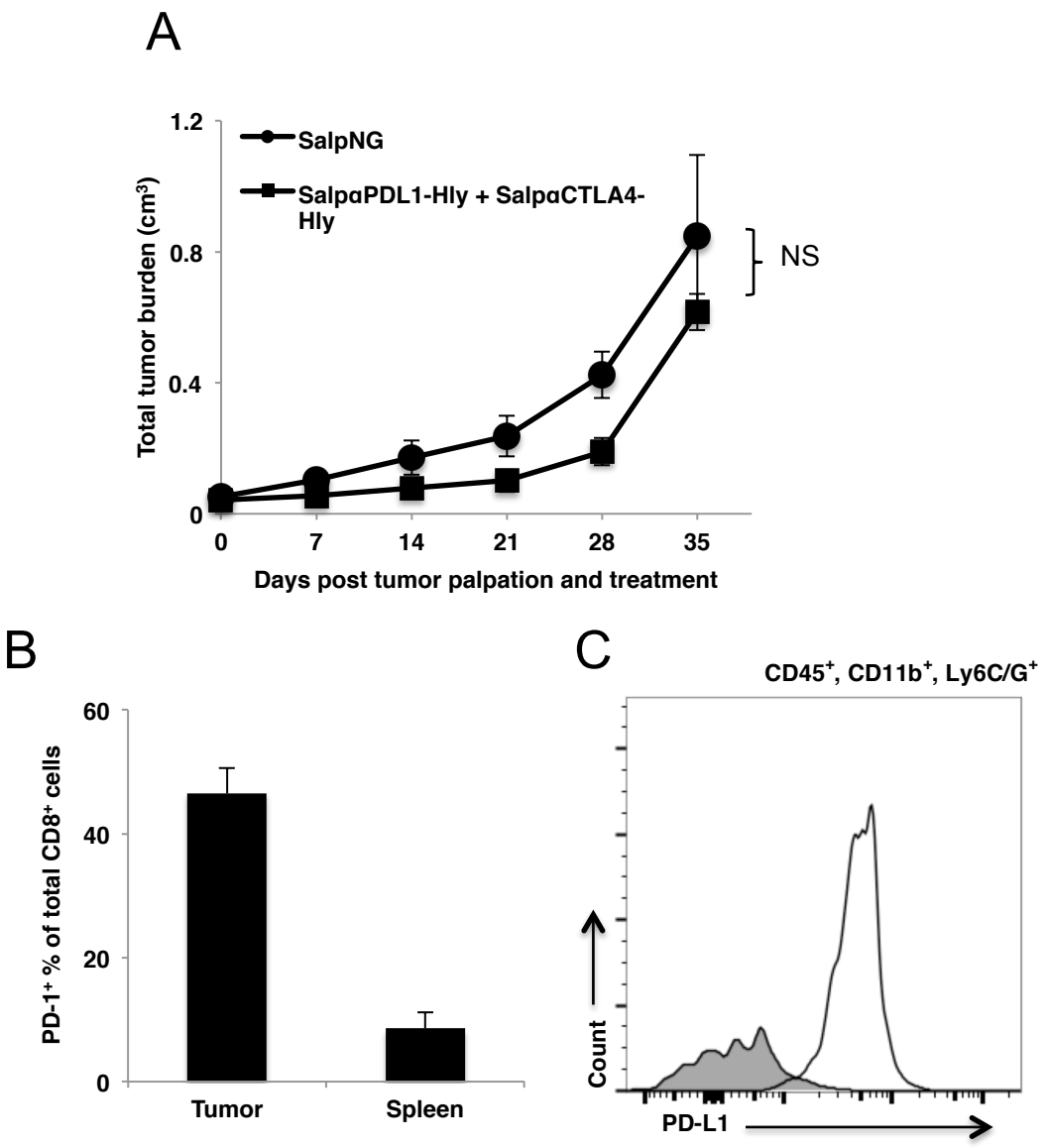

Figure 3-7: *S.* Typhimurium secreting αPD-L1 and αCTLA-4 scFvs does not improve efficacy in BALB-neuT mice, despite expression of PD-1 on infiltrating CD8 T-cells and PD-L1 on infiltrating MDSCs.

Figure 3-7: *S.* Typhimurium secreting αPD-L1 and αCTLA-4 scFvs does not improve efficacy in BALB-neuT mice, despite expression of PD-1 on infiltrating CD8 T-cells and PD-L1 on infiltrating MDSCs. (A) BALB/neuT mice were treated as in (Figure 3-4) with either 6x10^4 CFU SalpNG or a combination of SalpαPDL1-Hly and SalpαCTLA-4-Hly (3x10^4 CFU each). Total tumor burden was measured overtime. Data displayed is an average + 1 standard deviation of 4 mice per group. **(B)** Cells isolated from homogenized tumors and spleens were stained for CD8 and PD-1 and examined using flow cytometry. The average percent PD-1^+ CD8 T-cell fraction is displayed for 3 mice + 1stdev. **(C)** MDSCs isolated from tumors on BALB-neuT mice were stained for PD-L1 expression (open histogram) or isotype control (shaded histogram).

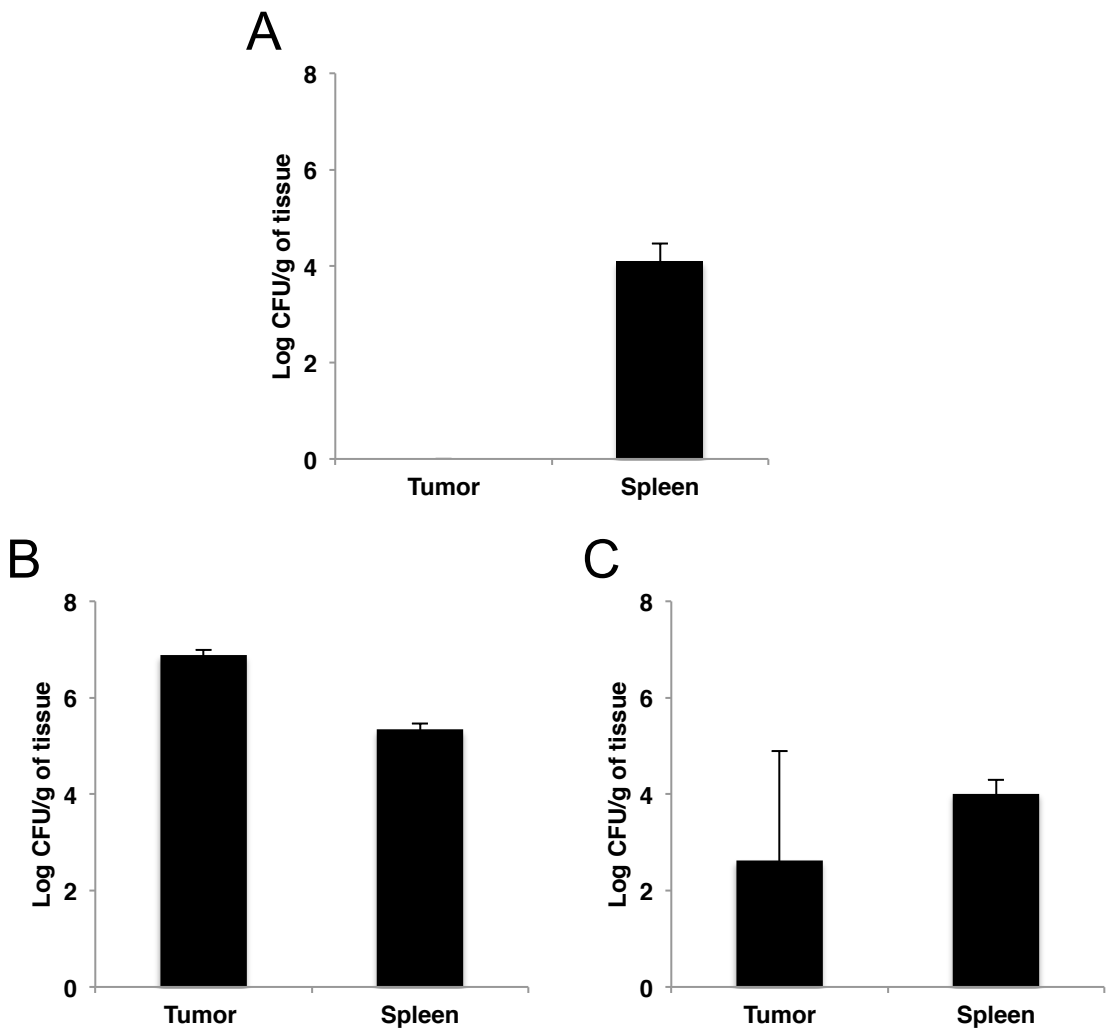

Figure 3-8: The tumor-targeting propensity of SalpNG is inconsistent between tumor models.

Figure 3-8: The tumor-targeting propensity of SalpNG is inconsistent between tumor models. BALB-neuT mice bearing palpable tumors **(A),** BALB/c mice bearing subcutaneous 4T1 tumors **(B)**, or BALB/c mice incoculated with IV K7M2 cells **(C)** were treated with IV SalpNG. Depending on mouse health, mice were sacrificed 17-21 days post bacterial treatment and their tissues were harvested, homogenized, and plated on LB agar overnight for CFU enumeration. Bars indicate the averages of 6 mice in (A), 3 mice in (B), and 3 mice in (C). Error bars indicate 1 standard deviation.

CHAPTER 4

BACTERIAL TARGETING OF AUTOCHTHONOUS TUMORS IS ENHANCED BY VASCULAR DISRUPTION AND PD-L1 INHIBITION

Authorship Note: Jeremy Drees performed all experimental work in this chapter alone or with assistance from colleagues including Michael Mertensotto (Research Scientist U of MN Dept. Surgery), Lance Augustin (Assistant Prof. U of MN Dept. Surgery), and David Urso (Research Scientist U of MN Dept. Surgery).

Reprint Disclaimers:
Sections of this chapter have been adapted with permission from the *Journal of Cancer,* Ivy Spring International Publisher
Citation: *Drees JJ, Mertensotto MJ, Augustin LB, Schottel JL, Saltzman DA. Vasculature Disruption Enhances Bacterial Targeting of Autochthonous Tumors. J Cancer 2015; 6(9): 843-848.*

INTRODUCTION

Many published reports demonstrate the efficacy of attenuated *Salmonella enterica* Typhimurium (*S.* Typhimurium) strains in mouse models of cancer, either by themselves or as vectors to deliver recombinant therapeutic proteins directly to the tumor microenvironment (94). In addition to efficacy, these studies report reproducibly high tumor colonization numbers of 10^8-10^9 colony-forming units (CFU) of *S.* Typhimurium per gram of tumor tissue with ratios of over 1000:1 when compared to healthy tissue (171).

When tested clinically, the results were largely disappointing. This was most likely due to insufficient tumor colonization. When tumors from 32 patients in clinical trials of parenterally administered *S.* Typhimurium strain VNP20009 were biopsied, less than 20% contained any measurable *S.* Typhimurium colonization (107-109). The results of the VNP20009 trials were unexpected given the preclinical demonstrations of bacterial colonization of subcutaneous tumors. Since all of the preclinical studies were performed in mouse transplant models of cancer, it may be that the tumor-targeting observed in

these models is due, at least partially, to characteristics of transplanted tumors that do not accurately mimic the autochthonous tumors that develop in human cancer. Necrotic tissue and hemorrhage of tumor blood vessels have been demonstrated to be important for the colonization of murine tumors (95, 118). Moreover, both necrosis and immature vasculature have been shown to be present at artificially high levels in transplant models. Indeed, transplantation tumors often contain large necrotic regions due to rapid growth of the inoculated tumor cells, inflammation and lack of mature vasculature, whereas human tumors develop much more slowly from a single cell and tend to be less necrotic due to suppression of an inflammatory immune response and coincident development of vasculature (111, 116, 117). These observations may help explain the difference between the high bacterial colonization of tumors in transplantation mouse models and the low colonization observed in clinical studies.

The BALB-neuT model is a genetically engineered mouse (GEM) model in which mammary tumor development is driven by expression of a constitutively active rat homolog of human epidermal growth factor receptor 2 (161). In this model, autochthonous tumors develop over several months and are palpable in the mammary pads of female mice around 16 weeks of age. In Chapter 3 of this thesis, anti-tumor efficacy was observed in the BALB-neuT model with attenuated *S.* Typhimurium treatment. Yet, similar to results reported in human trials, no bacteria were observed in tumor tissue of treated mice at the time point tested, and the reduction in tumor burden was concluded to be due to a systemic immune response.

To address bacterial tumor-targeting, we compared colonization of the transplantation tumors that develop in BALB/c mice subcutaneously inoculated with the syngeneic 4T1 breast cancer cell line to colonization of the autochthonous tumors that develop sporadically in the mammary glands of BALB-neuT mice. One approach that

has been used to cause necrosis in tumors and enhance the targeting of anaerobic *Clostridium* spores to transplant tumors is the administration of the vascular-disrupting agent (VDA) combretastatin A-4 phosphate (CA4P) (172). Therefore, we also investigated the use of CA4P to improve *S.* Typhimurium targeting of autochthonous tumors in BALB-neuT mice.

METHODS

S*. Typhimurium strain growth and preparation for treatment*

S. Typhimurium strains VNP20009 (Δ*msb*, Δ*purI*) (106) and SL3261 (Δ*aroA*, Δ*hisG*) (173) were obtained from The American Type Culture Collection (ATCC #202165) and The *Salmonella* Genetic Stock Centre (SGSC #439), respectively. Cultures of VNP20009 and SL3261 were grown from single colonies in lysogeny broth (LB) and MSB broth (174), respectively, at 37ºC until reaching mid-log phase at approximately 10^8 Colony Forming Units per ml (CFU/ml). Cultures were then chilled by swirling the flasks in ice water, and diluted in ice-cold PBS to concentrations required for injections.

Mouse maintenance

All mice were maintained in specific pathogen free conditions and fed standard mouse chow (Harlan). Research Animal Resources at the University of Minnesota provided animal care. All protocols were approved by the Institutional Animal Care and Use Committee.

4T1 experiments

4T1 cells (ATCC #CRL-2539) were grown in RPMI-1640 medium containing 10% fetal bovine serum. Cells were detached from flasks using 0.05% trypsin-EDTA, counted with a hemocytometer, washed with sterile PBS, and diluted to the appropriate concentration prior to injection. Female BALB/c mice of approximately 12 weeks of age were given a subcutaneous injection of 1×10^5 4T1 cells in 50 µL of sterile PBS superficial to the right inguinal mammary fat pad. Tumor growth was measured over time by caliper. Mice were treated with *S.* Typhimurium by IV injection when tumors reached approximately 400 mm^3 volume calculated as an ellipsoid (length × width × depth × 0.52).

BALB-neuT experiments

BALB-neuT colony maintenance and husbandry was performed as previously described (175). Tumor growth was monitored over time. Mice were treated by IV injection with *S.* Typhimurium when a single tumor reached the indicated sizes. In most cases, mice had additional smaller tumors on other mammary pads; these tumors were not considered in the analyses. Mice were either euthanized for bacterial CFU enumeration or measured over time for tumor response to treatment. Tumors were measured with a digital caliper, and tumor volumes were calculated as length × width × depth × 0.52.

Treatment of mice

Mice were injected IV with the indicated CFU of the appropriate *S.* Typhimurium strain in 100 µL of PBS via the tail vein. In some cases as indicated, bacteria were injected twice, 3 hours apart. For VDA pre-treatment, mice were given two IV injections of 0.4 mg (20 mg/kg) of combretastatin A-4 phosphate (CA4P): one injection 48 hours

prior to and one injection immediately before *S.* Typhimurium treatment. Similarly as indicated, some mice were injected with the same CA4P dose twice, 3 hours apart (i.e. four VDA injections total). For mice treated with anti-IL-6, 1 mg of anti-mouse IL-6 (αIL-6) monoclonal antibody (mAb) (MP5-20F3, BioXCell) was injected IP immediately following the first *S.* Typhimurium injection.

Tissue harvest and CFU enumeration

Mice were euthanized 48 hours post-*S.* Typhimurium administration. Tumors and spleens were harvested and minced with sterile razor blades to about 1 mm diameter pieces. Minced tissues were homogenized in 3 ml of sterile PBS using gentleMACS M Tubes (Miltenyi Biotec) with a gentleMACS Tissue Dissociator (program RNA_01). The homogenate was serially diluted in sterile PBS, plated on LB agar, and incubated for 16-18 hours at 37°C for CFU enumeration. For histology, tumors were harvested from untreated control mice and from mice 48 hours after administration of 0.4 mg CA4P. Tissue was fixed in 10% neutral-buffered formalin solution for two days followed by 70% ethanol for two days. Tissues were then paraffin-embedded, sectioned and stained with hematoxylin and eosin (H&E) according to standard protocols.

*Generation of luminescent (*lux*)* S*. Typhimurium strains*

The *luxCDABE* operon was inserted into the chromosome of DS3262 (see Chapter 2 methods for the generation of DS3262) using a Tn7 transposon method as described by McKenzie and Craig (176). Briefly, the *luxCDABE* operon was PCR-amplified from the pAKlux2 plasmid (Addgene plasmid #14080) using the primers: Fwd: 5'ATGACTAAAAAAATTTCATTCATTATTAACGGC and Rev: 5' TTATCAACTATCAAAC GCTTCGGTTAAG. The *luxCDABE* operon was then inserted into a plasmid containing

the *lacUV5* promoter and re-amplified with the *lacUV5* promoter with primers containing PacI and Xho1 sites to generate *lacUV5-lux*CDABE. The pGRG36 plasmid (Addgene plasmid #16666; temperature sensitive for replication) and *lacUV5-luxCDABE* were digested with PacI and XhoI restriction endonucleases and ligated with T4 DNA ligase (New England Biolabs). The resulting plasmid was amplified in *Stbl3 E. coli* cells and then used to transform electrocompetent DS3262 cells. Transformed cells were then cured of the delivery plasmid by growing at 42°C. The resulting DS3262-*lux* strain was transformed with pNG or pTrc-αPDL1-Hly to generate the luminescent *S.* Typhimurium strains DSpNG-*lux* and DSpαPDL1-Hly-*lux*, respectively. The pNG and pTrc-αPDL1-Hly plasmids were described in Chapter 2 of this thesis.

In vivo imaging of tumor colonization

To measure the radiance of tumors in mice treated with luminescent bacteria, mice were anesthetized by isoflurane inhalation at 3.5% in oxygen and imaged using an IVIS Spectrum *In Vivo* Imaging System with Living Image software (PerkinElmer). Total flux (luminescence) was acquired for 60 seconds and recorded as radiance (photons/sec/cm^2/sr) for the tumors of interest.

RESULTS

Attenuated S. *Typhimurium targets subcutaneous transplant but not autochthonous tumors.*

Reports of cancer treatment using the attenuated *S.* Typhimurium strain VNP20009 demonstrated successful targeting of transplanted mouse tumors with IV

injections. In a phase I clinical trial, the maximum tolerable dose of IV VNP20009 in human cancer patients was 3×10^8 CFU/m^2 (177). This dose translates to 2×10^6 CFU per 20 g mouse. In order to avoid toxic effects, we used a dose of 5×10^5 CFU. IV administration of this dose to mice did not result in significant weight loss compared to saline-treated controls (data not shown). To verify successful tumor-targeting in a transplant model of breast cancer, 4T1 cells were injected subcutaneously superficial to the mammary fat pads of female BALB/c mice. When tumors reached 400 mm^3 in volume, mice were given a single IV injection of VNP20009. Mice were harvested 48 hours post injection and their tissues were examined for bacterial colonization. In agreement with published studies (94), we observed invariably high tumor colonization of greater than 1×10^8 CFU/gram of tumor tissue, which was more than 1000-fold greater than colonization of the spleen (Figure 4-1A). To investigate the colonization of autochthonous tumors, BALB-neuT mice with size-matched mammary tumors were given the same injection of VNP20009 and examined 48 hours later for tumor colonization. Compared to 4T1 tumors, the autochthonous BALB-neuT tumors contained approximately 10,000-fold fewer CFU/g (Figure 4-1A). While tumor colonization was greatly reduced in the autochthonous tumors, splenic colonization was similar when compared to mice bearing 4T1 tumors (Figure 4-1A).

It has been suggested that the failure of VNP20009 to successfully target human tumors may be due to its lack of lipopolysaccharide (LPS) endotoxin, which may elicit a cytokine-dependent blood influx that is critical for tumor colonization (90, 95). To address whether a Lipid A^+ strain would result in better BALB-neuT tumor colonization, we treated both 4T1 and BALB-neuT tumor-bearing mice as before using the attenuated *S.* Typhimurium strain SL3261. This strain has been studied for tumor colonization

extensively (for background on this strain, see Chapter 2 of this thesis). As observed with VNP20009, SL3261 readily colonized 4T1 tumors, but not autochthonous BALB-neuT tumors (Figure 4-1B). In attempts to improve tumor colonization, we tested doses of SL3261 and VNP20009 containing up to 5×10^6 CFU and also included "primer" doses of varying sizes, which have been reported to improve tumor-targeting in some instances (178). While increasing colonization marginally, these dosing strategies were limited by toxicity, as mice that received 2×10^6-3×10^6 total CFU of either strain experienced significant weight loss, and doses $>3\times10^6$ CFU were lethal in some cases (data not shown).

Vascular disruption improves bacterial targeting of autochthonous mammary tumors.

As an alternative approach to improve tumor-targeting, we investigated whether pre-treatment of mice with a vasculature-disrupting agent (VDA) would make autochthonous tumors more susceptible to colonization by affecting vasculature and necrosis. VDAs cause the destruction of immature vasculature that is often found in tumor tissue, which leads to hemorrhagic necrosis (179). Female BALB-neuT mice with autochthonous mammary tumors were given two IV injections of the VDA combretastatin A-4 phosphate (CA4P) at 20 mg/kg, 48 hours apart. Immediately following the second CA4P injection, mice were injected IV with 5×10^5 CFU of SL3261 and harvested two days later to determine tissue colonization. When SL3261 injection was combined with CA4P pre-treatment, there was an approximate 1000-fold CFU/g increase in tumors when compared to mice not pre-treated with CA4P, while splenic colonization was not affected (Figure 4-1B). The combination of CA4P pre-treatment with SL3261 treatment

in this manner did not cause any overt behavioral changes or significant weight loss of the mice.

To verify the necrotic effect of CA4P pre-treatment on tumor tissue, tumors from BALB-neuT mice treated with CA4P were excised two days post-treatment and histologically compared to tumors from untreated mice. As expected, CA4P treatment induced the formation of necrotic regions that were largely absent in the tumors of untreated mice (Figure 4-2A-B); however, the extent of necrosis was somewhat less than expected. This may have been due to the more mature vasculature of autochthonous tumors being less responsive to the disruption caused by CA4P than is typically observed for transplanted tumors. Hill and colleagues demonstrated an improved effect of CA4P on spontaneous tumors when administered twice in a 3-hour period rather than once (115). Similarly, we observed more extensive necrosis of BALB-neuT tumors when CA4P was administered in two equal doses separated by 3 hours (Figure 4-2C).

Split dosing of VDA and S. Typhimurium further improves the targeting of autochthonous tumors.

BALB-neuT mice bearing 400mm^3 tumors typically have greater than a cubic cm of systemic tumor burden, which may be physiologically unrealistic for efficacy studies. Therefore we investigated the VDA-assisted targeting of smaller tumors. When CA4P pretreatment was administered as described previously (Figure 4-3A), and mice were treated IV with 5×10^5 CFU of DSpNG (SL3261-based strain carrying an empty expression vector), 150-200mm^3 tumors were examined for colonization. A similar degree of colonization was observed for some tumors; however, colonization was less consistent (Figure 4-4). In light of the increased necrosis observed with the split CA4P

dose (Figure 4-2C) and the reported advantage of incorporating a similar primer dosing strategy for bacterial tumor-targeting (178), we investigated whether combining these approaches would further improve the consistency of autochthonous tumor-targeting. When CA4P and bacterial injections were administered as a dose that was split between 3 hours (illustrated in Figure 4-3B), the resulting tumor colonization was more consistent (Figure 4-4); however, this treatment strategy also caused an acute toxicity that led to weight loss and, in rare cases, death of the treated mice. This toxic effect was only observed when both CA4P and *S.* Typhimurium were administered together, as neither agent alone was notably toxic at these levels (Figure 4-5). We hypothesized that the toxicity observed was caused by a systemic cytokine release in response to the bacteria, the effects of which were augmented by the vasculature disrupting effects of CA4P. One strategy that has been used to prevent the toxic effects of a systemic cytokine release is the blockade of IL-6/IL-6-receptor signaling. To investigate whether IL-6 antagonism could prevent the toxic effects of the split CA4P and *S.* Typhimurium dosing strategy, treated mice were given a single 1 mg IP dose of an αIL-6 mAb following the first bacterial injection (Figure 4-3C). The addition of αIL-6 not only reduced the toxic effects of mice given 5×10^5 total CFU of DSpNG (split into two 2.5×10^5 doses) but also allowed an increased non-toxic administration of 1×10^6 total CFU (Figure 4-5).

Anti-PD-L1 scFv expression may improve tumor colonization in BALB-neuT tumors, leading to improved tumor suppression.

While VDA treatment improved the colonization of autochthonous BALB-neuT tumors, not all tumors were colonized equally, and it was unclear how long *S.* Typhimurium remained in tumor tissue. This made it difficult to correlate tumor colonization with anti-tumor efficacy. In order to follow individual tumor colonization

overtime, DSpNG and DSpαPD-L1-Hly were engineered to express bacterial luciferase (*lux*) by inserting the *luxCDABE* operon into the bacterial chromosome. This allowed an estimation of tumor colonization of individual tumors over time by measuring the radiance (photons/second/cm^2/steradian) of live mice (Figure 4-6). Due to the single copy chromosomal expression of *lux,* only tumors that contained an approximate minimum colonization of 5×10^6 CFU/g were detectable; tumors that contained fewer bacteria were below the background radiance of the mice (approximately 1.3×10^4).

To examine tumor colonization and growth overtime after *S.* Typhimurium treatment, BALB-neuT mice bearing at least one tumor between 150-250 mm^3 were treated with CA4P, αIL-6 and 1×10^6 CFU of DSpNG-*lux* as illustrated in Figure 4-3C. By measuring tumor radiance, initial tumor colonization was observed at 2-3 days for most mice; however most colonization dissipated to undetectable levels within approximately one-week post-bacterial injection (Figure 4-7A,C). When mice were treated similarly with DSpαPD-L1-Hly-*lux*, a higher degree of tumor colonization was observed for many tumors, which was often measurable for more than 20 days (Figure 4-7B,C). To determine whether this improved tumor colonization affected the anti-tumor efficacy of *S.* Typhimurium, the growth of tumors with "high" colonization ($>1\times10^5$ radiance) and tumors with "low" colonization ($<1\times10^5$ radiance) was compared for treated mice. The growth of individual tumors from untreated mice was also included for comparison. Untreated BALB-neuT tumors between 150-250 mm^3 grew an average of 463% in 19 days (Figure 4-7D). Tumors from treated mice with low bacterial colonization showed significantly less growth than those from untreated mice, with an average volume increase of 207% in the same time frame (Figure 4-7D), corroborating the systemic anti-tumor effects of *S.* Typhimurium treatment that was described in Chapter 3. The growth of tumors in treated mice that displayed high tumor colonization was further reduced to

43% over 19 days, indicating a significantly improved therapeutic effect of *S.* Typhimurium treatment when tumors were adequately colonized. Tumors from mice treated with αPD-L1 mAb were also examined for growth and did not differ significantly from tumors on untreated control mice (Figure 4-7D)

DISCUSSION

Vasculature disruption enhances bacterial targeting of autochthonous tumors.

The use of bacteria as nontoxic cancer therapy is based on the ability of virulence-attenuated bacterial strains to specifically target tumor tissue. This characteristic is highly reproducible in murine tumors developed from transplanted cells or tissues (94). In the current study, however, we observed that the more clinically relevant autochthonous BALB-neuT tumors are much less readily colonized by IV-administered bacteria than are transplanted subcutaneous 4T1 tumors. These results are consistent with *S.* Typhimurium failing to colonize tumors when tested in a clinical setting and may explain the lack of significant efficacy observed in the clinical trials (107-109). Therefore, it is important for future preclinical studies of bacterial tumor colonization to consider the utilization of autochthonous models that more closely mimic the development of human tumors.

Recently reported studies suggest that *S.* Typhimurium colonization of tumors is constrained by both the amount of necrotic space and the capacity of tumor vasculature to facilitate bacterial extravasation (95, 110, 118). Because CA4P causes hemorrhagic necrosis by breaking down the epithelial wall of immature vasculature in tumors (179), we tested its ability to enhance colonization of autochthonous tumors by IV administered *S.* Typhimurium. The observed 1000-fold average increase in colonization with CA4P pre-treatment confirmed the ability of this VDA to enhance tumor colonization. While

CA4P increased necrotic regions in the tumors of BALB-neuT mice, it is not clear if extravasation of bacteria from vasculature, establishment of necrotic regions, or both contributed to the colonization of BALB-neuT tumors. However, in preliminary optimization experiments (not shown), we found that the timing of the two CA4P doses was important, and a single dose of CA4P was ineffective at improving tumor colonization. The dosing strategy described in this report that included two administrations 48 hours apart followed immediately by bacterial injection was optimal. We suspect that the first dose causes the development of necrotic regions important for the colonization (Figure 4-2) and the second injection disrupts the nascent vasculature that begins to form after the first injection causing hemorrhage of the tumor blood vessels and facilitating entry of bacteria into the tumor. Experimentation to optimize the timing and concentration of CA4P dosing may clarify the relative contribution of each mechanism to improved bacterial colonization.

Much of the literature describing the effects of VDAs on tumor vasculature and necrosis includes studies performed in transplanted subcutaneous models. Conclusions drawn from these models may overestimate the effects of VDA treatment due to the unnaturally immature vasculature that characterizes the rapidly growing inoculated tumors. One of the few studies published that characterized the effects of VDA treatment in autochthonous tumors reported a reduced effect of CA4P on autochthonous tumors compared to transplanted tumors. The study reported a single CA4P dose induced a 40% reduction of the functional vasculature of subcutaneous transplanted CaNT adenocarcinoma tumors, whereas significant vasculature disruption was not observed in autochthonous T138 mammary tumors. However, when mice bearing autochthonous T138 tumors were given the same CA4P dose administered as two half-doses three hours apart, functional vasculature in the tumor was reduced approximately 50% (115).

Similarly, we observed a greater extent of necrosis in the tumors of mice treated with two CA4P injections three hours apart than those from mice that were injected once, and the combination of CA4P and *S.* Typhimurium, when similarly injected twice 2 days following the CA4P pretreatment, improved the consistency and the degree of bacterial tumor-targeting. However, this treatment strategy also caused an adverse toxic effect that we suspect is due to a systemic cytokine release in response to the combination of intravenous bacteria and CA4P. In support of this hypothesis, the IP administration of an anti-mouse IL-6 antibody immediately after the first bacterial injection abrogated the toxic effect and allowed an increase bacterial dose without increased toxicity. Continued investigation of how autochthonous tumors can be conditioned in this manner to increase bacterial colonization will increase the likelihood of successful clinical translation of bacterial cancer therapy.

Anti-PD-L1 scFv expression may improve tumor colonization in BALB-neuT tumors, leading to improved tumor suppression.

When DSpαPDL1-Hly was examined for tumor-targeting propensity, we observed a higher degree and duration of colonization than the same bacterium carrying an empty expression vector (DSpNG-*lux*). All tumors that displayed lasting radiance of greater than 1×10^5 (p/s/cm^2/st), corresponding to approximately 2.5×10^7 CFU/g, were in mice treated with DSpαPDL1-Hly. It has recently been shown that functional PD-L1 is important for the clearance of *Salmonella* infections in mice (180). Additionally, PD-L1 can act as a positive co-stimulatory molecule in *Listeria* infections (181) and may be important for the survival of activated CD8 T-cells (182). In light of these counterintuitive reports, it may be that expression and secretion of αPDL1 scFv from *S.* Typhimurium gives it a degree of protection that allows more robust and lasting tumor colonization.

When highly colonized (radiance > 1×10^5) tumors were compared to those with low colonization, a significant improvement in tumor growth reduction was observed. However, because the only tumors with high colonization over longer time periods were observed in mice treated with DSpαPDL1-Hly, it is unclear whether the increased anti-tumor efficacy was due to the T-cell stimulatory activity of the αPD-L1 scFv in the tumor microenvironment or due to the higher concentration of bacterial cells augmenting the native cytotoxic effects of tumor colonization in mice treated with this strain. We suspect the latter to be the primary cause, as mice treated with αPD-L1 mAb did not show significant growth reduction compared to those from untreated controls. Further experiments that investigate DSpαPDL1-Hly tumor-targeting may elucidate the mechanisms involved and their relative contributions to the efficacy observed.

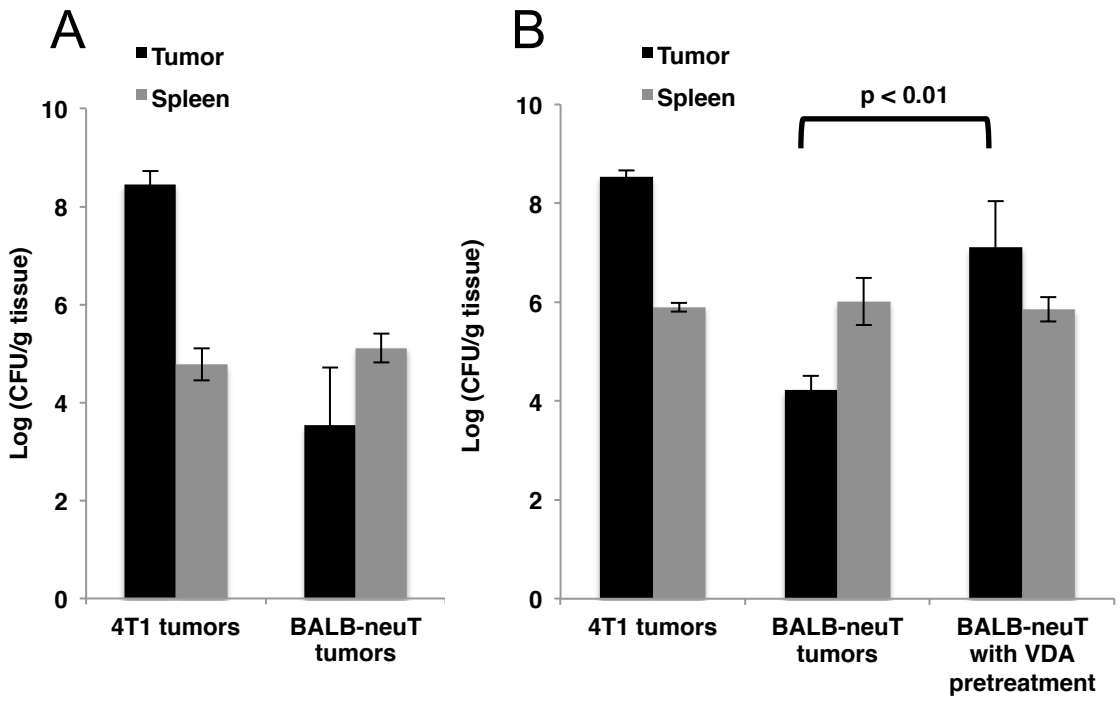

Figure 4-1 Figure 1: VDA improves tumor-targeting of attenuated *S.* Typhimurium in autochthonous breast cancer.

Figure 4-1 Figure 1: VDA improves tumor-targeting of attenuated *S. Typhimurium* in autochthonous breast cancer. A: BALB/c mice bearing subcutaneous 4T1 breast tumors or BALB-neuT mice bearing size-matched sporadic tumors were administered 5×10^5 CFU of log phase VNP20009 by tail vein injection. Tumors and spleens were harvested from mice two days post bacterial injection and were homogenized and plated for CFU determination. **B:** Mice bearing 4T1 or BALB-neuT tumors were treated as in (A) with log phase SL3261 and similarly plated for CFU determination. The VDA pre-treatment group was administered 0.4 mg CA4P 48 hours prior to, and once again immediately before, injection of SL3261 (as illustrated in Figure 4-3A). For panels A and B, the $\log_{10}$ of individual CFU/g values were used to calculate average and standard deviation of each group. Displayed is the average +/- one standard deviation of two separate experiments. Total mice for either the VNP20009 or SL3261 experiments: 4T1 N = 4; BALB-neuT N = 6. p-value was calculated using a Student's unpaired T-test.

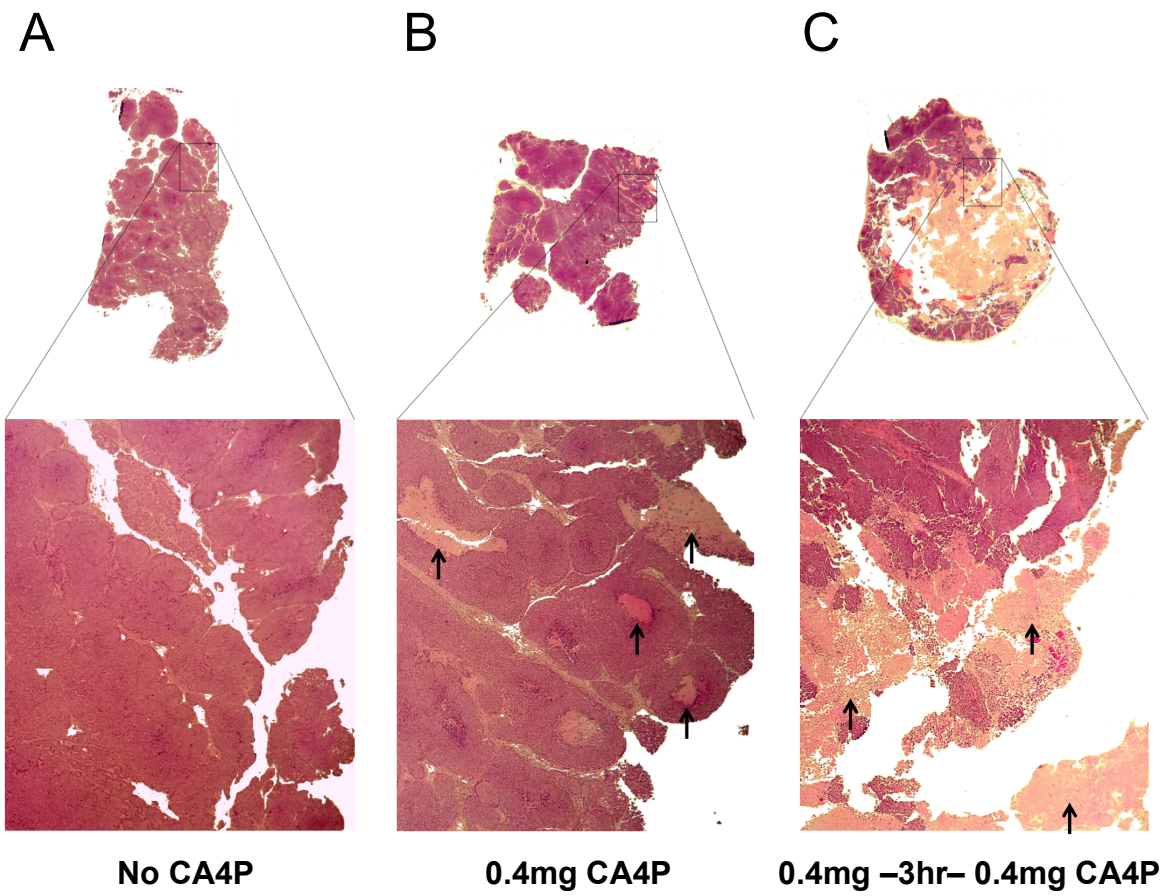

Figure 4-2: VDA treatment leads to development of necrotic areas in autochthonous BALB-neuT tumors.

Figure 4-2: VDA treatment leads to development of necrotic areas in autochthonous BALB-neuT tumors. BALB-neuT mice with autochthonous mammary tumors were administered a single tail vein injection of 0.4 mg of CA4P or two injections separated by 3 hours. Tumors were excised two days later for slide preparation and H&E staining. **(A)** Necrotic regions were largely absent from CA4P (-) control tumors. **(B)** CA4P treatment caused the development of necrotic regions, indicated by black arrows. **(C)** The extent of necrosis was further increased with two CA4P injections 3 hours apart.
Histology and H&E staining were performed by David Urso (Dept. of Surgery, University of Minnesota)

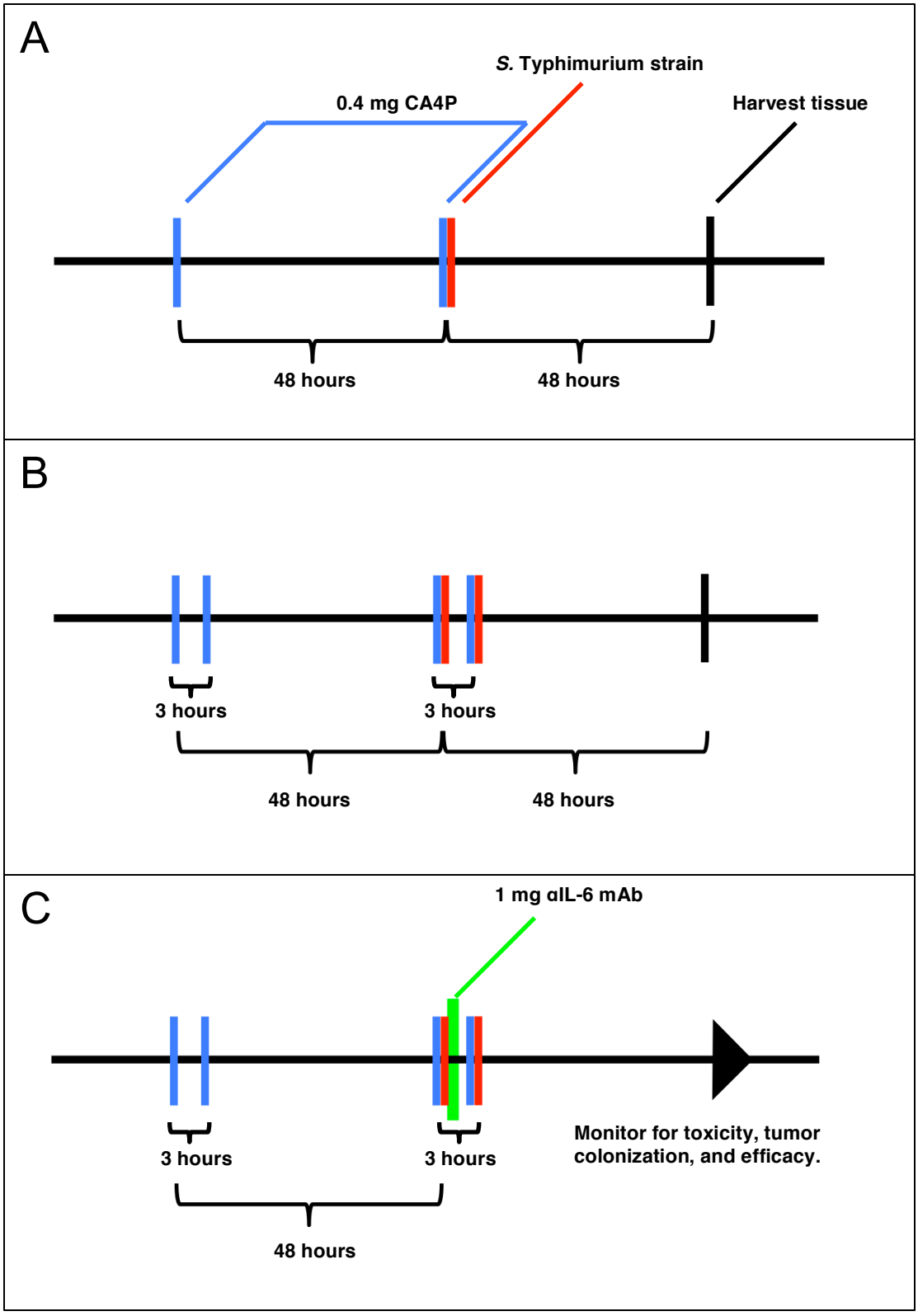

Figure 4-3: Schematics illustrating the injection strategies used for tumor-targeting in the BALB-neuT model.

Figure 4-3: Schematics illustrating the injection strategies used for tumor-targeting in the BALB-neuT model. All CAP4 injections were given 2 days before and again on the day of bacterial injections. For “split” injections in (B) and (C), CA4P and bacterial injections were administered twice, separated by 3 hours. All CA4P and bacterial injections were administered IV via the tail vein. The αIL-6 mAb in (C) was administered IP immediately following the first bacterial injection. Blue, red, green, and black bars indicate CA4P, *S.* Typhimurium, αIL-6 mAb, and tissue harvest, respectively (bars are also labeled within the figure).

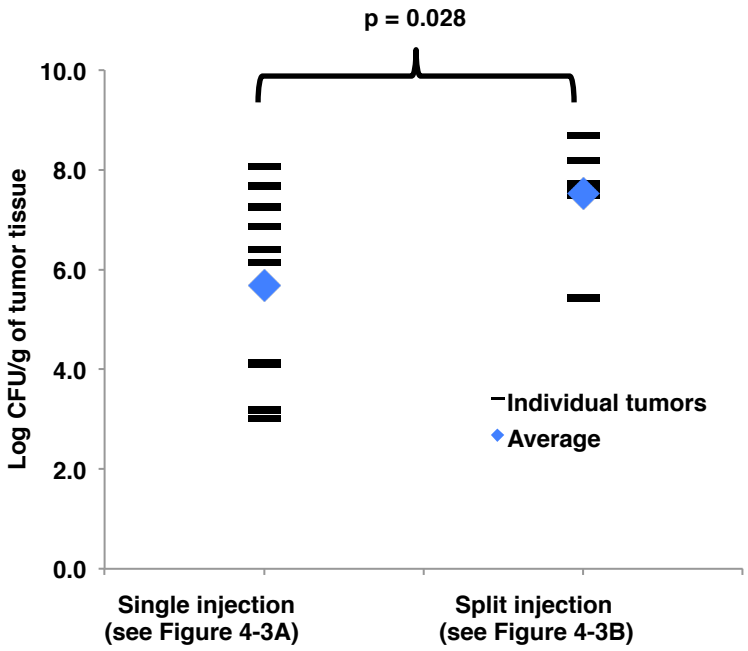

Figure 4-4: Split dosing of VDA and CA4P improves the consistency of BALB-neuT tumor colonization.

Figure 4-4: Split dosing of VDA and CA4P improves the consistency of BALB-neuT tumor colonization. BALB-neuT mice bearing tumors ranging in size from 150-250 mm were treated with 0.4 mg CA4P and 5×10^5 CFU of DSpNG in single injections as before (illustrated in Figure 4-3A) or with both CA4P and DSpNG split into two doses separated by 3 hours (illustrated in Figure 4-3B). For the split injections, both CA4P and DSpNG were administered on the bacterial treatment day as two half doses of 0.2 mg and 2.5×10^5 CFU, respectively. Tumors were harvested, homogenized and plated two days after the bacterial injection(s). The colonization of individual tumors is displayed (symbol: −) along with the average colonization (symbol: ◆) of each group. The combined results of two experiments are displayed. N=10 total tumors for the single injection group and 6 tumors for the split injection group. p-value was calculated using a Student's' unpaired T-test.

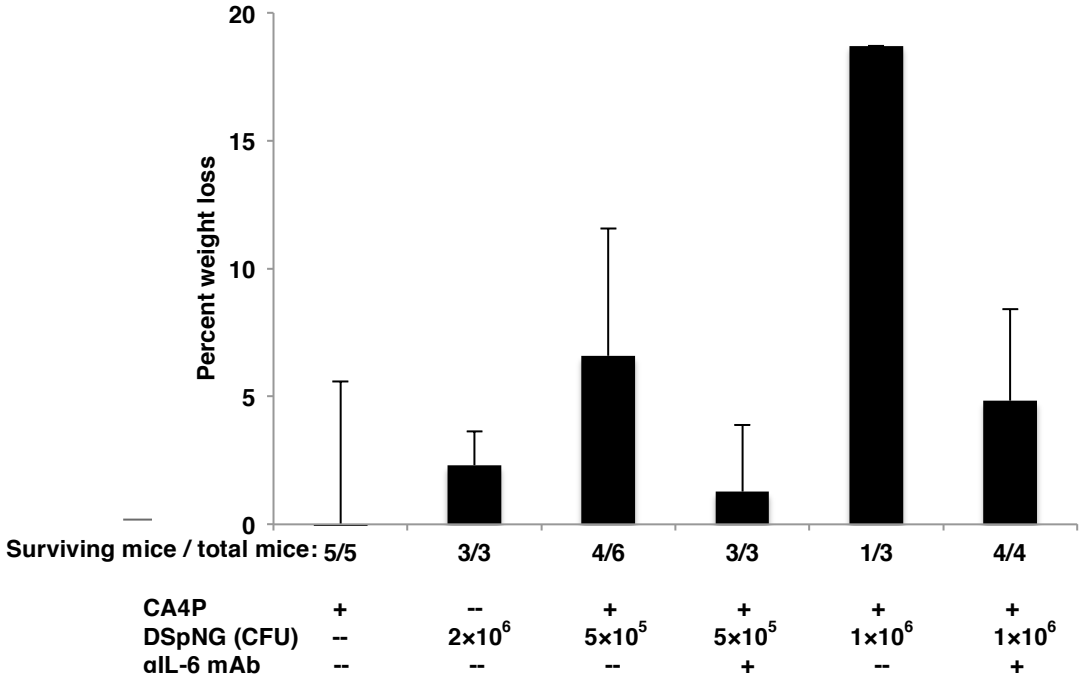

Figure 4-5: IL-6 treatment reduces the toxic effects of CA4P and *S.* Typhimurium treatment.

Figure 4-5: IL-6 treatment reduces the toxic effects of CA4P and *S.* Typhimurium treatment. Mice were treated with DSpNG, CA4P, and/or αIL-6 as indicated. Bacteria and CAP4 were administered as split injections as illustrated in Figure 4-3B and C. All CA4P doses were 0.4 mg per injection (e.g. $CA4P^{+}$ mice were given four 0.4 mg injections of CA4P as illustrated in Figure 3C for a total of 1.6 mg over 2 days). Bacterial CFU numbers indicate the total number for each injection; i.e. "1×10^{6}" represents two 5×10^{5} CFU injections 3 hours apart, or 1×10^{6} total CFU. Mice were monitored for weight loss and survival after treatment. The surviving mice/total mice treated in each group is depicted as a fraction below each column. The y-value represents the average percent weight loss of the surviving mice in each group.

A

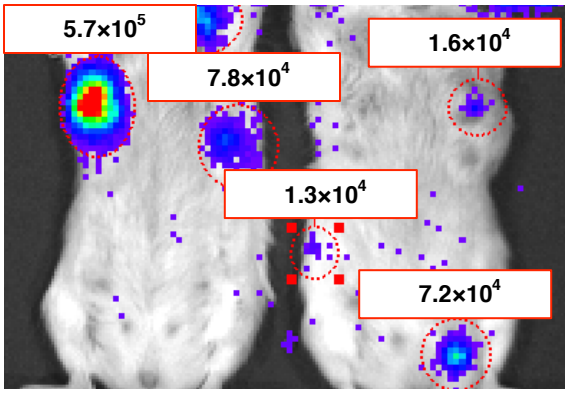

B

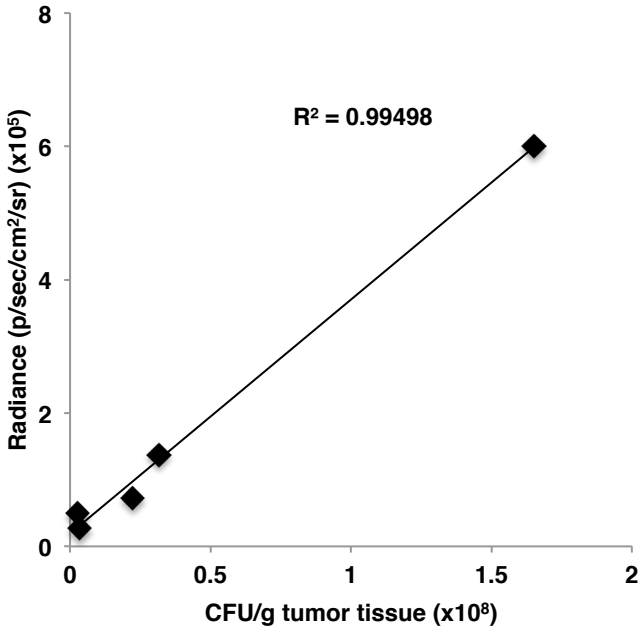

Figure 4-6: Tumor radiance of mice treated with luminescent *S.* Typhimurium allows quantification of tumor colonization in live mice.

Figure 4-6: Tumor radiance of mice treated with luminescent *S.* Typhimurium allows quantification of tumor colonization in live mice. (A) Representative image depicting the luminescence quantification of individual tumors (radiance) in a mouse treated with luminescent *S.* Typhimurium. **(B)** Tumors of varying luminescence from treated mice were homogenized and plated for CFU enumeration. CFU/gram of tissue correlated with tumor radiance.

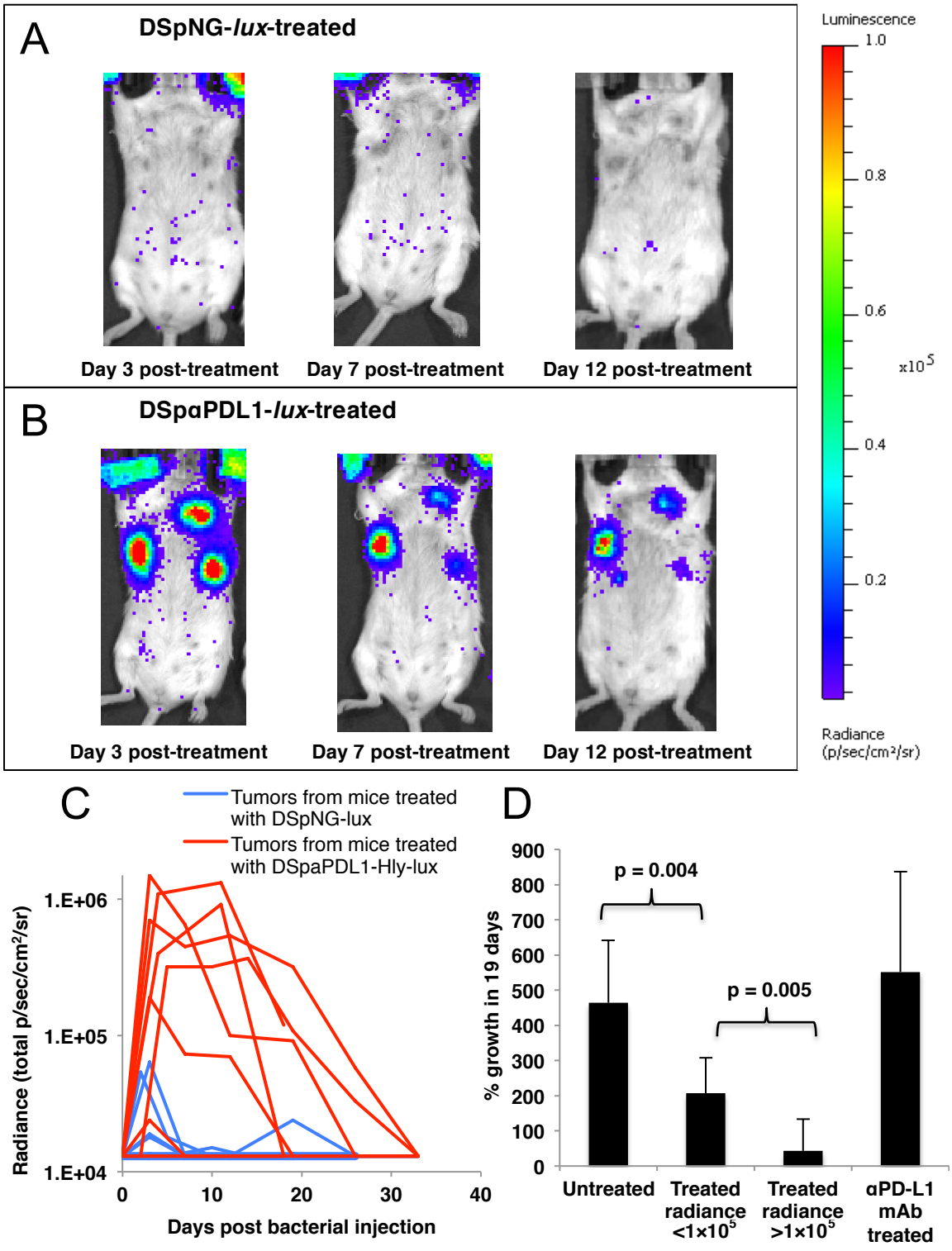

Figure 4-7: Anti-PD-L1 scFv expression may improve tumor colonization and decrease growth of BALB-neuT tumors.

Figure 4-7: Anti-PD-L1 scFv expression may improve tumor colonization and decrease growth of BALB-neuT tumors. BALB-neuT mice bearing 150-250 mm^3 tumors were treated with CA4P, αIL-6, and 5×10^5 CFU of either DSpNG-*lux* or DSpαPDL1-Hly-*lux* with the injection strategy illustrated in Figure 4-3A. Luminescence and tumor growth were measured over time. Images demonstrating the luminescence of representative mice are shown in **(A)** and **(B)**. **(C):** The radiance of multiple individual tumors from treated mice was measured over time. Only tumors that were between 150-250mm^3 upon treatment were graphed (N=9 for DSpαPDL1-Hly-*lux* treated and N=8 for DSpNG-*lux* treated). **(D):** The average percent growth 19 days post-treatment of all tumors shown in (C) that reached radiance greater than 1×10^5 (N=6) were compared to those consistently below 1×10^5 (N=11). For comparison, the average growth of tumors between 150-250mm^3 from untreated mice (N=8) as well as mice treated twice weekly with 125μg of IP αPD-L1 mAb (N=4) were also included. p-values were calculated using Student's unpaired T-test.

CHAPTER 5

DISCUSSION AND FUTURE DIRECTIONS

Discussion

Immunotherapy is an exciting advancement in the treatment of cancer. The specificity and memory of the immune system give it potential advantages over conventional therapies for lasting therapeutic responses. However, the adverse effects of sustained or off-target immune responses can cause serious autoimmune disorders, graft or organ transplant rejection, and general symptoms associated with the inflammatory response. The immune-related adverse events of systemic checkpoint blockade and cytokine therapy limit their therapeutic potential (for review, see introduction section “Toxicity of checkpoint blockade”). One method to remove the limitation of systemic toxicity is to target the therapeutic agent(s) specifically to the tumor microenvironment. The ideal targeting vector would specifically accumulate in tumor tissue where it would generate and secrete the immunotherapeutic agent. In this thesis, the potential of *Salmonella enterica* serovar Typhimurium (*S.* Typhimurium) as a tumor targeting immunotherapy vector was investigated.

The native cytotoxicity of S. *Typhimurium*

One advantage of *S.* Typhimurium as an immunotherapy vector is its native tumoricidal activity in the absence of any recombinant protein expression. In Chapter 3, we demonstrated the anti-tumor efficacy of *S.* Typhimurium in metastatic and primary tumor models of osteogenic sarcoma and transplanted and autochthonous breast cancer models. Interestingly, this efficacy was observed in the absence of bacterial tumor targeting in both metastatic osteosarcoma and BALB-neuT autochthonous breast

cancer. Therefore, we suspect that the efficacy was due to the systemic immunostimulatory effects of *Salmonella* treatment. The immunosuppressive tumor microenvironment is characterized by a Th2/M2 immune polarization. *S.* Typhimurium, a potent driver of a Th1 immune response (183), may have induced a Th1 shift that prevented tumor growth and/or caused the destruction of tumor cells. The increased infiltration of $IFN\gamma^+$ $CD4^+$ Th1 cells in K7M2 tumors in response to *S.* Typhimurium treatment supports this hypothesis. Additionally, we observed a reduction in the T-reg population in K7M2 tumors, indicating a less immunosuppressive tumor environment in response to *S.* Typhimurium treatment in the absence of bacterial tumor colonization.

In addition to the systemic efficacious effect of *S.* Typhimurium*,* we observed an apparent tumor colonization-specific anti-tumor effect in highly colonized BALB-neuT tumors that was significantly greater than what was observed for tumors with low colonization in treated mice. This interesting observation differentiated the systemic efficacious effects of *S.* Typhimurium treatment from a tumor colonization-specific effect. Additional work in the BALB-neuT model may further elucidate these two effects (see "Future Directions" section below).

S. Typhimurium *is able to secrete immune checkpoint-blocking scFvs*

Another beneficial characteristic of bacterial cancer therapy is the ability to engineer strains like *S.* Typhimurium to express therapeutic proteins. In Chapter 2, we demonstrated this capability with the expression and secretion of antagonistic single chain variable fragments (scFvs) against the immunoinhibitory checkpoints CTLA-4 and PD-L1. Full-length antibodies are difficult to produce in prokaryotic hosts. Whereas scFvs, being single chain peptides that include the variable heavy and variable light regions of one arm of a full-length antibody, should maintain antigen-binding affinity in a

structure simple enough for relatively easy prokaryotic expression (184). However due to the lack of a stabilizing framework region, scFvs will occasionally encounter problems with proper folding and stability (129). This is particularly common when scFvs are generated from B-cell hybridomas or other monoclonal cell lines, as there is no guarantee that scFvs will retain stability or even binding affinity when the majority of the remaining antibody structure is absent. In order to sidestep these issues, we used a phage display and panning approach to select for functional scFvs. Using this method, only scFv sequences that expressed and folded correctly in bacteria and retained high binding affinity in the absence of the rest of the antibody structure were selected during panning. Using an immunized chicken library for our selection pool, we successfully isolated antagonistic scFvs against CTLA-4 and PD-L1. αPD-L1 scFv was readily expressed and purified from bacterial cultures and displayed an antigen-binding affinity in the picomolar range, similar to antagonistic anti-mouse PD-L1 mAbs that are regularly used in research. When tested for antagonistic biological activity, both αPD-L1 and αCTLA-4 scFvs demonstrated biological activity similar to antagonistic mAbs. Therefore apart from their use in bacterial cancer therapy, the scFvs may be alternative immune checkpoint-binding reagents for other experimental or therapeutic applications. Using the hemolysin type I secretion system from *E. coli*, we generated *S.* Typhimurium strains that actively secrete the scFvs from their cytoplasm into the extracellular space. We encountered some difficulty with the larger scale production and characterization of αCTLA-4 scFv, which prevented the more detailed characterization of this scFv, such as the determination of its binding affinity. While these issues were largely resolved with hemolysin secretion, we decided to focus the subsequent investigation of *S.* Typhimurium as a vector for checkpoint blockade on the delivery of the better characterized αPD-L1 scFv.

Tumor-targeting propensity of S*. Typhimurium in transplant versus autochthonous tumor models*

Central to its applicability as a tumor-targeting vector is *S.* Typhimurium's propensity to preferentially colonize tumor tissue over healthy tissue. This property has been described in numerous preclinical studies using transplanted mouse tumor models. However, when tested clinically, less than 20% of biopsied tumors contained any measurable *S.* Typhimurium colonization. These results were unexpected in light of the numerous preclinical demonstrations of tumor targeting. When we examined the colonization of transplanted subcutaneous 4T1 tumors, we observed invariably high colony-forming units/gram of tumor, similar to other published studies in this field. However, when the colonization of sized matched autochthonous tumors was examined in BALB-neuT mice, little to no tumor colonization was observed, similar to what was observed for human tumors in clinical trials. It may be that the reproducibly high bacterial tumor colonization in much of the published literature is due in part to the artificiality of transplanted tumor models used, which often contain exaggerated levels of necrosis and/or immature vasculature than what is encountered in human disease (111, 116, 117). Conversely tumors in autochthonous cancer models, having developed from a single cell in their place of origin, have vasculature and necrosis patterns that more closely resemble human tumors (111, 117). Hemorrhage of tumor vasculature and the presence of necrotic regions have been demonstrated to be important for bacterial colonization (95, 118). Therefore, the differences between transplanted and autochthonous tumors in this regard may account for the differences in colonization that we observed. In addressing this idea with the hope of improving the bacterial targeting of autochthonous tumors (and ultimately human tumors), we sought to condition the

autochthonous tumors of the BALB-neuT model to “act” like transplant tumors by administering the vasculature disrupting agent (VDA) Combretastatin A-4 phosphate (CA4P). CA4P disrupts vasculature by binding to tubulin causing depolymerization and disruption of the cytoskeleton of vascular endothelial cells (179). The chaotic vasculature of tumor tissue is more susceptible to the effects of CA4P than the vasculature of healthy tissue, and CA4P treatment can cause a decreased tumor blood flow in as little as five minutes and complete shutdown of tumor blood flow in as little as 20 minutes in animal models while leaving healthy vasculature largely unaffected (179). This causes the development of necrotic regions in tumors within two days post treatment in animal models, which may subsequently be re-vascularized with neovasculature (185). These changes may cause autochthonous (and ultimately human) tumors to appear more “transplant-like,” making them more susceptible to bacterial colonization.

When BALB-neuT mice bearing autochthonous tumors were treated with CA4P two days prior to *S.* Typhimurium treatment (pre-treatment) and again with CA4P co-administered with *S.* Typhimurium, we observed an approximate 1000-fold increase in tumor colonization. Dosing regimens that excluded either of these two CA4P doses did not improve tumor targeting (not shown). Wang and colleagues showed that nascent vasculature forms in the necrotic regions that form after CA4P administration (185). We suspect that our first CA4P dose induced the formation of necrosis, while the second dose caused hemorrhage of the nascent tumor vasculature that facilitated entry of the bacteria into the tumor. Additionally, we found that splitting each CAP4 dose into two half-doses or two full doses three hours apart (for a total of four doses) improved the consistency of tumor colonization. Further experimentation may help to optimize and illuminate the mechanisms behind VDA-assisted bacterial tumor targeting.

At least two conclusions can be drawn from these results. First, bacterial tumor targeting studies should be performed in autochthonous models if possible. The difficulty encountered in the colonization of human tumors is not modeled well in transplanted orthotopic or subcutaneous mouse tumors, which are readily colonized by *S.* Typhimurium. In contrast, we did not see adequate tumor colonization when *S.* Typhimurium was injected as a single agent in BALB-neuT mice bearing autochthonous tumors, which is consistent with the poor colonization of human tumors. Second, since treatment with a VDA improved the colonization of autochthonous tumors, which more closely mimic human tumors, this strategy may also improve the targeting of human tumors. At a minimum, these studies illustrate the potential of conditioning tumors to improve bacterial targeting by treatment with VDAs or other agents.

Tumor targeting and efficacious effects of bacterial αPD-L1 scFv expression

When attenuated *S.* Typhimurium secreting αPD-L1 scFv (DSpαPDL1-Hly-*lux*) was compared to the same strain carrying an empty expression vector (DSpNG-*lux*) for tumor colonization in the BALB-neuT autochthonous breast cancer model (Chapter 4), the majority of tumors examined in DSpαPDL1-Hly-*lux* treated mice were colonized at a higher level and for a longer period of time than those in mice treated with DSpNG-*lux*. As mentioned in the Chapter 4 discussion, it has recently been demonstrated that functional PD-L1 is important in the clearance of both *Salmonella* (180) and *Listeria* (181) infections in mice, and this may be due to a role that PD-L1 plays in CD8 T-cell survival (182). Therefore, the secreted αPD-L1 scFv may gave a degree of protection to the *S.* Typhimurium that prevented its immune-mediated clearance and allowed longer lasting and more robust tumor colonization. Two additional observations further support this hypothesis. First, in Chapter 3 (page 83) we described a lethal toxicity that occurred

when αPD-L1 mAb was combined with SalpNG, which prevented the inclusion of this control group in 4T1 tumor studies. This toxicity corroborated the published effects of PD-L1 blockade on *Salmonella* infections. Second, when testing for *in vivo* survivability of our recombinant strains in Chapter 2, we saw that the χ4550-based *S.* Typhimurium strain that secreted αPD-L1 scFv (SalpαPD-L1-Hly) not only survived as well as SalpNG, but also appeared to have colonized tumors at one to two orders of magnitude higher than SalpNG (Figure 2-9B). Therefore we suggest that blocking PD-L1 systemically with αPD-L1 mAbs prevents the clearance of *S.* Typhimurium and is lethal. However, when the blocking agents are secreted by DSpαPDL1-Hly-lux or SalpαPD-L1, the PD-L1 block is localized to areas of higher bacterial concentrations in the tumor microenvironment where the secreted αPD-L1 scFvs can accumulate to functional concentrations to prevent the clearance of the bacteria.

When tumors that contained high levels of bacterial colonization were measured over time for growth, a significantly greater anti-tumor effect was observed than for those with low colonization. It is unclear whether this efficacy is the effect of the higher degree of bacterial colonization augmenting the native anti-tumor effects of the colonizing bacteria, or if it is due to an anti-tumor immunostimulatory activity of the secreted αPD-L1 scFv. Differentiating between the relative contributions of these mechanisms is difficult, as the only strain that achieved robust lasting colonization was DSpαPDL1-Hly-lux; therefore we were unable to compare highly colonized DSpαPDL1-Hly-lux tumors to highly colonized DSpNG tumors. We suspect the former explanation to play a more significant role, as tumors in BALB-neuT mice treated with a PD-L1 mAb blockade did not show a significant growth difference compared to tumors in untreated mice (Figure 4-7D), which suggests that PD-L1 may play a secondary role in the immunosuppressive microenvironment of BALB-neuT tumors. However, it is possible that the immunological

changes of *S.* Typhimurium colonization may have caused BALB-neuT tumors to respond more readily to PD-L1 blockade, resulting in improved efficacy. A proper control for this mechanism would involve administering a combination of *S.* Typhimurium treatment and αPD-L1 blockade with mAb; however as mentioned, this treatment regimen was lethal in mice, making the comparison difficult. Further experimentation is needed to elucidate the mechanisms behind the targeting and efficacious properties of DSpαPDL1-Hly-lux (see “Future Directions” section).

Future Directions

Elucidate the tumor-targeting effects of αPD-L1 scFv secretion

The observation that αPD-L1 scFv improves the robustness and duration of *S.* Typhimurium tumor colonization was surprising but may prove useful for the advancement of *Salmonella*-based cancer therapy. In order to validate this result, the strains should be re-constructed and examined again for their tumor-colonization effectiveness; this would rule out the unlikely possibility that a simple cloning variation or mutation produced a strain that colonized tumors more effectively, independent of αPD-L1 scFv secretion.

The DSpαPDL1-Hly strain may be useful in downstream applications as a “colonization driver” strain to improve the tumor colonization of other recombinant strains. For example if an IL-2-secreting strain requires a threshold colonization concentration for effectiveness, the co-administration of DSpαPDL1-Hly may improve the colonization to meet that threshold. This property could be tested by performing an experiment in two groups of BALB-neuT mice. Group A would be treated with non-luminescent DSpαPDL1-Hly and luminescent DSpNG-*lux*, and Group B would be treated with an equal dose of non-luminescent DSpNG and the same DSpNG-*lux* dose.

According to the colonization driver hypothesis, the tumors in mice treated in Group A would have greater DSpNG-*lux* colonization, measured by increased tumor radiance.

Due to the apparent toxic effects of systemic PD-L1 blockade and *S.* Typhimurium infection that we observed, and in light of the published reports demonstrating the importance of PD-L1 in *Salmonella* clearance, there may be a danger of the DSpαPD-L1-Hly strain avoiding systemic clearance and causing an unmanageable infection during its initial dissemination. Therefore, the expression of αPD-L1 scFv may increase the virulence of the attenuated *S.* Typhimurium strains. In support of this, we have preliminary data that suggests DSpαPDL1-Hly may be slightly more toxic than DSpNG (not shown). One approach to prevent this adverse effect of αPD-L1 scFv secretion is to limit its expression to the tumor microenvironment. We are currently investigating the use of tumor-specific promoters, including the *212b* (186) and *NirB* (187) promoters, which are activated in tumor tissue and in hypoxic conditions, respectively. This strategy would localize the effects of αPD-L1 scFv expression on survivability exclusively to the tumor microenvironment.

Apart from its effect on bacterial survivability, the anti-tumor function of bacterially delivered anti-immune checkpoint scFvs was not specifically addressed. This would be most clearly tested in a tumor model known to respond to immune checkpoint blockade. In Chapter 3, our attempts to demonstrate this functionality in the 4T1 tumor model are described. The combination of αPD-L1 mAb blockade and a stimulatory agonistic CD137 mAb was reported by Hirano and colleagues to cause the complete regression of established 4T1 tumors (163). Therefore, in light of the high bacterial tumor colonization that we observed in this model, we sought to replicate this efficacy with αPD-L1 scFv-secreting *S.* Typhimurium instead of αPD-L1 mAb. As a positive control for efficacy, one group was treated with the same αPD-L1 and αCD137 mAb treatment regimen used by

Hirano and colleagues. In these experiments, we were unable to reproduce the efficacy that was reported for 4T1 tumor-bearing mice given the mAb treatment, as tumors in these mice continued to grow similarly to those in other treatment groups. Therefore, it was difficult to draw conclusions about the comparable *in vivo* function of the bacterially delivered αPD-L1 scFv. Future experiments in a tumor model that is known to respond to checkpoint blockade in which bacterial colonization would be expected, such as MB49 bladder cancer for αCTLA-4 (188) and B16 melanoma treated in combination with adoptive transfer of IFNα-stimulated T-cells for αPD-L1 (189), would provide a proof of principle for bacterially delivered checkpoint-blocking scFvs functioning comparably to systemic mAb administration.

Combination of immune checkpoint-blocking scFvs with direct immunostimulatory agents

As outlined in the Introduction chapter, multiple immunotherapeutic agents used in combination have demonstrated greater anti-tumor efficacy than the agents used individually, but this strategy is also associated with greater toxicities. One of the benefits of tumor-specific bacterial delivery is the theoretical potential to deliver a cocktail of stimulatory agents specifically to the tumor microenvironment, thereby avoiding the adverse effects that may result from the combinatorial systemic administration. Ultimately, our goal is to combine multiple immune checkpoint-blocking scFvs with direct immunostimulatory molecules such as cytokines. Our lab has experience treating mice with *S.* Typhimurium expressing recombinant IL-2 (121-125). Since then, subsequent cytokines of even greater anti-tumor interest have been characterized, such as IL-15. Both IL-2 and IL-15 require three receptor molecules working in concert for optimal signaling. Both molecules share two receptors, the common γ chain and IL-2Rβ. The third receptor, IL-2Rα (aka CD25) for IL-2 and IL-15Rα

for IL-15, is largely responsible for the cytokines' unique functions. The α receptors are expressed on the surface of different cellular subsets at different stages of an immune response. IL-2Rα and IL15rα are both expressed on activated effector T-cells, but IL-2Rβ is also constitutively expressed at relatively high levels on T-regs, while IL15rα is constitutively found on memory T-cells. While both cytokines assist in effector T-cell function, this α receptor expression pattern makes IL-2 important for the development and maintenance of T-regs and IL-15 important for the maintenance of immunological memory. The T-reg-promoting effect of IL-2 lessens its potential as a cancer immunotherapy, whereas the memory-promoting effects of IL-15 make it a more attractive alternative to IL-2 (190). It has also been demonstrated that IL-15 administered in a complex covalently bound to its IL-15rα (IL-15/IL15Rα) greatly improves its CD8 T-cell stimulatory effects compared to purified IL-15 alone, by removing the requirement of IL15rα expression for its activity (191, 192). We have generated recombinant strains that express and secrete functional murine cytokines such as IL-2 (DSpIL2-Hly) and an IL-15/IL-15Rα fusion protein (DSpIL15-Hly) via the hemolysin system. Both molecules are functional when secreted from attenuated *S.* Typhimurium, and the IL-15/IL-15Rα fusion protein isolated from bacterial cultures is actually greater than 100-fold more biologically active than purified recombinant mouse IL-15 (Figure 5-1). Future experiments investigating the efficacy of these strains alone and in combination with checkpoint-blocking strains are currently planned or underway.

Systemic versus tumor-specific effects of S*. Typhimurium treatment*

An interesting observation that may warrant further investigation is the efficacious effect of *S.* Typhimurium treatment in K7M2 ostosarcoma and BALB-neuT breast cancer in the absence of tumor targeting. We suspect this efficacy is due to a systemic

immunostimulation in response to the initial bacterial dissemination, probably not unlike that which William Coley observed with his toxins several years ago (See Introduction pages 15-16). When examining the recent existing bacterial cancer therapy literature (reviewed in (94)), the efficacy observed is most often associated with bacterial tumor targeting; however as discussed, most of these reports utilize subcutaneous transplant tumor models, in which tumor colonization is almost always present. Therefore the observations in these experiments cannot be differentiated into systemic effects and tumor-targeted effects. The BALB-neuT model and luminescent *S.* Typhimurium strains may be useful tools to elucidate these differences. Using the BALB-neuT model, immunological changes and growth or reduction of four different "types" of tumors could be investigated: 1) colonized tumors in treated mice, 2) uncolonized tumors in treated mice in which other tumors are colonized, 3) uncolonized tumors in treated mice in which no tumors are colonized, and 4) tumors in untreated mice. These groups could potentially address questions regarding: 1) the tumor colonization-specific effects of *S.* Typhimurium treatment, 2) the off-target or immunological memory effects on uncolonized tumors when other tumors are targeted (differentiated based on tumor radiance) and 3) the systemic effects of *S.* Typhimurium treatment on tumor growth independent of tumor targeting. Chapter 4 of this thesis begins to compare these groups (Figure 4-7), but a more exhaustive investigation may help interpret the results of existing literature in this field and thereby increase our understanding of bacterial cancer therapy.

Investigate the tumor-targeting and efficacious effects of S. *Typhimurium in other autochthonous models*

We observed differences in bacterial tumor targeting between autochthonous tumors and transplanted tumors, and we suspect this was due to differences in vasculature and necrosis patterns in these tumors. However, it may be premature to generalize these results to autochthonous and transplant tumor models. The requirement of VDA treatment for tumor colonization in the BALB-neuT model may be unique to that model and not representative of other autochthonous models or human tumors. Therefore further validation of these results in other preclinical autochthonous cancer models is needed. The Department of Surgery at the University of Minnesota has available genetically engineered KPC mice that spontaneously develop *p53*$^{-}$, *kras*-driven pancreatic cancer. A non-oncogene driven autochthonous model, such as 3-methylcholanthrene-induced sarcoma, could be used as well. Testing our strains in these autochthonous models and comparing colonization and efficacy to the corresponding transplant models would substantiate the targeting differences between autochthonous and transplanted tumors and the colonization-enhancing effects of VDA treatment.

Additional considerations

Immune response generated against recombinant scFvs

We may find that mice develop immunity and antibody titers against the chicken-derived scFvs, which would lower their half-life *in vivo.* This possibility may be significant since they are being delivered by a highly immunostimulatory bacterium that may act as an adjuvant. The immunogenicity of the scFvs could be reduced by removing the purification tags (hemagglutinin and poly-histidine) from their sequences. Additionally, the scFvs could be “mouseized” by substituting the framework regions of the scFv

variable regions with those from mouse immunoglobulin. This strategy also may be necessary for the eventual humanization of the proteins before any clinical applications.

The functional concentration of immunostimulatory agents delivered by S*. Typhimurium*

The potential of *S.* Typhimurium to deliver therapeutic proteins specifically to the tumor environment assumes that the delivered proteins will accumulate within tumor tissues to therapeutic concentrations. We may find that bacterially delivered cytokines or antagonistic scFvs do not reach high enough concentrations in the tumor immune microenvironment to have a significant effect. One way to overcome this pitfall would be to continue to improve bacterial tumor targeting, as there is a correlation between CFU/g of tumor tissue and recombinant protein/g of tumor tissue in colonized tumors (Figure 5-2). Chapter 4 of this thesis reported methods to increase the levels of tumor colonization, and continuing investigations to further improve colonization are underway, which in turn should increase the concentrations of therapeutic proteins in the tumors. We have noticed additional enhancement in the degree of tumor colonization when bacterial doses are pushed to higher levels (Figure 5-3); however this also increases the acute toxicity of the treatment (data not shown). Recent experiments to address toxicity included supplementing mouse food with the anti-inflammatory drug celecoxib in addition to treating the mice with anti-IL-6 mAb; these treatments seemed to reduce toxicity (data not shown), illustrating a balancing act between increased bacterial dosing and toxicity. Further dosing and toxicity studies will continue to optimize the targeting of autochthonous tumors in order to deliver higher concentrations of therapeutic proteins. Additionally, other strategies, such as radiation therapy, may condition tumors for improved bacterial colonization.

The effective concentration of anti-immune checkpoint scFvs will likely depend on how much of their antigen is expressed in different tumor tissues. If tumor colonization and recombinant protein expression limit is reached, and this is still inadequate for a functional therapeutic response, an alternative approach would be to concentrate on the development of strains that secrete stimulatory agents that require lower functional concentrations. One candidate is the immunostimulatory cytokine IL-12, which is biologically active at low picomolar concentrations (193), which would be relatively easy to achieve using *S.* Typhimurium. This cytokine is also a great candidate for bacterial expression because, despite its beneficial effects for cancer immunity, its systemic administration was found to be to be prohibitively toxic in humans (64).

Summary and conclusions

In this thesis, the potential of *S.* Typhimurium as a tumor-targeting immunotherapy vector was investigated. To this end, functional antagonistic single chain antibodies against CTLA-4 (αCTLA-4 scFv) and PD-L1 (αPD-L1 scFv) were isolated from an immunized chicken library and engineered for secretion from *S.* Typhimurium. The inherent anti-tumor properties and tumor-targeting capability of *S.* Typhimurium were then investigated in transplanted primary and metastatic tumor models as well as in a genetically engineered autochthonous BALB-neuT breast cancer model. In each model tested, *S.* Typhimurium demonstrated native anti-tumor efficacy; however it did not adequately colonize autochthonous tumors, reflecting the lack of human tumor colonization reported in clinical studies. Disruption of tumor vasculature by treating BALB-neuT mice with the VDA CA4P improved the bacterial targeting of autochthonous tumors to levels similar to those observed for transplanted tumors. Subsequent comparison of the tumor targeting capability and efficacy of *S.* Typhimurium engineered

to secrete αPD-L1 scFv versus a control strain showed that αPD-L1 scFv secretion may further improve the colonization of autochthonous tumors, leading to a greater reduction in tumor burden of treated mice.

Several conclusions can be drawn from this work. First, the genetic manipulability of *S.* Typhimurium makes it capable of expressing and secreting single chain antibody fragments that block CTLA-4 and PD-L1 signaling. This provides a proof of principle that would likely be true of scFvs sequences specific to any target of interest and illustrates *S.* Typhimurium's potential as an immunotherapy vector. Second, *S.* Typhimurium displays native tumoricidal activity independent of any recombinant protein expression. This activity is likely due to systemic immunostimulatory effects of the bacterium and is observable in many different cancer models. Third, while readily targeting transplanted tumors, *S.* Typhimurium did not by itself target more clinically representative autochthonous tumors, suggesting that subsequent bacterial tumor colonization studies should be performed in autochthonous models or other models that more accurately mimic the results reported in human trials. Fourth, disruption of tumor vasculature with CA4P improved the bacterial targeting of autochthonous tumors, illustrating the potential of this VDA-assisted approach for targeting human tumors. And finally, expression and secretion of recombinant proteins such as αPD-L1 scFv, may affect *S.* Typhimurium's tumor colonization and *in vivo* viability, which may improve its effectiveness for cancer therapy. Taken together, these conclusions support the hypothesis that *S.* Typhimurium is a promising tumor targeting immunotherapy vector.

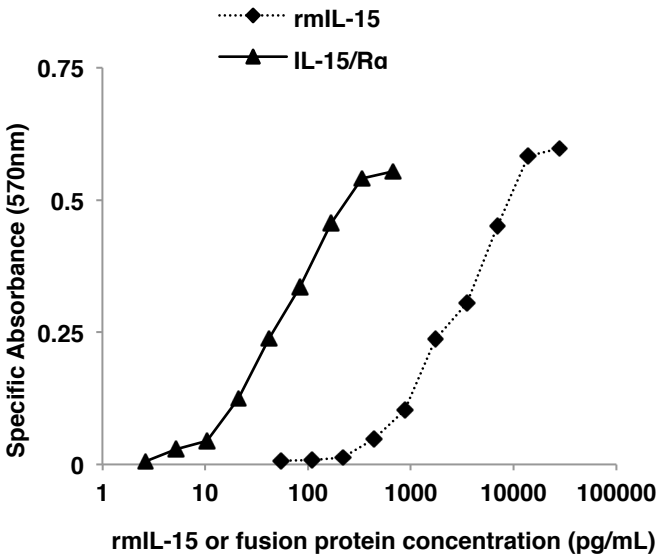

Figure 5-1: IL-15/IL-15ra fusion protein expressed in *S.* Typhimurium demonstrates improved bioactivity over IL-15.

Figure 5-1: IL-15/IL-15ra fusion protein expressed in *S.* Typhimurium demonstrates improved bioactivity over IL-15. IL-15/IL-15Ra expressed in *S.* Typhimurium was compared to purified recombinant mouse IL-15 for its ability to induce the proliferation of the IL-2/IL-15 growth dependent CTLL-2 cells. CTLL-2 cells maintained in RPMI supplemented with 10% FBS and T-STIM^{TM} T-cell supplement were harvested at log-phase growth at >90% viability, washed 2x with PBS and 1x with RPMI (with no T-STIM). Cells were counted and suspended in RPMI at 4×10^5 cells/ml. The cell suspension was added to individual wells of a 96-well plate at 50µL per well followed by 50µl of a SalpIL-15/Rα protein preparation. Recombinant mouse IL-15 standard was added to protein similarly prepared from *S.* Typhimurium control culture for comparison. Cells were incubated at 37°C, 5% CO_2 for 44 hours. Alamar blue dye (Life Technologies) was diluted to 30% in RPMI medium, and 50ul of this solution was added to experimental wells for a 10% final concentration. Plates were incubated for an additional 4 hours at 37°C, 5% CO_2. Following incubation, plates were measured for "specific absorbance," calculated by: $Absorbance_{570nm} - Absorbance_{600nm}$. A separate IL-15 ELISA was performed on bacterial cultures to determine the concentration of IL15/IL-15Ra added to each well.
Cloning of the IL-15/IL-15Rα strain and biological activity experiments were performed by Michael Mertensotto (Research Scientist, Dept. of Surgery, University of Minnesota).

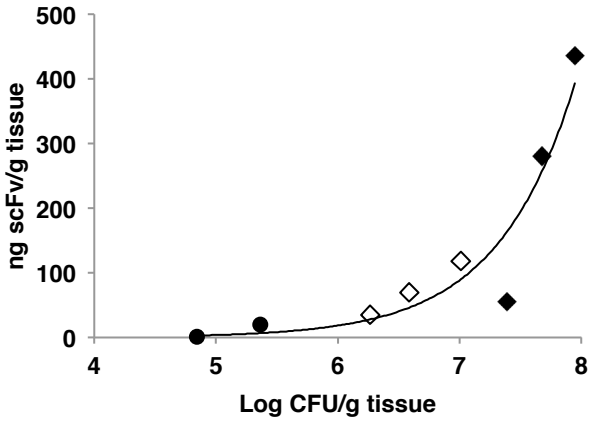

Figure 5-2: *S.* Typhimurium tissue colonization correlates with secreted scFv concentration.

Figure 5-2: *S.* Typhimurium tissue colonization correlates with secreted scFv concentration. BALB-neuT tumors (open diamonds), 4T1 tumors (filled diamonds), and spleens (filled circles) were harvested from mice 5-7 days after treatment with DSpαPDL1-Hly. Tissues were homogenized and plated for CFU determination as previously described (Chapter 4). In addition, supernatants from tissue homogenates were diluted and added to plates coated with recombinant PD-L1-Fc protein, and incubated for 120 minutes at room temperature. Bound αPD-L1 scFv was detected using an anti-6xHisTag/HRP conjugate and visualized with OptEIA^{TM} HRP substrate (BD). Absorbance at 450 nm was corrected for background by subtracting the absorbance at 570 nm. Values were then fitted to a standard curve of purified αPD-L1-scFv and used to calculate scFv tissue concentration in ng of scFv/g of tissue.

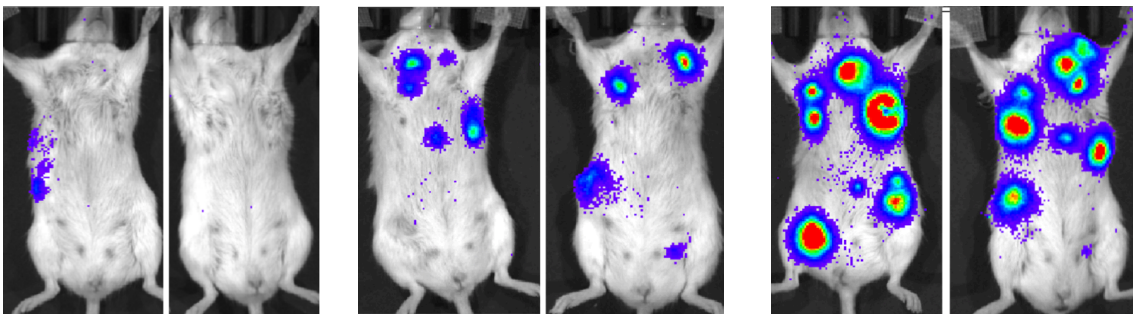

Figure 5-3: Increased bacterial dosing increases tumor colonization.

Figure 5-3: Increased bacterial dosing increases tumor colonization. BALB-neuT mice bearing multiple tumors ranging from 30-200mm^3 were treated with CA4P and anti-IL-6 mAb as illustrated in Figure 4-3C and a combination of four recombinant luminescent *S.* Typhimurium strains (DSpαPDL1-Hly-lux, DSpαCTLA-4-Hly-lux, DSpIL-2-Hly, and DSpIL-15/Rα-Hly). The indicated CFU is the total number of bacteria, split evenly between the four strains and administered as two doses 3 hours apart as in Figure 4-3C. Tumor radiance was measured four or five days post-treatment.
Experiments shown in panel (B) were performed by Michael Mertensotto (Research Scientist, Dept. of Surgery, University of Minnesota).

REFERENCES

1. Hanahan D (2014) Rethinking the war on cancer. *Lancet* 383(9916):558-563.
2. Dunn GP, Old LJ, & Schreiber RD (2004) The three Es of cancer immunoediting. *Annu. Rev. Immunol.* 22:329-360.
3. Ehrlich P (1909) *Beiträge zur experimentellen Pathologie und Chemotherapie* (Akademische Verlagsgesellschaft, Leipzig,) pp vii p., 2 l., 3 -247 p.
4. Lawrence HS (1959) *Cellular and humoral aspects of the hypersensitive states; a symposium held at the New York Academy of Medicine* (P.B. Hoeber, New York,) pp xii, 667 p.
5. Burnet FM (1970) The concept of immunological surveillance. *Prog. Exp. Tumor Res.* 13:1-27.
6. Grulich AE, van Leeuwen MT, Falster MO, & Vajdic CM (2007) Incidence of cancers in people with HIV/AIDS compared with immunosuppressed transplant recipients: a meta-analysis. *Lancet* 370(9581):59-67.
7. Sternlicht MD & Werb Z (2001) How matrix metalloproteinases regulate cell behavior. *Annu. Rev. Cell Dev. Biol.* 17:463-516.
8. Vicari AP & Caux C (2002) Chemokines in cancer. *Cytokine Growth Factor Rev.* 13(2):143-154.
9. Benlagha K & Bendelac A (2000) CD1d-restricted mouse V alpha 14 and human V alpha 24 T cells: lymphocytes of innate immunity. *Semin. Immunol.* 12(6):537-542.
10. Bancroft GJ, Schreiber RD, & Unanue ER (1991) Natural immunity: a T-cell-independent pathway of macrophage activation, defined in the scid mouse. *Immunol. Rev.* 124:5-24.
11. Bromberg JF, Horvath CM, Wen Z, Schreiber RD, & Darnell JE, Jr. (1996) Transcriptionally active Stat1 is required for the antiproliferative effects of both interferon alpha and interferon gamma. *Proc. Natl. Acad. Sci. U. S. A.* 93(15):7673-7678.
12. Kumar A, Commane M, Flickinger TW, Horvath CM, & Stark GR (1997) Defective TNF-alpha-induced apoptosis in STAT1-null cells due to low constitutive levels of caspases. *Science* 278(5343):1630-1632.
13. Coughlin CM, Salhany KE, Gee MS, LaTemple DC, Kotenko S, Ma X, Gri G, Wysocka M, Kim JE, Liu L, Liao F, Farber JM, Pestka S, Trinchieri G, & Lee WM (1998) Tumor cell responses to IFNgamma affect tumorigenicity and response to IL-12 therapy and antiangiogenesis. *Immunity* 9(1):25-34.
14. Qin Z & Blankenstein T (2000) CD4+ T cell--mediated tumor rejection involves inhibition of angiogenesis that is dependent on IFN gamma receptor expression by nonhematopoietic cells. *Immunity* 12(6):677-686.
15. Takeda K, Hayakawa Y, Smyth MJ, Kayagaki N, Yamaguchi N, Kakuta S, Iwakura Y, Yagita H, & Okumura K (2001) Involvement of tumor necrosis factor-related apoptosis-inducing ligand in surveillance of tumor metastasis by liver natural killer cells. *Nat. Med.* 7(1):94-100.
16. Smyth MJ, Cretney E, Takeda K, Wiltrout RH, Sedger LM, Kayagaki N, Yagita H, & Okumura K (2001) Tumor necrosis factor-related apoptosis-inducing ligand (TRAIL) contributes to interferon gamma-dependent natural killer cell protection from tumor metastasis. *J. Exp. Med.* 193(6):661-670.

17. Gerosa F, Baldani-Guerra B, Nisii C, Marchesini V, Carra G, & Trinchieri G (2002) Reciprocal activating interaction between natural killer cells and dendritic cells. *J. Exp. Med.* 195(3):327-333.
18. Srivastava P (2002) Interaction of heat shock proteins with peptides and antigen presenting cells: chaperoning of the innate and adaptive immune responses. *Annu. Rev. Immunol.* 20:395-425.
19. Murshid A, Gong J, & Calderwood SK (2012) The role of heat shock proteins in antigen cross presentation. *Frontiers in immunology* 3:63.
20. MartIn-Fontecha A, Sebastiani S, Hopken UE, Uguccioni M, Lipp M, Lanzavecchia A, & Sallusto F (2003) Regulation of dendritic cell migration to the draining lymph node: impact on T lymphocyte traffic and priming. *J. Exp. Med.* 198(4):615-621.
21. Sallusto F, Mackay CR, & Lanzavecchia A (2000) The role of chemokine receptors in primary, effector, and memory immune responses. *Annu. Rev. Immunol.* 18:593-620.
22. Albert ML, Sauter B, & Bhardwaj N (1998) Dendritic cells acquire antigen from apoptotic cells and induce class I-restricted CTLs. *Nature* 392(6671):86-89.
23. Yu P, Spiotto MT, Lee Y, Schreiber H, & Fu YX (2003) Complementary role of CD4+ T cells and secondary lymphoid tissues for cross-presentation of tumor antigen to CD8+ T cells. *J. Exp. Med.* 197(8):985-995.
24. Cavallo F, De Giovanni C, Nanni P, Forni G, & Lollini PL (2011) 2011: the immune hallmarks of cancer. *Cancer Immunol. Immunother.* 60(3):319-326.
25. Hanahan D & Weinberg RA (2011) Hallmarks of cancer: the next generation. *Cell* 144(5):646-674.
26. Garcia-Lora A, Algarra I, & Garrido F (2003) MHC class I antigens, immune surveillance, and tumor immune escape. *J. Cell. Physiol.* 195(3):346-355.
27. Seliger B (2008) Molecular mechanisms of MHC class I abnormalities and APM components in human tumors. *Cancer Immunol. Immunother.* 57(11):1719-1726.
28. Colombo MP & Piconese S (2007) Regulatory-T-cell inhibition versus depletion: the right choice in cancer immunotherapy. *Nat. Rev. Cancer* 7(11):880-887.
29. Facciabene A, Motz GT, & Coukos G (2012) T-regulatory cells: key players in tumor immune escape and angiogenesis. *Cancer Res.* 72(9):2162-2171.
30. Noy R & Pollard JW (2014) Tumor-associated macrophages: from mechanisms to therapy. *Immunity* 41(1):49-61.
31. Nucera S, Biziato D, & De Palma M (2011) The interplay between macrophages and angiogenesis in development, tissue injury and regeneration. *Int. J. Dev. Biol.* 55(4-5):495-503.
32. Quail DF & Joyce JA (2013) Microenvironmental regulation of tumor progression and metastasis. *Nat. Med.* 19(11):1423-1437.
33. Bonde AK, Tischler V, Kumar S, Soltermann A, & Schwendener RA (2012) Intratumoral macrophages contribute to epithelial-mesenchymal transition in solid tumors. *BMC Cancer* 12:35.
34. Brown D, Trowsdale J, & Allen R (2004) The LILR family: modulators of innate and adaptive immune pathways in health and disease. *Tissue Antigens* 64(3):215-225.
35. Noman MZ, Desantis G, Janji B, Hasmim M, Karray S, Dessen P, Bronte V, & Chouaib S (2014) PD-L1 is a novel direct target of HIF-1alpha, and its blockade under hypoxia enhanced MDSC-mediated T cell activation. *J. Exp. Med.* 211(5):781-790.

36. Curiel TJ, Coukos G, Zou L, Alvarez X, Cheng P, Mottram P, Evdemon-Hogan M, Conejo-Garcia JR, Zhang L, Burow M, Zhu Y, Wei S, Kryczek I, Daniel B, Gordon A, Myers L, Lackner A, Disis ML, Knutson KL, Chen L, & Zou W (2004) Specific recruitment of regulatory T cells in ovarian carcinoma fosters immune privilege and predicts reduced survival. *Nat. Med.* 10(9):942-949.
37. Savage ND, de Boer T, Walburg KV, Joosten SA, van Meijgaarden K, Geluk A, & Ottenhoff TH (2008) Human anti-inflammatory macrophages induce Foxp3+ GITR+ CD25+ regulatory T cells, which suppress via membrane-bound TGFbeta-1. *J. Immunol.* 181(3):2220-2226.
38. Daurkin I, Eruslanov E, Stoffs T, Perrin GQ, Algood C, Gilbert SM, Rosser CJ, Su LM, Vieweg J, & Kusmartsev S (2011) Tumor-associated macrophages mediate immunosuppression in the renal cancer microenvironment by activating the 15-lipoxygenase-2 pathway. *Cancer Res.* 71(20):6400-6409.
39. Oh SA & Li MO (2013) TGF-beta: guardian of T cell function. *J. Immunol.* 191(8):3973-3979.
40. Ng TH, Britton GJ, Hill EV, Verhagen J, Burton BR, & Wraith DC (2013) Regulation of adaptive immunity; the role of interleukin-10. *Frontiers in immunology* 4:129.
41. Sica A & Mantovani A (2012) Macrophage plasticity and polarization: in vivo veritas. *J. Clin. Invest.* 122(3):787-795.
42. Gabrilovich DI, Ostrand-Rosenberg S, & Bronte V (2012) Coordinated regulation of myeloid cells by tumours. *Nat. Rev. Immunol.* 12(4):253-268.
43. Dolcetti L, Peranzoni E, Ugel S, Marigo I, Fernandez Gomez A, Mesa C, Geilich M, Winkels G, Traggiai E, Casati A, Grassi F, & Bronte V (2010) Hierarchy of immunosuppressive strength among myeloid-derived suppressor cell subsets is determined by GM-CSF. *Eur. J. Immunol.* 40(1):22-35.
44. Youn JI, Nagaraj S, Collazo M, & Gabrilovich DI (2008) Subsets of myeloid-derived suppressor cells in tumor-bearing mice. *J. Immunol.* 181(8):5791-5802.
45. Movahedi K, Guilliams M, Van den Bossche J, Van den Bergh R, Gysemans C, Beschin A, De Baetselier P, & Van Ginderachter JA (2008) Identification of discrete tumor-induced myeloid-derived suppressor cell subpopulations with distinct T cell-suppressive activity. *Blood* 111(8):4233-4244.
46. Rodriguez PC, Quiceno DG, Zabaleta J, Ortiz B, Zea AH, Piazuelo MB, Delgado A, Correa P, Brayer J, Sotomayor EM, Antonia S, Ochoa JB, & Ochoa AC (2004) Arginase I production in the tumor microenvironment by mature myeloid cells inhibits T-cell receptor expression and antigen-specific T-cell responses. *Cancer Res.* 64(16):5839-5849.
47. Srivastava MK, Sinha P, Clements VK, Rodriguez P, & Ostrand-Rosenberg S (2010) Myeloid-derived suppressor cells inhibit T-cell activation by depleting cystine and cysteine. *Cancer Res.* 70(1):68-77.
48. Schmielau J & Finn OJ (2001) Activated granulocytes and granulocyte-derived hydrogen peroxide are the underlying mechanism of suppression of t-cell function in advanced cancer patients. *Cancer Res.* 61(12):4756-4760.
49. Mazzoni A, Bronte V, Visintin A, Spitzer JH, Apolloni E, Serafini P, Zanovello P, & Segal DM (2002) Myeloid suppressor lines inhibit T cell responses by an NO-dependent mechanism. *J. Immunol.* 168(2):689-695.
50. Nagaraj S, Gupta K, Pisarev V, Kinarsky L, Sherman S, Kang L, Herber DL, Schneck J, & Gabrilovich DI (2007) Altered recognition of antigen is a mechanism of CD8+ T cell tolerance in cancer. *Nat. Med.* 13(7):828-835.

51. Hanson EM, Clements VK, Sinha P, Ilkovitch D, & Ostrand-Rosenberg S (2009) Myeloid-derived suppressor cells down-regulate L-selectin expression on CD4+ and CD8+ T cells. *J. Immunol.* 183(2):937-944.
52. Pan PY, Ma G, Weber KJ, Ozao-Choy J, Wang G, Yin B, Divino CM, & Chen SH (2010) Immune stimulatory receptor CD40 is required for T-cell suppression and T regulatory cell activation mediated by myeloid-derived suppressor cells in cancer. *Cancer Res.* 70(1):99-108.
53. Huang B, Pan PY, Li Q, Sato AI, Levy DE, Bromberg J, Divino CM, & Chen SH (2006) Gr-1+CD115+ immature myeloid suppressor cells mediate the development of tumor-induced T regulatory cells and T-cell anergy in tumor-bearing host. *Cancer Res.* 66(2):1123-1131.
54. Serafini P, Mgebroff S, Noonan K, & Borrello I (2008) Myeloid-derived suppressor cells promote cross-tolerance in B-cell lymphoma by expanding regulatory T cells. *Cancer Res.* 68(13):5439-5449.
55. Hoechst B, Gamrekelashvili J, Manns MP, Greten TF, & Korangy F (2011) Plasticity of human Th17 cells and iTregs is orchestrated by different subsets of myeloid cells. *Blood* 117(24):6532-6541.
56. Fife BT & Bluestone JA (2008) Control of peripheral T-cell tolerance and autoimmunity via the CTLA-4 and PD-1 pathways. *Immunol. Rev.* 224:166-182.
57. Wing K, Onishi Y, Prieto-Martin P, Yamaguchi T, Miyara M, Fehervari Z, Nomura T, & Sakaguchi S (2008) CTLA-4 control over Foxp3+ regulatory T cell function. *Science* 322(5899):271-275.
58. Friedline RH, Brown DS, Nguyen H, Kornfeld H, Lee J, Zhang Y, Appleby M, Der SD, Kang J, & Chambers CA (2009) CD4+ regulatory T cells require CTLA-4 for the maintenance of systemic tolerance. *J. Exp. Med.* 206(2):421-434.
59. Chemnitz JM, Parry RV, Nichols KE, June CH, & Riley JL (2004) SHP-1 and SHP-2 associate with immunoreceptor tyrosine-based switch motif of programmed death 1 upon primary human T cell stimulation, but only receptor ligation prevents T cell activation. *J. Immunol.* 173(2):945-954.
60. Zitvogel L & Kroemer G (2012) Targeting PD-1/PD-L1 interactions for cancer immunotherapy. *Oncoimmunology* 1(8):1223-1225.
61. Dranoff G (2004) Cytokines in cancer pathogenesis and cancer therapy. *Nat. Rev. Cancer* 4(1):11-22.
62. Steel JC, Waldmann TA, & Morris JC (2012) Interleukin-15 biology and its therapeutic implications in cancer. *Trends Pharmacol. Sci.* 33(1):35-41.
63. Schwartz RN, Stover L, & Dutcher J (2002) Managing toxicities of high-dose interleukin-2. *Oncology (Williston Park)* 16(11 Suppl 13):11-20.
64. Atkins MB, Robertson MJ, Gordon M, Lotze MT, DeCoste M, DuBois JS, Ritz J, Sandler AB, Edington HD, Garzone PD, Mier JW, Canning CM, Battiato L, Tahara H, & Sherman ML (1997) Phase I evaluation of intravenous recombinant human interleukin 12 in patients with advanced malignancies. *Clin. Cancer Res.* 3(3):409-417.
65. Weber JS, O'Day S, Urba W, Powderly J, Nichol G, Yellin M, Snively J, & Hersh E (2008) Phase I/II study of ipilimumab for patients with metastatic melanoma. *J. Clin. Oncol.* 26(36):5950-5956.
66. Hodi FS, O'Day SJ, McDermott DF, Weber RW, Sosman JA, Haanen JB, Gonzalez R, Robert C, Schadendorf D, Hassel JC, Akerley W, van den Eertwegh AJ, Lutzky J, Lorigan P, Vaubel JM, Linette GP, Hogg D, Ottensmeier CH, Lebbe C, Peschel C, Quirt I, Clark JI, Wolchok JD, Weber JS, Tian J, Yellin MJ, Nichol

GM, Hoos A, & Urba WJ (2010) Improved survival with ipilimumab in patients with metastatic melanoma. *N. Engl. J. Med.* 363(8):711-723.
67. Robert C, Thomas L, Bondarenko I, O'Day S, Weber J, Garbe C, Lebbe C, Baurain JF, Testori A, Grob JJ, Davidson N, Richards J, Maio M, Hauschild A, Miller WH, Jr., Gascon P, Lotem M, Harmankaya K, Ibrahim R, Francis S, Chen TT, Humphrey R, Hoos A, & Wolchok JD (2011) Ipilimumab plus dacarbazine for previously untreated metastatic melanoma. *N. Engl. J. Med.* 364(26):2517-2526.
68. Yang JC, Hughes M, Kammula U, Royal R, Sherry RM, Topalian SL, Suri KB, Levy C, Allen T, Mavroukakis S, Lowy I, White DE, & Rosenberg SA (2007) Ipilimumab (anti-CTLA4 antibody) causes regression of metastatic renal cell cancer associated with enteritis and hypophysitis. *J. Immunother.* 30(8):825-830.
69. van den Eertwegh AJ, Versluis J, van den Berg HP, Santegoets SJ, van Moorselaar RJ, van der Sluis TM, Gall HE, Harding TC, Jooss K, Lowy I, Pinedo HM, Scheper RJ, Stam AG, von Blomberg BM, de Gruijl TD, Hege K, Sacks N, & Gerritsen WR (2012) Combined immunotherapy with granulocyte-macrophage colony-stimulating factor-transduced allogeneic prostate cancer cells and ipilimumab in patients with metastatic castration-resistant prostate cancer: a phase 1 dose-escalation trial. *Lancet Oncol.* 13(5):509-517.
70. Carthon BC, Wolchok JD, Yuan J, Kamat A, Ng Tang DS, Sun J, Ku G, Troncoso P, Logothetis CJ, Allison JP, & Sharma P (2010) Preoperative CTLA-4 blockade: tolerability and immune monitoring in the setting of a presurgical clinical trial. *Clin. Cancer Res.* 16(10):2861-2871.
71. Hodi FS, Butler M, Oble DA, Seiden MV, Haluska FG, Kruse A, Macrae S, Nelson M, Canning C, Lowy I, Korman A, Lautz D, Russell S, Jaklitsch MT, Ramaiya N, Chen TC, Neuberg D, Allison JP, Mihm MC, & Dranoff G (2008) Immunologic and clinical effects of antibody blockade of cytotoxic T lymphocyte-associated antigen 4 in previously vaccinated cancer patients. *Proc. Natl. Acad. Sci. U. S. A.* 105(8):3005-3010.
72. Brahmer JR, Tykodi SS, Chow LQ, Hwu WJ, Topalian SL, Hwu P, Drake CG, Camacho LH, Kauh J, Odunsi K, Pitot HC, Hamid O, Bhatia S, Martins R, Eaton K, Chen S, Salay TM, Alaparthy S, Grosso JF, Korman AJ, Parker SM, Agrawal S, Goldberg SM, Pardoll DM, Gupta A, & Wigginton JM (2012) Safety and activity of anti-PD-L1 antibody in patients with advanced cancer. *N. Engl. J. Med.* 366(26):2455-2465.
73. Powles T, Eder JP, Fine GD, Braiteh FS, Loriot Y, Cruz C, Bellmunt J, Burris HA, Petrylak DP, Teng SL, Shen X, Boyd Z, Hegde PS, Chen DS, & Vogelzang NJ (2014) MPDL3280A (anti-PD-L1) treatment leads to clinical activity in metastatic bladder cancer. *Nature* 515(7528):558-562.
74. Sharma P & Allison JP (2015) The future of immune checkpoint therapy. *Science* 348(6230):56-61.
75. Tivol EA, Borriello F, Schweitzer AN, Lynch WP, Bluestone JA, & Sharpe AH (1995) Loss of CTLA-4 leads to massive lymphoproliferation and fatal multiorgan tissue destruction, revealing a critical negative regulatory role of CTLA-4. *Immunity* 3(5):541-547.
76. Waterhouse P, Penninger JM, Timms E, Wakeham A, Shahinian A, Lee KP, Thompson CB, Griesser H, & Mak TW (1995) Lymphoproliferative disorders with early lethality in mice deficient in Ctla-4. *Science* 270(5238):985-988.
77. Hurwitz AA, Sullivan TJ, Krummel MF, Sobel RA, & Allison JP (1997) Specific blockade of CTLA-4/B7 interactions results in exacerbated clinical and histologic

disease in an actively-induced model of experimental allergic encephalomyelitis. *J. Neuroimmunol.* 73(1-2):57-62.
78. Perrin PJ, Maldonado JH, Davis TA, June CH, & Racke MK (1996) CTLA-4 blockade enhances clinical disease and cytokine production during experimental allergic encephalomyelitis. *J. Immunol.* 157(4):1333-1336.
79. Luhder F, Hoglund P, Allison JP, Benoist C, & Mathis D (1998) Cytotoxic T lymphocyte-associated antigen 4 (CTLA-4) regulates the unfolding of autoimmune diabetes. *J. Exp. Med.* 187(3):427-432.
80. Weber JS, Kahler KC, & Hauschild A (2012) Management of immune-related adverse events and kinetics of response with ipilimumab. *J. Clin. Oncol.* 30(21):2691-2697.
81. Gelao L, Criscitiello C, Esposito A, Goldhirsch A, & Curigliano G (2014) Immune checkpoint blockade in cancer treatment: a double-edged sword cross-targeting the host as an "innocent bystander". *Toxins* 6(3):914-933.
82. Postow MA, Chesney J, Pavlick AC, Robert C, Grossmann K, McDermott D, Linette GP, Meyer N, Giguere JK, Agarwala SS, Shaheen M, Ernstoff MS, Minor D, Salama AK, Taylor M, Ott PA, Rollin LM, Horak C, Gagnier P, Wolchok JD, & Hodi FS (2015) Nivolumab and Ipilimumab versus Ipilimumab in Untreated Melanoma. *N. Engl. J. Med.*
83. Callahan MK & Wolchok JD (2013) At the bedside: CTLA-4- and PD-1-blocking antibodies in cancer immunotherapy. *J. Leukoc. Biol.* 94(1):41-53.
84. Robert C, Soria JC, & Eggermont AM (2013) Drug of the year: programmed death-1 receptor/programmed death-1 ligand-1 receptor monoclonal antibodies. *Eur. J. Cancer* 49(14):2968-2971.
85. Topalian SL, Hodi FS, Brahmer JR, Gettinger SN, Smith DC, McDermott DF, Powderly JD, Carvajal RD, Sosman JA, Atkins MB, Leming PD, Spigel DR, Antonia SJ, Horn L, Drake CG, Pardoll DM, Chen L, Sharfman WH, Anders RA, Taube JM, McMiller TL, Xu H, Korman AJ, Jure-Kunkel M, Agrawal S, McDonald D, Kollia GD, Gupta A, Wigginton JM, & Sznol M (2012) Safety, activity, and immune correlates of anti-PD-1 antibody in cancer. *N. Engl. J. Med.* 366(26):2443-2454.
86. Wolchok JD, Neyns B, Linette G, Negrier S, Lutzky J, Thomas L, Waterfield W, Schadendorf D, Smylie M, Guthrie T, Jr., Grob JJ, Chesney J, Chin K, Chen K, Hoos A, O'Day SJ, & Lebbe C (2010) Ipilimumab monotherapy in patients with pretreated advanced melanoma: a randomised, double-blind, multicentre, phase 2, dose-ranging study. *Lancet Oncol.* 11(2):155-164.
87. Yu P, Steel JC, Zhang M, Morris JC, & Waldmann TA (2010) Simultaneous blockade of multiple immune system inhibitory checkpoints enhances antitumor activity mediated by interleukin-15 in a murine metastatic colon carcinoma model. *Clin. Cancer Res.* 16(24):6019-6028.
88. Yu P, Steel JC, Zhang M, Morris JC, Waitz R, Fasso M, Allison JP, & Waldmann TA (2012) Simultaneous inhibition of two regulatory T-cell subsets enhanced Interleukin-15 efficacy in a prostate tumor model. *Proc. Natl. Acad. Sci. U. S. A.* 109(16):6187-6192.
89. Barbe S, Van Mellaert L, & Anne J (2006) The use of clostridial spores for cancer treatment. *J. Appl. Microbiol.* 101(3):571-578.
90. Leschner S & Weiss S (2010) *Salmonella*-allies in the fight against cancer. *J Mol Med (Berl)* 88(8):763-773.

91. Coley WB (1991) The treatment of malignant tumors by repeated inoculations of erysipelas. With a report of ten original cases. 1893. *Clin. Orthop. Relat. Res.* (262):3-11.
92. Bickels J, Kollender Y, Merinsky O, & Meller I (2002) Coley's toxin: historical perspective. *Isr. Med. Assoc. J.* 4(6):471-472.
93. Hoption Cann SA, van Netten JP, & van Netten C (2003) Dr William Coley and tumour regression: a place in history or in the future. *Postgrad. Med. J.* 79(938):672-680.
94. Forbes NS (2010) Engineering the perfect (bacterial) cancer therapy. *Nat. Rev. Cancer* 10(11):785-794.
95. Leschner S, Westphal K, Dietrich N, Viegas N, Jablonska J, Lyszkiewicz M, Lienenklaus S, Falk W, Gekara N, Loessner H, & Weiss S (2009) Tumor invasion of *Salmonella enterica* serovar Typhimurium is accompanied by strong hemorrhage promoted by TNF-alpha. *PLoS ONE* 4(8):e6692.
96. Kasinskas RW & Forbes NS (2006) *Salmonella typhimurium* specifically chemotax and proliferate in heterogeneous tumor tissue in vitro. *Biotechnol. Bioeng.* 94(4):710-721.
97. Kasinskas RW & Forbes NS (2007) *Salmonella typhimurium* lacking ribose chemoreceptors localize in tumor quiescence and induce apoptosis. *Cancer Res.* 67(7):3201-3209.
98. Zhao M, Yang M, Li XM, Jiang P, Baranov E, Li S, Xu M, Penman S, & Hoffman RM (2005) Tumor-targeting bacterial therapy with amino acid auxotrophs of GFP-expressing Salmonella typhimurium. *Proc. Natl. Acad. Sci. U. S. A.* 102(3):755-760.
99. Sznol M, Lin SL, Bermudes D, Zheng LM, & King I (2000) Use of preferentially replicating bacteria for the treatment of cancer. *J. Clin. Invest.* 105(8):1027-1030.
100. Jain RK (1998) The next frontier of molecular medicine: delivery of therapeutics. *Nat. Med.* 4(6):655-657.
101. Dang LH, Bettegowda C, Huso DL, Kinzler KW, & Vogelstein B (2001) Combination bacteriolytic therapy for the treatment of experimental tumors. *Proc. Natl. Acad. Sci. U. S. A.* 98(26):15155-15160.
102. Hoffman RM & Zhao M (2014) Methods for the development of tumor-targeting bacteria. *Expert opinion on drug discovery* 9(7):741-750.
103. Westphal K, Leschner S, Jablonska J, Loessner H, & Weiss S (2008) Containment of tumor-colonizing bacteria by host neutrophils. *Cancer Res.* 68(8):2952-2960.
104. Yu YA, Shabahang S, Timiryasova TM, Zhang Q, Beltz R, Gentschev I, Goebel W, & Szalay AA (2004) Visualization of tumors and metastases in live animals with bacteria and vaccinia virus encoding light-emitting proteins. *Nat. Biotechnol.* 22(3):313-320.
105. Curtiss R, 3rd & Kelly SM (1987) *Salmonella typhimurium* deletion mutants lacking adenylate cyclase and cyclic AMP receptor protein are avirulent and immunogenic. *Infect. Immun.* 55(12):3035-3043.
106. Low KB, Ittensohn M, Le T, Platt J, Sodi S, Amoss M, Ash O, Carmichael E, Chakraborty A, Fischer J, Lin SL, Luo X, Miller SI, Zheng L, King I, Pawelek JM, & Bermudes D (1999) Lipid A mutant *Salmonella* with suppressed virulence and TNFalpha induction retain tumor-targeting in vivo. *Nat. Biotechnol.* 17(1):37-41.
107. Nemunaitis J, Cunningham C, Senzer N, Kuhn J, Cramm J, Litz C, Cavagnolo R, Cahill A, Clairmont C, & Sznol M (2003) Pilot trial of genetically modified,

attenuated *Salmonella* expressing the *E. coli* cytosine deaminase gene in refractory cancer patients. *Cancer Gene Ther.* 10(10):737-744.
108. Toso JF, Gill VJ, Hwu P, Marincola FM, Restifo NP, Schwartzentruber DJ, Sherry RM, Topalian SL, Yang JC, Stock F, Freezer LJ, Morton KE, Seipp C, Haworth L, Mavroukakis S, White D, MacDonald S, Mao J, Sznol M, & Rosenberg SA (2002) Phase I study of the intravenous administration of attenuated *Salmonella typhimurium* to patients with metastatic melanoma. *J. Clin. Oncol.* 20(1):142-152.
109. Heimann DM & Rosenberg SA (2003) Continuous intravenous administration of live genetically modified *Salmonella typhimurium* in patients with metastatic melanoma. *J. Immunother.* 26(2):179-180.
110. Zhang M, Swofford CA, & Forbes NS (2014) Lipid A controls the robustness of intratumoral accumulation of attenuated *Salmonella* in mice. *Int. J. Cancer* 135(3):647-657.
111. Lee JC, Kim DC, Gee MS, Saunders HM, Sehgal CM, Feldman MD, Ross SR, & Lee WM (2002) Interleukin-12 inhibits angiogenesis and growth of transplanted but not in situ mouse mammary tumor virus-induced mammary carcinomas. *Cancer Res.* 62(3):747-755.
112. Holash J, Maisonpierre PC, Compton D, Boland P, Alexander CR, Zagzag D, Yancopoulos GD, & Wiegand SJ (1999) Vessel cooption, regression, and growth in tumors mediated by angiopoietins and VEGF. *Science* 284(5422):1994-1998.
113. Benjamin LE, Hemo I, & Keshet E (1998) A plasticity window for blood vessel remodelling is defined by pericyte coverage of the preformed endothelial network and is regulated by PDGF-B and VEGF. *Development* 125(9):1591-1598.
114. Benjamin LE, Golijanin D, Itin A, Pode D, & Keshet E (1999) Selective ablation of immature blood vessels in established human tumors follows vascular endothelial growth factor withdrawal. *J. Clin. Invest.* 103(2):159-165.
115. Hill SA, Chaplin DJ, Lewis G, & Tozer GM (2002) Schedule dependence of combretastatin A4 phosphate in transplanted and spontaneous tumour models. *Int. J. Cancer* 102(1):70-74.
116. Schreiber K, Rowley DA, Riethmuller G, & Schreiber H (2006) Cancer immunotherapy and preclinical studies: Why we are not wasting our time with animal experiments. *Hematology-Oncology Clinics of North America* 20(3):567-584.
117. Falk P (1982) Differences in vascular pattern between the spontaneous and the transplanted C3H mouse mammary carcinoma. *Eur. J. Cancer Clin. Oncol.* 18(2):155-165.
118. Yu YA, Zhang Q, & Szalay AA (2008) Establishment and characterization of conditions required for tumor colonization by intravenously delivered bacteria. *Biotechnol. Bioeng.* 100(3):567-578.
119. DuPage M & Jacks T (2013) Genetically engineered mouse models of cancer reveal new insights about the antitumor immune response. *Curr. Opin. Immunol.* 25(2):192-199.
120. Garbe AI, Vermeer B, Gamrekelashvili J, von Wasielewski R, Greten FR, Westendorf AM, Buer J, Schmid RM, Manns MP, Korangy F, & Greten TF (2006) Genetically induced pancreatic adenocarcinoma is highly immunogenic and causes spontaneous tumor-specific immune responses. *Cancer Res.* 66(1):508-516.

121. Barnett SJ, Soto LJ, 3rd, Sorenson BS, Nelson BW, Leonard AS, & Saltzman DA (2005) Attenuated *Salmonella typhimurium* invades and decreases tumor burden in neuroblastoma. *J. Pediatr. Surg.* 40(6):993-997; discussion 997-998.
122. Sorenson BS, Banton KL, Frykman NL, Leonard AS, & Saltzman DA (2008) Attenuated *Salmonella typhimurium* with IL-2 gene reduces pulmonary metastases in murine osteosarcoma. *Clin. Orthop. Relat. Res.* 466(6):1285-1291.
123. Saltzman DA, Katsanis E, Heise CP, Hasz DE, Vigdorovich V, Kelly SM, Curtiss R, 3rd, Leonard AS, & Anderson PM (1997) Antitumor mechanisms of attenuated *Salmonella typhimurium* containing the gene for human interleukin-2: a novel antitumor agent? *J. Pediatr. Surg.* 32(2):301-306.
124. Feltis BA, Miller JS, Sahar DA, Kim AS, Saltzman DA, Leonard AS, Wells CL, & Sielaff TD (2002) Liver and circulating NK1.1(+)CD3(-) cells are increased in infection with attenuated *Salmonella typhimurium* and are associated with reduced tumor in murine liver cancer. *J. Surg. Res.* 107(1):101-107.
125. Soto LJ, 3rd, Sorenson BS, Kim AS, Feltis BA, Leonard AS, & Saltzman DA (2003) Attenuated *Salmonella typhimurium* prevents the establishment of unresectable hepatic metastases and improves survival in a murine model. *J. Pediatr. Surg.* 38(7):1075-1079.
126. Peterson E, Owens SM, & Henry RL (2006) Monoclonal antibody form and function: manufacturing the right antibodies for treating drug abuse. *AAPS J.* 8(2):E383-390.
127. Persson J, Beyer I, Yumul R, Li Z, Kiem HP, Roffler S, & Lieber A (2011) Immuno-therapy with anti-CTLA4 antibodies in tolerized and non-tolerized mouse tumor models. *PLoS ONE* 6(7):e22303.
128. Tuve S, Chen BM, Liu Y, Cheng TL, Toure P, Sow PS, Feng Q, Kiviat N, Strauss R, Ni S, Li ZY, Roffler SR, & Lieber A (2007) Combination of tumor site-located CTL-associated antigen-4 blockade and systemic regulatory T-cell depletion induces tumor-destructive immune responses. *Cancer Res.* 67(12):5929-5939.
129. Rothlisberger D, Honegger A, & Pluckthun A (2005) Domain interactions in the Fab fragment: a comparative evaluation of the single-chain Fv and Fab format engineered with variable domains of different stability. *J. Mol. Biol.* 347(4):773-789.
130. Finlay WJ, Bloom L, & Cunningham O (2011) Phage display: a powerful technology for the generation of high specificity affinity reagents from alternative immune sources. *Methods Mol. Biol.* 681:87-101.
131. McCormack WT, Tjoelker LW, & Thompson CB (1993) Immunoglobulin gene diversification by gene conversion. *Prog. Nucleic Acid Res. Mol. Biol.* 45:27-45.
132. Finlay WJ, deVore NC, Dobrovolskaia EN, Gam A, Goodyear CS, & Slater JE (2005) Exploiting the avian immunoglobulin system to simplify the generation of recombinant antibodies to allergenic proteins. *Clin. Exp. Allergy* 35(8):1040-1048.
133. Chiliza TE, Van Wyngaardt W, & Du Plessis DH (2008) Single-chain antibody fragments from a display library derived from chickens immunized with a mixture of parasite and viral antigens. *Hybridoma (Larchmt)* 27(6):413-421.
134. Hof D, Hoeke MO, & Raats JM (2008) Multiple-antigen immunization of chickens facilitates the generation of recombinant antibodies to autoantigens. *Clin. Exp. Immunol.* 151(2):367-377.
135. Finlay WJ, Bloom L, & Cunningham O (2011) Optimized generation of high-affinity, high-specificity single-chain Fv antibodies from multiantigen immunized chickens. *Methods Mol. Biol.* 681:383-401.

136. Galan JE, Nakayama K, & Curtiss R, 3rd (1990) Cloning and characterization of the asd gene of *Salmonella typhimurium*: use in stable maintenance of recombinant plasmids in *Salmonella* vaccine strains. *Gene* 94(1):29-35.
137. Datsenko KA & Wanner BL (2000) One-step inactivation of chromosomal genes in *Escherichia coli* K-12 using PCR products. *Proc. Natl. Acad. Sci. U. S. A.* 97(12):6640-6645.
138. Andris-Widhopf J, Rader C, Steinberger P, Fuller R, & Barbas CF, 3rd (2000) Methods for the generation of chicken monoclonal antibody fragments by phage display. *J. Immunol. Methods* 242(1-2):159-181.
139. Brosius J, Erfle M, & Storella J (1985) Spacing of the -10 and -35 regions in the *tac* promoter. Effect on its in vivo activity. *J. Biol. Chem.* 260(6):3539-3541.
140. de Marco A (2009) Strategies for successful recombinant expression of disulfide bond-dependent proteins in *Escherichia coli*. *Microb Cell Fact* 8:26.
141. Schaefer JV & Pluckthun A (2010) Improving Expression of scFv Fragments by Co-expression of Periplasmic Chaperones. *Antibody Engineering, Vol 2, Second Edition*:345-361.
142. Gentschev I, Dietrich G, & Goebel W (2002) The E. coli alpha-hemolysin secretion system and its use in vaccine development. *Trends Microbiol.* 10(1):39-45.
143. Foote J & Eisen HN (1995) Kinetic and affinity limits on antibodies produced during immune responses. *Proc. Natl. Acad. Sci. U. S. A.* 92(5):1254-1256.
144. Zhang X, Schwartz JC, Guo X, Bhatia S, Cao E, Lorenz M, Cammer M, Chen L, Zhang ZY, Edidin MA, Nathenson SG, & Almo SC (2004) Structural and functional analysis of the costimulatory receptor programmed death-1. *Immunity* 20(3):337-347.
145. Kumagai, Izumi, and Tsumoto, Kouhei (2010) Antigen–Antibody Binding. In: *eLS*. John Wiley & Sons Ltd, Chichester. http://www.els.net
146. Worn A & Pluckthun A (2001) Stability engineering of antibody single-chain Fv fragments. *J. Mol. Biol.* 305(5):989-1010.
147. Choi GH, Lee DH, Min WK, Cho YJ, Kweon DH, Son DH, Park K, & Seo JH (2004) Cloning, expression, and characterization of single-chain variable fragment antibody against mycotoxin deoxynivalenol in recombinant *Escherichia coli*. *Protein Expr. Purif.* 35(1):84-92.
148. Lombardi A, Sperandei M, Cantale C, Giacomini P, & Galeffi P (2005) Functional expression of a single-chain antibody specific for the *HER2* human oncogene in a bacterial reducing environment. *Protein Expr. Purif.* 44(1):10-15.
149. Wang H, Liu X, He Y, Dong J, Sun Y, Liang Y, Yang J, Lei H, Shen Y, & Xu X (2010) Expression and purification of an anti-clenbuterol single chain Fv antibody in *Escherichia coli*. *Protein Expr. Purif.* 72(1):26-31.
150. Lamberski JA, Thompson NE, & Burgess RR (2006) Expression and purification of a single-chain variable fragment antibody derived from a polyol-responsive monoclonal antibody. *Protein Expr. Purif.* 47(1):82-92.
151. Chen LH, Huang Q, Wan L, Zeng LY, Li SF, Li YP, Lu XF, & Cheng JQ (2006) Expression, purification, and in vitro refolding of a humanized single-chain Fv antibody against human CTLA4 (CD152). *Protein Expr. Purif.* 46(2):495-502.
152. Loeffler M, Le'Negrate G, Krajewska M, & Reed JC (2007) Attenuated Salmonella engineered to produce human cytokine LIGHT inhibit tumor growth. *Proc. Natl. Acad. Sci. U. S. A.* 104(31):12879-12883.

153. Lloyd SA, Sjostrom M, Andersson S, & Wolf-Watz H (2002) Molecular characterization of type III secretion signals via analysis of synthetic N-terminal amino acid sequences. *Mol. Microbiol.* 43(1):51-59.
154. Dobo J, Varga J, Sajo R, Vegh BM, Gal P, Zavodszky P, & Vonderviszt F (2010) Application of a short, disordered N-terminal flagellin segment, a fully functional flagellar type III export signal, to expression of secreted proteins. *Appl. Environ. Microbiol.* 76(3):891-899.
155. Zhang G, Brokx S, & Weiner JH (2006) Extracellular accumulation of recombinant proteins fused to the carrier protein YebF in *Escherichia coli*. *Nat. Biotechnol.* 24(1):100-104.
156. Fernandez LA, Sola I, Enjuanes L, & de Lorenzo V (2000) Specific secretion of active single-chain Fv antibodies into the supernatants of *Escherichia coli* cultures by use of the hemolysin system. *Appl. Environ. Microbiol.* 66(11):5024-5029.
157. Hotz C, Fensterle J, Goebel W, Meyer SR, Kirchgraber G, Heisig M, Furer A, Dietrich G, Rapp UR, & Gentschev I (2009) Improvement of the live vaccine strain *Salmonella enterica* serovar Typhi Ty21a for antigen delivery via the hemolysin secretion system of *Escherichia coli*. *Int. J. Med. Microbiol.* 299(2):109-119.
158. Ferguson WS & Goorin AM (2001) Current treatment of osteosarcoma. *Cancer Invest.* 19(3):292-315.
159. Khanna C, Prehn J, Yeung C, Caylor J, Tsokos M, & Helman L (2000) An orthotopic model of murine osteosarcoma with clonally related variants differing in pulmonary metastatic potential. *Clin. Exp. Metastasis* 18(3):261-271.
160. Pulaski BA & Ostrand-Rosenberg S (2001) Mouse 4T1 breast tumor model. *Curr Protoc Immunol* Chapter 20:Unit 20 22.
161. Conti L, Ruiu R, Barutello G, Macagno M, Bandini S, Cavallo F, & Lanzardo S (2014) Microenvironment, oncoantigens, and antitumor vaccination: lessons learned from BALB-neuT mice. *BioMed research international* 2014:534969.
162. Anderson KG, Mayer-Barber K, Sung H, Beura L, James BR, Taylor JJ, Qunaj L, Griffith TS, Vezys V, Barber DL, & Masopust D (2014) Intravascular staining for discrimination of vascular and tissue leukocytes. *Nat. Protoc.* 9(1):209-222.
163. Hirano F, Kaneko K, Tamura H, Dong H, Wang S, Ichikawa M, Rietz C, Flies DB, Lau JS, Zhu G, Tamada K, & Chen L (2005) Blockade of B7-H1 and PD-1 by monoclonal antibodies potentiates cancer therapeutic immunity. *Cancer Res.* 65(3):1089-1096.
164. Greifenberg V, Ribechini E, Rossner S, & Lutz MB (2009) Myeloid-derived suppressor cell activation by combined LPS and IFN-gamma treatment impairs DC development. *Eur. J. Immunol.* 39(10):2865-2876.
165. Ray P, Arora M, Poe SL, & Ray A (2011) Lung myeloid-derived suppressor cells and regulation of inflammation. *Immunol. Res.* 50(2-3):153-158.
166. Tam JW, Kullas AL, Mena P, Bliska JB, & van der Velden AW (2014) CD11b+ Ly6Chi Ly6G- immature myeloid cells recruited in response to *Salmonella enterica* serovar Typhimurium infection exhibit protective and immunosuppressive properties. *Infect. Immun.* 82(6):2606-2614.
167. Langdon SP (2012) Animal modeling of cancer pathology and studying tumor response to therapy. *Curr. Drug Targets* 13(12):1535-1547.

168. Schreiber K, Rowley DA, Riethmuller G, & Schreiber H (2006) Cancer immunotherapy and preclinical studies: why we are not wasting our time with animal experiments. *Hematol. Oncol. Clin. North Am.* 20(3):567-584.
169. Peters LJ & Hewitt HB (1974) The influence of fibrin formation on the transplantability of murine tumour cells: implications for the mechanism of the Revesz effect. *Br. J. Cancer* 29(4):279-291.
170. Forbes NS (2010) Engineering the perfect (bacterial) cancer therapy. *Nat. Rev. Cancer* 10(11):785-794.
171. Pawelek JM, Low KB, & Bermudes D (1997) Tumor-targeted *Salmonella* as a novel anticancer vector. *Cancer Res.* 57(20):4537-4544.
172. Theys J, Landuyt W, Nuyts S, Van Mellaert L, Bosmans E, Rijnders A, Van Den Bogaert W, van Oosterom A, Anne J, & Lambin P (2001) Improvement of Clostridium tumour targeting vectors evaluated in rat rhabdomyosarcomas. *FEMS Immunol. Med. Microbiol.* 30(1):37-41.
173. Hoiseth SK & Stocker BA (1981) Aromatic-dependent *Salmonella typhimurium* are non-virulent and effective as live vaccines. *Nature* 291(5812):238-239.
174. Murray SR, Bermudes D, de Felipe KS, & Low KB (2001) Extragenic suppressors of growth defects in *msbB Salmonella*. *J. Bacteriol.* 183(19):5554-5561.
175. Drees J, Mertensotto M, Liu G, Panyam J, Leonard A, Augustin L, Schottel J, & Saltzman D (2015) Attenuated *Salmonella enterica* Typhimurium Reduces Tumor Burden in an Autochthonous Breast Cancer Model. *Anticancer Res* 35(2):843-849.
176. McKenzie GJ & Craig NL (2006) Fast, easy and efficient: site-specific insertion of transgenes into enterobacterial chromosomes using Tn7 without need for selection of the insertion event. *BMC Microbiol.* 6:39.
177. Toso JF, Gill VJ, Hwu P, Marincola FM, Restifo NP, Schwartzentruber DJ, Sherry RM, Topalian SL, Yang JC, Stock F, Freezer LJ, Morton KE, Seipp C, Haworth L, Mavroukakis S, White D, MacDonald S, Mao J, Sznol M, & Rosenberg SA (2002) Phase I study of the intravenous administration of attenuated *Salmonella typhimurium* to patients with metastatic melanoma. *Journal of clinical oncology : official journal of the American Society of Clinical Oncology* 20(1):142-152.
178. Tome Y, Zhang Y, Momiyama M, Maehara H, Kanaya F, Tomita K, Tsuchiya H, Bouvet M, Hoffman RM, & Zhao M (2013) Primer dosing of *S. typhimurium* A1-R potentiates tumor-targeting and efficacy in immunocompetent mice. *Anticancer Res.* 33(1):97-102.
179. Tozer GM, Kanthou C, & Baguley BC (2005) Disrupting tumour blood vessels. *Nat. Rev. Cancer* 5(6):423-435.
180. Lee SJ, O'Donnell H, & McSorley SJ (2010) B7-H1 (programmed cell death ligand 1) is required for the development of multifunctional Th1 cells and immunity to primary, but not secondary, *Salmonella* infection. *J. Immunol.* 185(4):2442-2449.
181. Xu D, Fu HH, Obar JJ, Park JJ, Tamada K, Yagita H, & Lefrancois L (2013) A potential new pathway for PD-L1 costimulation of the CD8-T cell response to *Listeria monocytogenes* infection. *PLoS ONE* 8(2):e56539.
182. Pulko V, Harris KJ, Liu X, Gibbons RM, Harrington SM, Krco CJ, Kwon ED, & Dong H (2011) B7-h1 expressed by activated CD8 T cells is essential for their survival. *J. Immunol.* 187(11):5606-5614.

183. O'Donnell H & McSorley SJ (2014) *Salmonella* as a model for non-cognate Th1 cell stimulation. *Frontiers in immunology* 5:621.
184. Terpe K (2006) Overview of bacterial expression systems for heterologous protein production: from molecular and biochemical fundamentals to commercial systems. *Appl. Microbiol. Biotechnol.* 72(2):211-222.
185. Wang H, Sun X, Chen F, De Keyzer F, Yu J, Landuyt W, Vandecaveye V, Peeters R, Bosmans H, Hermans R, Marchal G, & Ni Y (2009) Treatment of rodent liver tumor with combretastatin a4 phosphate: noninvasive therapeutic evaluation using multiparametric magnetic resonance imaging in correlation with microangiography and histology. *Invest. Radiol.* 44(1):44-53.
186. Leschner S, Deyneko IV, Lienenklaus S, Wolf K, Bloecker H, Bumann D, Loessner H, & Weiss S (2012) Identification of tumor-specific *Salmonella Typhimurium* promoters and their regulatory logic. *Nucleic Acids Res.* 40(7):2984-2994.
187. Chatfield SN, Charles IG, Makoff AJ, Oxer MD, Dougan G, Pickard D, Slater D, & Fairweather NF (1992) Use of the nirB promoter to direct the stable expression of heterologous antigens in *Salmonella* oral vaccine strains: development of a single-dose oral tetanus vaccine. *Biotechnology. (N. Y.)* 10(8):888-892.
188. Mangsbo SM, Sandin LC, Anger K, Korman AJ, Loskog A, & Totterman TH (2010) Enhanced tumor eradication by combining CTLA-4 or PD-1 blockade with CpG therapy. *J. Immunother.* 33(3):225-235.
189. Gerner MY, Heltemes-Harris LM, Fife BT, & Mescher MF (2013) Cutting edge: IL-12 and type I IFN differentially program CD8 T cells for programmed death 1 re-expression levels and tumor control. *J. Immunol.* 191(3):1011-1015.
190. Rochman Y, Spolski R, & Leonard WJ (2009) New insights into the regulation of T cells by gamma(c) family cytokines. *Nat. Rev. Immunol.* 9(7):480-490.
191. Rubinstein MP, Kovar M, Purton JF, Cho JH, Boyman O, Surh CD, & Sprent J (2006) Converting IL-15 to a superagonist by binding to soluble IL-15R{alpha}. *Proc. Natl. Acad. Sci. U. S. A.* 103(24):9166-9171.
192. Stoklasek TA, Schluns KS, & Lefrancois L (2006) Combined IL-15/IL-15Ralpha immunotherapy maximizes IL-15 activity in vivo. *J. Immunol.* 177(9):6072-6080.
193. Kobayashi M, Fitz L, Ryan M, Hewick RM, Clark SC, Chan S, Loudon R, Sherman F, Perussia B, & Trinchieri G (1989) Identification and purification of natural killer cell stimulatory factor (NKSF), a cytokine with multiple biologic effects on human lymphocytes. *J. Exp. Med.* 170(3):827-845.